Digitized Theses   Digitized Special Collections

2011

Pressure-Equalized Rainscreen Wall System: A Full-Scale Experiment

Samar D. Dernayka
Western University, sdernayk@alumni.uwo.ca

PRESSURE-EQUALIZED RAINSCREEN WALL SYSTEM:
A FULL-SCALE EXPERIMENT

(Thesis format: Monograph)

By

Samar D. <u>Dernayka</u>

Faculty of Engineering

Department of Civil and Environmental Engineering

Submitted in partial fulfillment

of the requirements for the degree of

Master of Engineering Science

School of Graduate and Postdoctoral Studies

The University of Western Ontario

London, Ontario, Canada

May 2011

THE UNIVERSITY OF WESTERN ONTARIO
SCHOOL OF GRADUATE AND POSTDOCTORAL STUDIES

CERTIFICATE OF EXAMINATION

Supervisor   Examiners

_____   _____
Dr. Craig Miller   Dr. Horia Hangan

                                                          _____
                                                          Dr. Eric Savory

                                                          _____
                                                          Dr. Clare Robinson

The thesis by
Samar D. Dernayka

entitled

Pressure-Equalized Rainscreen Wall System: A Full-Scale Experiment

is accepted in partial fulfillment of the

requirements for the degree of

Master of Engineering Science

Date_____   _____
                                                          Chair of the Thesis Examination Board

ABSTRACT

The pressure equalized rainscreen wall, considered as the most effective building envelope against wind–induced rain penetration, requires continuous investigations to reach better performance. This research seeks the optimum pressure equalization process under external pressure conditions and wall parameters that have not previously been studied in detail. For this purpose, a single compartment full-scale wall model was built in a controlled facility at the University of Western Ontario. The cavity pressure response to external fluctuations was experimentally examined with respect to the rainscreen venting area ratio, under two types of real wind pressure distributions generated mechanically at zero degree incidence: 1) single pressure and, 2) pressure gradient caused by the application of three different signals varying horizontally across the rainscreen.

As the rainscreen venting area ratio increases, the pressure equalization performance improves, irrespective of the nature of the applied pressure, implying an increase in the critical damping frequency. However, an applied pressure gradient leads to a lower degree of pressure equalization at a constant venting area. Moreover, the change of the vent openings layout has an impact on the wall performance, mainly at low venting areas. Locating the vent openings at the bottom of the rainscreen gives better pressure equalization rather than distributing them between top and bottom.

Using a numerical model, the cavity pressure measurements were underestimated under a uniform pressure and overestimated when subject to a pressure gradient. The agreement in the frequency domain between experimental and predicted signals was satisfactory in the high frequency regions at high venting area ratios. However, transfer functions and phase angles were overpredicted at low venting rates. Based on numerical simulations, the cavity volume change does not significantly affect the performance of the model under an external pressure gradient. When a single pressure is applied, the pressure equalization is reduced at a larger cavity depth, which is only apparent at low venting areas.

Keywords: rainscreen, wind pressure gradient, frequency domain

ACKNOWLEDGEMENTS

I would like to express my thanks to Dr. Diana R. Inculet, who introduced the Pressure Equalized Rainscreen systems field to me. She gave me the opportunity to do this research under her guidance and insightful ideas.

I am also grateful to Dr. Craig Miller, a great supervisor I was so lucky to have during the last semester. He offered me help and support, and provided many hours of valuable discussions. His understanding, encouragement and advice have made this thesis completed at the end of the day.

I also acknowledge the technical staff at the Three Little Pigs facility for their assistance. Similarly, it would have been so difficult to accomplish the experimental part of the work without the aid of many graduate students; among them, I would like to mention Murray Morrison. I really appreciate his excellent knowledge and patience in providing the solutions for the electrical and technical problems that I have encountered through the course of this work.

The build up of the full-scale model was realized by the University Machine Shop staff who offered valuable guidance in terms of the design and the actual performance of the model.

Finally, I would like to thank my lovely parents for their encouragement. And I wonder if I could have ever done this research without the continuous support of my husband Zaher. I would like to express my deepest gratitude to him for being so patient and helpful during the last two years. This work is dedicated to him, and to our coming baby...

TABLE OF CONTENTS

LIST OF TABLES

LIST OF FIGURES

x

NOMENCLATURE

A	Opening area
A_{ab}	Air barrier leakage area
A_{rs}	Rainscreen venting area
A_w	Wall panel area
$A_V = A_{rs}/A_w$	Rainscreen Venting area ratio
a	Opening area of a rainscreen
C_L	Loss coefficient
C_p	Pressure coefficient
C_{pe}	External pressure coefficient
C_{pi0}	Internal pressure coefficient
C_{pc}	Pressure coefficient inside the cavity
d	Opening diameter
d_c	Cavity depth
f	Frequency
g	Peak factor
H	PER wall height
H_m	Height of the building model in the wind tunnel
$H_\Delta(\omega)$	Transfer function
H_g	Instantaneous horizontal pressure gradient coefficient
K	Discharge coefficient
K_A	Bulk modulus of air
K_B	Bulk modulus of the building
l_e	Effective length
l_0	Opening length

m	number of openings
m_c	Mass of air inside the cavity
n	Flow exponent
p_0	Atmospheric static pressure
P_a	Area-averaged pressure
P_c	Cavity pressure
P_e	External pressure
P_i	Internal pressure
P_t	Instantaneous pressure measured by a pressure transducer
P_1	External pressure applied to the first pressure box from the left
P_2	External pressure applied to the second pressure box in the middle
P_3	External pressure applied to the third pressure box from the left
Δp	Differential pressure
Q	Flow rate
R_e	Reynolds number
$S(f)$	Power spectral density function
t	Time lag
U	Air velocity
V	Velocity
V_0	Internal volume for a low-rise building
V_c	Cavity volume
x	Horizontal coordinate from the bottom left corner of the air barrier
x	Distance the air slug moves
x_m	Horizontal coordinate from the bottom left corner of the wind tunnel pressure model face
x_r	Horizontal coordinate from the bottom left corner of the rainscreen

y_m	Vertical coordinate from the bottom left corner of the wind tunnel pressure model face
y	Vertical coordinate from the bottom left corner of the air barrier
z_{ref}	Reference height in the wind tunnel
W	Width of the pressure equalized rainscreen wall
W_m	Width of the pressure model face in the wind tunnel
ω_0	Resonant gradient frequency
ϖ_d	Critical damping frequency
ρ_a	Air density
μ	Kinetic viscosity of the air
β	Polytropic exponent
γ	Ratio of specific heat of air
σ	Variance of the pressure signal

CHAPTER 1

INTRODUCTION

1.1 Principle of a Pressure-Equalized Rainscreen Wall System

The Pressure Equalized Rainscreen wall (PER) also referred to as an open rainscreen wall has gained a reputation among buildings envelopes, for being a defence-line against rainwater penetration.   It is constituted of: 1) the outer wall layer known as the rainscreen, 2) the inner wall layer called the air barrier and, 3) the cavity that separates them and which is vented to the exterior through deliberate openings in the rainscreen. Figures 1.1 and 1.2 show the components of a PER wall system and different images of the PER walls actually built in the industry.
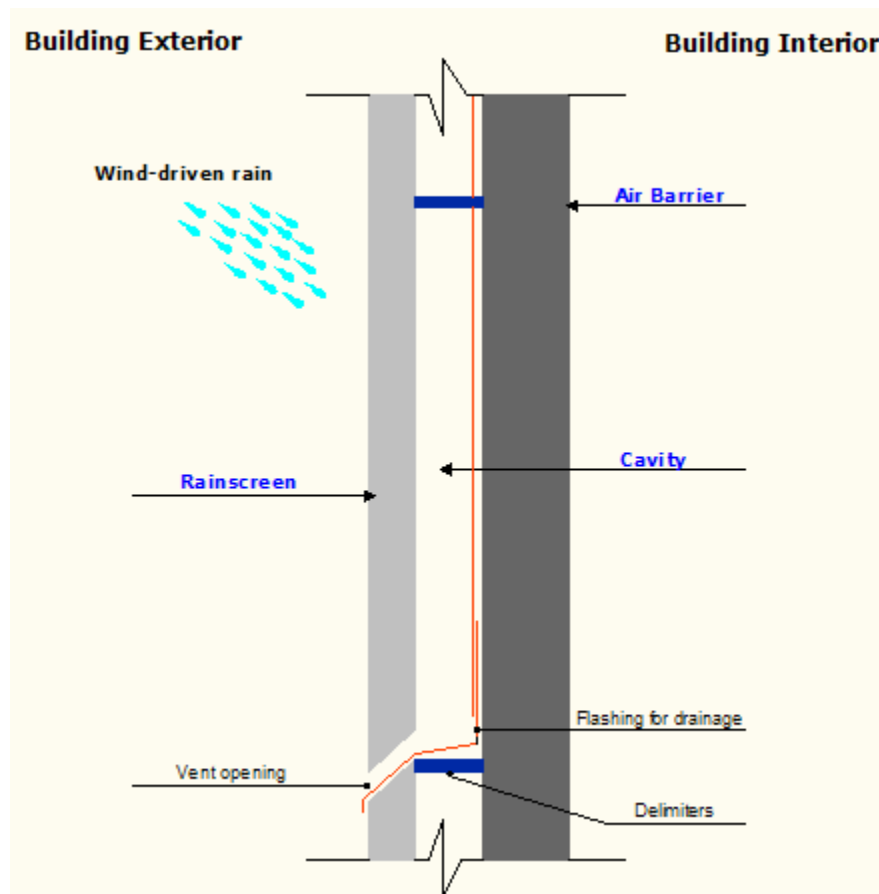
Figure 1.1 Components of a pressure equalized rainscreen wall (PER)
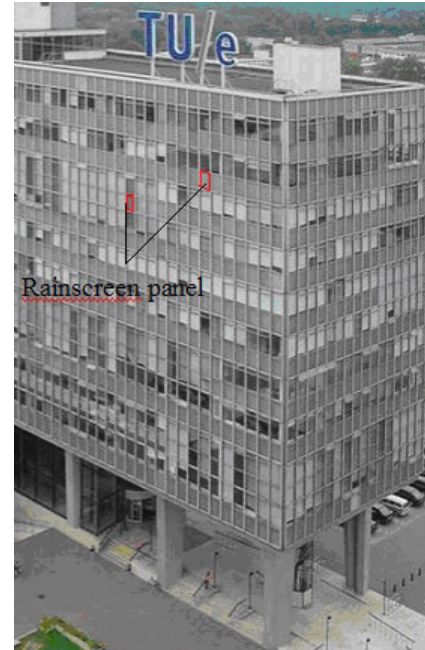
<table>
<tr><td>a) Metal PER</td><td>b) Technical University of Eindhoven</td></tr>
</table>

Figure 1.2 Examples of PER systems in the industry (a) and (b)

In general, for the rain to penetrate a building envelope, there must be both an opening for the water and a force to move the water through this opening. Many driving forces contribute to this process like the kinetic energy of the raindrop, surface tension, gravity, capillary suction and air pressure difference between the building exterior and interior. The PER wall design intent is to equalize external pressure with internal cavity pressure via vent openings that form the venting area, in order to eliminate the differential pressure across the rainscreen. Wind-induced pressure difference is considered as the most critical air driving forces, as being responsible of the rain, moisture and mould penetration into a building, especially under severe wind storms. The air barrier assembly, supposed to be stiff and airtight, has the role of resisting sustained and peak wind loads in case they are transferred to the cavity. Further, it transmits the load induced by the pressure difference between the cavity and building interior to the wall's structural components.

In theory, pressure equalization (PE) means a zero air pressure differential at all times across the rainscreen. In practice, however, perfect pressure equalization is neither achievable nor necessary for adequate rain penetration control; engineers claim that the wall assembly must be designed to tolerate the entry of a small amount of water without damage. According to Rousseau et al. (1998), the adequate pressure equalization for rain penetration control may be defined as not more than 25 Pa differential pressure across the rainscreen.

The pressure equalization technique was in fact early recognized in 1962 as O. Birkeland proposed in his Handbook "Curtain Walls" to "design the exterior rain-proof finishing so open that no super-pressure can be created over the joints or seams in the finishing". He considered that such process is provided by having "an air space behind the exterior finishing, but with connection to the outside air", so that air pressures due to wind gusts will be equalized on both sides of the exterior finishing. This principle was then enhanced in Garden's publication in 1963 "Rain penetration and its control", who settled the preliminary basics of the PER wall construction in terms of cavity depth and vent openings size. Later, others like Ganguli and Dalgliesh (1988), Baskaran and Brown (1992), Kumar (1999) and Inculet and Davenport (1996) carried on several researches, laboratory and tests on site in order to establish specific design guidelines for the different parameters for an optimum performance of the PER walls systems, under different conditions; like when the system is experiencing a leakage problem, which is an unavoidable issue in buildings.

Many recommendations have arisen based on their experiments, however this domain still need further investigation, especially in the absence of ready to use design guidelines for PER walls in codes and standards. The latter agree in general that a satisfactory differential pressure is available when the pressure load on the rainscreen is near zero.

1.2 Applications of Pressure Equalized Rainscreen Wall Concept

The PER walls systems are used for existing buildings experiencing general performance problems such as rain penetration, insufficient insulation, and deterioration of components. A new application has been introduced recently, known as overcladding. In fact, tens of thousands of highrises built during the building boom of the mid-1980s suffered water damage as wind-driven rain entered the walls. Under severe wind storms, sections of exterior cladding have let go and plunged to the ground for some building façades. A few today, like low-rise buildings, just show the same symptoms as leaky construction, wet spots and mould on walls, with an exterior wall assembly unable to sustain wind-induced pressure. Moreover, Canadian insurance companies have claimed that well over half of insured losses from building outer envelopes are wind related. In light of these problems, engineers decided to opt for PER wall as an outer building envelope that offers the most protection to the inner structural layer and requires less maintenance over its service life.

When applied to cladding panels, the pressure equalization technique is considered to be very expensive. A major part of the cost is highly related to materials that are unique for façade applications such as exterior rainscreen panels like molten cast glass, precast concrete, marble, aluminium, glass fibre reinforced concrete (GFRC), water jet cut stainless steel, copper, etc. The choice of rainscreen material is surely based on aesthetic criterion as well as on cost restrictions.

In Europe, the open rainscreen principle refers to back-ventilated rainscreen walls, instead of the pressure equalized rainscreen wall notion used mostly in the USA and Canada. In fact, it is a PER wall with incorporating additional large vents at the top of the rainscreen. Thus, the resulting airflow pattern in the cavity moves air in through the bottom vents (the original venting openings of the rainscreen) and out the top vents, helping to dry out any moisture that penetrates the wall. According to Inculet (1990), this design only strives to keep water from coming in contact with the air barrier; while the

PER wall system aims to eliminate any water penetration through the rainscreen, by addressing the wind's driving force with adequate vent openings.

1.3 Focus of the Current Research

The development of PER wall systems application is still slow, due to the comparative expense over a more conventional exterior wall system, according to leading designers of tall buildings in the United States. The motivation for the current research on pressure-equalized rain screen wall cladding stems from this point. Actually, the goal is to look at the performance of a PER wall panel under new exterior pressures conditions; that were not taken into account before. Also, the effect of some design parameters is examined, and a numerical model is used for the experimental results validation.

Previous works have investigated PER wall performance by measuring the differential pressure across the rainscreen as it is considered the key for optimum pressure equalization. Such tests were done either in the laboratories or in the field. However, in both cases, the researches were not able to take the self-control of the set-up conditions of the PER wall system or even the applied wind load. In the wind tunnel experiments, the modeling of PER wall system is subject to scaling problem; which gives incorrect representations of the PER features size and the characteristics, and would negatively influence conclusions made on the pressure equalization process.

On the other hand, in the field tests previously done (i.e. Ganguli and Dalgliesh (1988) and Kumar (1999)) the full-scale model of the PER wall panel was always tested after being installed on the constructed building. Thus, the data measurements were probably affected by the leakage status, an unavoidable issue that is hard to quantify in buildings. Further in such tests, no one could control the external wind fluctuations at any time, it all depends on the climate conditions and the location of the PER panel itself. In case the cavity response pressure needs to be examined for other wind loads, or for pressures gradients (i.e. at the corner of the building façade), the panel needs to be moved or other wall panels are then added at various locations of the façade which imply higher cost and

a more time consuming work. Moreover, it is necessary to recall that the majority of previous studies have focused on the examination of rainscreen venting over air barrier leakage ratio effect on the PER performance; without taking into consideration the effects of the other parameters.

In light of this discussion, it was decided to build a PER full-scale model in a controlled facility to vary the different parameters and applied wind conditions, and observe the way they affect the model performance, in a controlled environment and within a short time period. The roadmap of the research work is clarified through the chapters of this thesis.

Chapter 2 mainly presents a literature review on the previous studies made about PER walls. Full-scale and wind tunnel experiments are discussed providing the key conclusions on the effect of design parameters on the PER performance; and the validity of applied numerical models. At the beginning, a general overview was presented about the theoretical models with the involved equations, used for cavity pressure response prediction when an external load is applied to the wall.

Chapter 3 describes the experimental model set-up. It provides a clear detailing of the three components of the PER wall, and the test configurations as well. The equipments used for both wind load application and cavity pressure data acquisition, are also depicted.

Chapter 4 shows the experimental measurements of the cavity pressure with respect to rainscreen venting configurations and vent openings location, the cavity depth being constant. The data permit calculation of the differential pressure across the rainscreen, which leads to the evaluation of the PER model performance.

Two types of external signals were normally applied to the panel: a) a single pressure and, b) a pressure gradient; which results from the application of three different pressure signals varying horizontally on the rainscreen. In this case, each group of venting openings was subject to a different pressure depending on its location. Such test was

never done before using a full-scale model. It allows examination of the effect of an exterior pressure gradient applied to the same PER panel. Moreover, the influence of a building façade on the pressure equalization process can be seen, since two different pressure gradients are used, each has been extracted in reality from on a different pressure model face in a wind tunnel experiment.

Chapter 5 provides a comparison between experimental and numerical results. A theoretical model was programmed for cavity pressures predictions, using the actual exterior pressure signals applied on site as input. Numerical simulations are presented for all test configurations. In addition, the numerical model was used to predict the effect of the cavity depth variation on the wall's PE process; which has not been investigated yet, neither numerically, nor practically. In the current research, the cavity depth has been numerically varied within a practical range where the upper value is the maximum depth used in the industry.

Finally Chapter 6 presents conclusions from the current project results. It also claims further investigations in some points that would be of a useful contribution for the development of PER wall systems.

CHAPTER 2

LITERATURE REVIEW

This chapter presents the results of a literature survey on the research work concerning the pressure-equalized rainscreen wall studies for the past decades. It tends to show the continuous effort of researches in examining the possibility of achieving an optimum performance for a PER system via laboratory experiments, field measurements, wind tunnel models and computer simulations. Finally, a summary is provided herein for general design guidelines recommended by the authors for a better pressure equalized rainscreen wall.

2.1 Prediction of Cavity Response Pressure

2.1.1 Background Theory from Low-rise Buildings

The theory for the prediction of cavity response pressures for a PER wall originates from internal pressure predictions in low-rise buildings.

The cavity pressure responding to the external wind-induced fluctuations entering through vents is analogous to the internal pressure behaviour within a building (enclosure with rigid walls and roofs) with single or multiple openings. In fact, internal pressures are introduced inside a building throughout leakage or openings. They depend on several factors including: external pressure distributions near the openings, geometry of the openings, vents, the fluid properties (density, viscosity), internal volume, wind direction, turbulence in the upstream boundary layer, flexibility of the building "skin" and structure (Vickery and Bloxham 1992); and the compartmentalization within the building (Sharma and Richard 1997). The internal pressure response can be determined using two methods: 1) conservation of mass, 2) Helmholtz resonator model.

For a low-rise building with a single windward opening, the internal pressure is established after a response time t where t is the time taken for the internal pressure to become equal to a sudden increase in pressure outside the opening, caused for example by a sudden window failure. In steady flow, Holmes (2001) confirms that the internal

pressure will quickly develop in order to reach the external pressure on the windward wall in proximity of the opening. In the case of a turbulent boundary-layer wind, the increase of the external pressure will allow an increase in the density of air within the internal volume V_0, thus the internal pressure increases.

In the case of neglected inertial effects, the mass conservation concept is applied, so that the rate of mass flow through the opening $\rho_a Q$ must equal the rate of mass increase $(d\rho_a/dt)V_0$ inside the volume thus the time lag expression is given by

$$\tau = \frac{\rho_a V_0 \overline{U}}{\gamma K A p_0} \sqrt{C_{pe} - C_{pi0}} \tag{2.1}$$

by considering that for a turbulent flow through an orifice, the air flow is related to the pressure difference across the orifice $P_e - P_i$

When inertial effects are considered, Holmes (1979) suggested that a Helmholtz resonator model can be used for the prediction of the response to turbulent external pressures. Holmes observed that a building with a single dominant opening behaves like a Helmholtz resonator and internal pressure fluctuations are due to compressibility effects of the fluid. Thus, he considered it as a special case of "Helmholtz resonator", known in acoustics as describing the response of small volumes to fluctuating external pressures (Raylieh 1945, Malecki 1969). This can be applied to the case of external wind pressures 'driving' the internal pressures within a building: a 'slug' of air of length l_e is assumed to move in a distance " x " in and out of the opening in response to the external pressure changes as in Fig 2.1. The motion of the slug of air is expressed with the differential equation

$$\rho_a A l_e \ddot{x} + \frac{\rho_a A}{2K^2} \dot{x} |\dot{x}| + \frac{\gamma p_0 A^2}{V_0} x = A \Delta p_e(t) \tag{2.2}$$

known as the unsteady orifice discharge equation where the first term on the left hand side is an inertial term proportional to the acceleration $\ddot{x}$ of the air slug (whose mass is $\rho_a A l_e$, the second term is the loss term associated with energy losses for flow through the orifice, and the third term represents the "stiffness" explained as the resistance of the air pressure that is already available in the internal volume V_0 to the air slug motion.

Holmes (1979) developed from this model the expression of the undamped natural frequency for the resonance of the movement of the air slug, and of the internal pressure fluctuations, known as Helmholtz frequency, in case of a single windward opening

$$f = \frac{1}{2\pi}\sqrt{\frac{\gamma A p_0}{\rho_a l_e V_0}} = \frac{1}{2\pi}\sqrt{\frac{K_A A}{\rho_a l_e V_0}}$$ (2.3)

calculated given the opening area, internal volume and flexibility of roof and walls.

Using the atmospheric pressure $p_0 = 10^5 Pa$, $\rho = 1.2 Kg/m^3$, $\gamma = 1.4$, $l_e = 1.0\sqrt{A}$, and taking into consideration the flexibility of the building, the frequency becomes

$$f \approx 55\frac{A^{1/4}}{V_0^{1/2}\left[1+(K_A/K_B)\right]^{1/2}}$$ (2.4)

Holmes claims that a significant resonant excitation of the internal pressure fluctuations by natural wind turbulence is unlikely to occur, in the case of small volumes as shown in Table 2.1, since Helmholtz frequencies are higher than 1Hz.

Kumar (1999) adopted this viewpoint in case of PER systems. Using $\gamma = 1.2$ and $l_e = 0.89\sqrt{A}$, he checked the probability of resonance inside the cavity for the combination of smallest $A_{rs}/A_w = 0.0025$ and largest $d_c = 0.2m$ that can be used, and could give the lowest system frequency (f). The expression

$$f \approx 52.8\left[\frac{A_{rs}^{1/4}}{V_c^{1/2}}\right] \approx 52.8\frac{(A_{rs}/A_w)^{1/4}}{d_c^{1/2}A_w^{1/4}}$$ provided $f \approx 12Hz$ which is much higher than the

frequencies of external pressures (0.1Hz-2Hz). Thus, it is unlikely that resonance will occur inside the cavity of a PER wall at any given amplitude of external pressure. Generally, cavity pressure frequencies lie in the range of 50 to 150 Hz.

Type	Internal volume (m^3)	Opening area (m^2)	Stiffness ratio K_A/K_B	Helmholtz frequency (Hertz)
House	600	4	0.2	2.9
Warehouse	5000	10	0.2	1.3
Concert hall	15 000	15	0.2	0.8
Arena (flexible roof)	50 000	20	4	0.23

Table 2.1 Helmholtz resonance frequencies for some Typical buildings after (Holmes 2001)
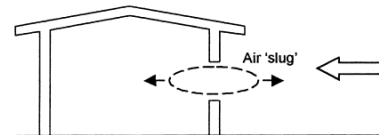
Figure 2.1 Helmholtz resonator model of fluctuating internal pressures with a single opening after (Holmes 2001)

2.2 Theoretical Models

The cavity pressure response of a PER wall subject to fluctuating pressures can be predicted using two theoretical models:

1) Model based on mass balance or first principle
2) Model based on Helmholtz resonator theory

For both analytical models, mathematical modelling of flow through the PER wall system is developed using the external pressure and wall characteristics as data input. The key for the cavity pressure simulation is the Bernoulli principle for incompressible fluids, which leads to flow rate expressions. The fluid here is air with $\rho_a = 1.3 Kg/m^3$. In general, for airflow to occur, there must be 1) a pressure difference between two points and 2) a continuous flow path or opening connecting the points. Those two requirements are represented by the vent holes of the rainscreen, which ensure the passage of the airflow from the exterior to the cavity generating a cavity pressure response P_c, and thus a differential pressure across the rainscreen.

The governing equation of motion corresponding to the "slug" of air moving throughout the vent hole of the rainscreen is given as

$$\rho_a l_e \frac{dU}{dt} + C_L \frac{\rho_a U^2}{2} = P_e - P_c \qquad (2.5)$$

This is the discharge equation for unsteady flow through an orifice, where l_e is the effective length of the air slug, $\rho_a l_e$ is the inertial effect, U is the fluid flow velocity, p_e is the external applied pressure. This equation comes from the Bernoulli equation, where a loss term C_L is introduced, since there is no absence of friction for the flow through an orifice.

2.2.1 Model Based on Mass Balance or First Principle (Model 1)

This category includes all models derived on the basis of mass continuity equation and equation of airflow through walls; without taking into consideration the inertial effect. The general form of the flow rate Q through vent hole was discussed first by Kimura (1977), where F is a function of Reynolds number and opening geometry:

$$Q = AF(R_e, \text{geometry of opening})\left(2dP_e \middle/ \rho_a\right)^{0.5} \qquad (2.6)$$

He considered that for openings greater than about 10mm, the function F may be regarded as a constant, and it is usually referred to the discharge coefficient K. A is the area of the orifice, and $dP_e = \Delta p = P_e - P_c$ is the differential pressure across the rainscreen. The conventional form of this equation is

$$Q = AK\sqrt{\frac{2\Delta p}{\rho_a}} \qquad (2.7)$$

originated from Eqn (2.5), with the assumption that the flow is steady $\left(dU \middle/ dt = 0\right)$. The discharge coefficient (also known as coefficient of discharge) allows the use of the ideal velocity and orifice area in calculating the flow for a jet through an orifice of a small wall thickness: It is negatively correlated with the loss coefficient $C_L = \dfrac{1}{K^2}$ which is affected by the time, the wind direction due to the exterior pressure field and the orifice length to diameter ratio (l_0 / d) (Chaplin et al. 2000). Its value is usually adjusted for the calculations, in order to get a match between the numerical model and the experiment as Table 2.2 shows.

Equation (2.7) is transformed to a general form that can be applied to different flow characteristics of rainscreen and air barrier walls:

$$Q = AK\sqrt{\frac{2}{\rho_a}(P_e - P_i)^n} \qquad (2.8)$$

Shaw (1981) considers that the flow exponent n varies according to the flow and the opening details (Table 2.3).

The conservation of mass of air inside the cavity generally requires that the rate of net mass flow into or out of the cavity must equal the rate of change of the mass of air inside the cavity m_c, as noted by Baskaran (1992). The general form of the continuity equation is

$$\rho_a(Q_1 + Q_2) = \frac{dm_c}{dt} = \frac{d}{dt}(\rho_a V_c) = \rho_a \frac{dV_c}{dt} + V_c \frac{d\rho_a}{dt} \qquad (2.9)$$

where Q_1 and Q_2 are respectively the flow rates through the rainscreen and the air barrier for a PER wall.

Assuming the walls are not flexible ($\frac{dV_c}{dt}=0$), and substituting to Eqn (2.9) the polytropic law relating pressure and density of air inside the cavity:

$$\frac{1}{P_c}\frac{dP_c}{dt}=\frac{\beta}{\rho_a}\frac{d\rho_a}{dt} \tag{2.10}$$

The practical continuity equation will be

$$\frac{dP_c}{dt}=\frac{\beta P_c}{V_c}\left[Q_1+Q_2\right] \tag{2.11}$$

with β is the polytropic exponent generally equal to 1.2 as an intermediate value as used by Holmes (1979) and Kumar (1999) ($\beta=1$ for isothermal condition, and $\beta=1.4$ for adiabatic condition).

2.2.2 Model Based on Helmholtz Resonator Theory (Model 2)

This model takes into consideration the inertial effects of air within the cavity, the losses due to the vent orifice and friction; as suggested by Holmes (1979). Helmholtz resonance is the phenomenon of air resonance in a cavity: the air has the tendency to oscillate at its maximum amplitude associated with resonant frequencies. When air is forced into a cavity, the pressure inside increases. Once the external force that pushes the air into the cavity disappears, the higher-pressure air inside will flow out. However, this surge of air flowing out will tend to over-compensate, due to the air inertia in the neck, and the cavity will be left at a pressure slightly lower than the outside, causing air to be drawn back in. This process repeats with the magnitude of the pressure changes decreasing each time.

Using the "slug" of air movement in a distance "x" in and out of the opening, Eqn (2.5) becomes

$$\rho_a l_e \ddot{x}+C_L\frac{\rho}{2}\dot{x}\left|\dot{x}\right|=P_e-P_c \tag{2.12}$$

where the term $\rho_a l_e$ is the inertial effect of the air slug proportional to the acceleration. The effective length l_e changes with shape and length of the opening (Table 2.4).

$C_L \dfrac{\rho}{2} \dot{x}|\dot{x}|$ represents the damping effect referring to energy losses when the flow passes

through the opening

Orifice-type loss: The pressure drop due to the Orifice-loss is then

$$|P_e - P_c| = |\dot{x}|^{1/n} \left[\frac{1}{K}\right]^{1/n} \left[\frac{\rho_a}{2}\right]^{1/2n} \tag{2.13}$$

Friction-type loss: For steady flow through an orifice-plate, it is essential to take into consideration the wall thickness, since the openings are very small. Thus, the solid wall shear stresses affect the pressure drop and the physical behaviour is more like a pipe flow than an orifice flow. The pressure drop due to friction loss as explained in Oh et al (2007) is

$$\Delta p = \frac{32 \mu l_0}{d^2} U \tag{2.14}$$

μ is the dynamic viscosity of air, and U is the wind velocity

Combining Eqns. (2.12), (2.13) and (2.14), "the single discharge equation for unsteady flow (SDE) through an opening or leak" is:

$$\rho_a l_e \ddot{x} + \left(\frac{1}{K}\right)^{1/n} \left(\frac{\rho_a}{2}\right)^{1/2n} \dot{x}|\dot{x}|^{(1/n)-1} + \frac{32 \mu l_0}{d^2} \dot{x} = P_e - P_c \tag{2.15}$$

For a number m of vent and leak openings, there will be $m+1$ unknowns $(P_c, x_1, x_2, ...x_m)$ giving

$$\rho_a l_{ei} \ddot{x}_i + \left(\frac{1}{K_i}\right)^{1/n_i} \left(\frac{\rho_a}{2}\right)^{1/2n_i} \dot{x}_i|\dot{x}_i|^{(1/n_i)-1} + \frac{32 \mu l_{0i}}{d_i^2} \dot{x}_i = P_{ei} - P_c \tag{2.16}$$

known as "Multiple discharge equations for unsteady flow through multiple openings or leaks (MDE)", (i=1… m) and an additional Continuity Equation (CE)

$$\rho_a(a_1 x_1 + a_2 x_2 + ... + a_m x_m) = \frac{\rho_a V_c}{\gamma p_0} P_c \tag{2.17}$$

This system provides the solution for the cavity response pressure prediction (Vickery 1986) for a PER wall system. P_{ei} is an external pressure at opening (i) , γ the ratio of specific heats of air, V_c the cavity volume, p_0 the static pressure and $Q = a\dot{x}$ is the flow rate through the vent .

Substituting the cavity pressure P_c in Eqn (2.16), we would observe Eqn (2.2) established by Holmes (1979) for a single windward opening for a low-rise building, but without the friction term.

Moreover, the damped Helmholtz resonator model theory has been a tool to calculate the undamped natural frequency (Irwin et al. (1984)) and the time lag of the cavity response Baskaran and Brown (1992).

Equation (2.16) can be written in terms of the pressure coefficients (Holmes (2001))

$$\frac{\rho_a l_e V_c}{\gamma p_0 A}\ddot{C}_{pc} + \left(\frac{\rho_a V_0 \bar{U}}{2K\gamma A p_0}\right)^2 \dot{C}_{Pc}\left|\dot{C}_{pc}\right| + C_{pc} = C_{pe} \qquad (2.18)$$

The generalized form is represented by $\dfrac{m_j}{K_j}\ddot{C}_{pc}(t) + \dfrac{C_j}{K_j}\dot{C}_{Pc}(t) + C_{pc}(t) = C_F(t)$ where m_j refers to the mass of the air slug, K_j indicates the stiffness associated with the resistance of air, and C_j is the equivalent linear damping coefficient.
$C_F(t)$ is the excitation pressure function. In the case of pressure –equalized rainscreen wall, the excitation of the system is brought by wind turbulence represented by a time-varying external signal, thus $C_F(t) = C_{pe}(t)$ (Sharma and Richards (2003))

The "undamped natural Helmholtz frequency" for the resonance of air slug movement, and of internal pressure fluctuations is $f = \dfrac{\omega}{2\pi} = \dfrac{\sqrt{K_j / m_j}}{2\pi}$ giving

$$f = \frac{1}{2\pi}\sqrt{\frac{\gamma A P_0}{\rho_a l_e V_c}} \qquad (2.19)$$

Previous studies	K	C_L	Comments
Holmes (1979)	0.63	2.5	Under steady flow conditions
	0.15	45	Under highly fluctuations and reversed flow conditions
Vickery (1994)	0.61	2.68	For sharp-edged circular openings
Inculet and Davenport (1994)	0.19	27	To get a matching between the experimental and numerical at high rainscreen venting area
Sharma and Richards (1997)	1	1.5	For long opening
	0.6	1.2	For thin opening
Ginger (1997)	0.633	2.5	To calculate Helmholtz frequency
Hee et al. (2007)	0.633	2.5	For dominant opening
	0.375	4.06	For leakage

Table 2.2 Previous values used for the discharge coefficient K and the loss coefficient C_L

Previous studies	n	Comments
Shaw (1981)	0.5	For laminar flow
	0.5 to 1	When openings in the air barrier are small cracks, the flow through the orifice is a mixture of laminar and turbulent
	0.7	For leakage openings
Kumar (1999)	0.5	For openings in a rainscreen (and air barrier where orifices are not small cracks)
	0.71	For leakage in air barrier as straw
	1	For leakage in air barrier as filter
ASHRAE (2001)	0.65	For leakage openings

Table 2.3 Previous values used for the flow coefficient n

Previous studies	l_e	Comments
Malecki (1969)	$0.89\sqrt{a}$	Correct for circular openings. Good approximation for rectangular openings of low aspect ratio
Holmes (1979)	$0.89\sqrt{a}$	For comparison with full-scale model
Vickery (1986)	$l_0 + 0.89\sqrt{a}$	
	$1.0\sqrt{a}$	For openings in thin walls
Hee et al. (2007)	$l_0 + 0.89\sqrt{a}$	For dominant opening and leakage

Table 2.4 Previous values used for the effective length l_e

$K_A = \gamma p_0 = 141999$ (Pa) is the bulk modulus of air.

This frequency depends on $A = A_{rs}$ the area of vent openings in the rainscreen, cavity volume V_c, effective length l_e of air slug at the opening, air density ρ_a, and the ratio of specific heats for air γ.

According to the equations, the two theoretical models assume the pressure inside the cavity to be uniform. Furthermore, Model 1 combines the flow rates through all the openings of the rainscreen into one term Q_1, the same applies to the air barrier. Thus, the model uses the averaged external pressures as a single pressure input applied on the rainscreen. Models 2 instead represents the flow rate through each opening or leak separately and, includes the associated applied pressure and losses terms, which leads to a more realistic prediction of cavity pressure inside the air barrier.

Davenport and Surry (1984) used the equations of Model 2 to develop an expression for a critical frequency ϖ_d (in radians) above which attenuation of the exterior pressure fluctuations will occur. Thus, frequencies less than ϖ_d will be fairly effectively transmitted to the cavity. Based on Eqn (2.15) and by including a forcing pressure as a function of the frequency, they got for only one opening in the rainscreen and no leakage through the air barrier, the expression

$$\frac{1}{\omega_0^2}\ddot{C}_{pc} + \frac{1}{\varpi_d}\dot{C}_{pc} + C_{pc} = C_{pe} \tag{2.20}$$

ω_0 is the resonant radian frequency. For $\varpi_d > \omega_0$, resonance may occur in the cavity.

Taking into consideration the multiple venting holes in the rainscreen, the distribution of mean exterior pressures and spatial correlation of exterior pressure fluctuations as well as the leakage characteristics, Davenport and Surry elaborated a frequency response function $H_\Delta(\omega)$ that describes the cavity pressure and pressure drops across the rainscreen

$$\Delta P_{ji} = H_{\Delta ji}(\omega) P_{ei} \tag{2.21}$$

ΔP_{ji} : pressure drop across the rainscreen at location j due to forcing pressure P_{ei} at i.

Such a function refers to the level of resistance that the vent holes exhibit as opposed to the flow, which suppresses the fluctuations, that is called aerodynamic damping. The greater the damping, the greater the magnitude of the differential pressures sustained by the rainscreen will be.

On the other hand, Baskaran and Brown (1992) used Helmholtz resonator model to establish an expression for the time lag of the cavity response pressure of a PER wall subject to sinusoidal pressure using

$$\tau = \frac{1}{57.48\sqrt{\dfrac{A_{rs}^{0.5}}{A_w d_c}}} \tag{2.22}$$

indicating that the time lag is constant for given wall parameters, and it can be reduced through better pressure equalization. Clearly, this formula assumes that the frequency of the signal is constant, thus it cannot be applied to the random fluctuations pressures that cause variation of the cavity fluctuations in the frequency domain.

Also, Baskaran carried out a numerical evaluation of the performance of pressure equalized rainscreen walls in (1994) being the first to use CFD. He applied sinusoidal external pressure variations only.

2.3 Previous Pressure-Equalized Rainscreen Walls Experiments

Previous experiments allowed estimation of the impact of various design parameters on the pressure equalization process. For this purpose, PER panels were subject to sets of configurations mainly in terms of rainscreen venting area, air barrier leakage areas and cavity compartmentalisation. The researchers were always seeking the ultimate combination of PER wall characteristics to get a full-pressure equalization, so that the wind-induced pressure is completely absorbed by the cavity.

2.3.1 Full-Scale Experiments

Most of these experiments were performed using wall-clad panels mounted on building façades and interacting with the real wind fluctuations. In spite of differences in the panels set-up and wind conditions, they all agree that two main factors contribute to the performance of a PER: 1) the rainscreen venting to wall area and, 2) the rainscreen venting to air barrier leakage area. The two ratios are equally important in case of leaky characteristics of the air barrier wall. In absence of leakage, increasing the venting area does not affect the transmission of external fluctuations into the cavity in the frequency domain. Furthermore, reasonable pressure equalization can be achieved by providing a relatively small venting area. The field experiments showed consistent results regarding the behaviour of the cavity pressure response under zero degree wind angle: with higher venting to wall area and venting to leakage ratios, the pressure equalization between external pressures fluctuations and cavity pressure improves. Ganguli and Guirouette (1987) were the first to evaluate the rainscreen venting area as a key controller for the rainscreen loading. They claimed that the peak pressure difference across glass cladding dropped when the ratio of cavity volume to venting area was decreased with a fixed volume.

Later, Ganguli and Dalgliesh (1988) showed a satisfactory PE performance of a precast open rainscreen panel by virtue of its large venting to volume ratio and its small compartment size, in addition to a well-sealed air barrier. It was suggested that the first parameter assists in equalizing the fluctuating pressures, the second limits both the mean and cross flows behind the rainscreen under mean external pressure gradients. The ratio of vent area to air barrier leakage was greater than 10 to 1, and that what caused the cavity pressure to equalize fully with the exterior pressure .

On the contrary, poor pressure equalization was revealed with Brown et al. (1995) and Inculet and Davenport (1994) models due to a small venting rate and low ratio of rainscreen venting to air barrier leakage area (two to one in the first case and one in the second case). The differences in these ratios influence the load sharing between the

rainscreen and cavity. Brown et al. (1995) observed that only 70% of the pressure drop across the wall was transferred to the air barrier under static pressure. Also under positive pressure, the brick veneer was receiving about 64% of the instantaneous load across the wall, and was capturing 90% under negative wind loading, due to the rapid variation in the external pressure. On the other hand, Inculet and Davenport (1994) said that the rainscreen was carrying 58% of the total mean load.

In 1998, Kumar showed that his experimental results are in agreement with the trends already observed. He claims that the pressure equalization improves as the leakage rate reduces, for the same amount of venting. Similarly, it gets better with a higher rainscreen venting area when the leakage is constant (Fig 2.2). He concluded that the highest rainscreen load is associated to smallest venting area and leaky air barrier, thus a low venting to leakage area ratio.

●No leakage   ▲ Leakage straw   ■ Leakage filter
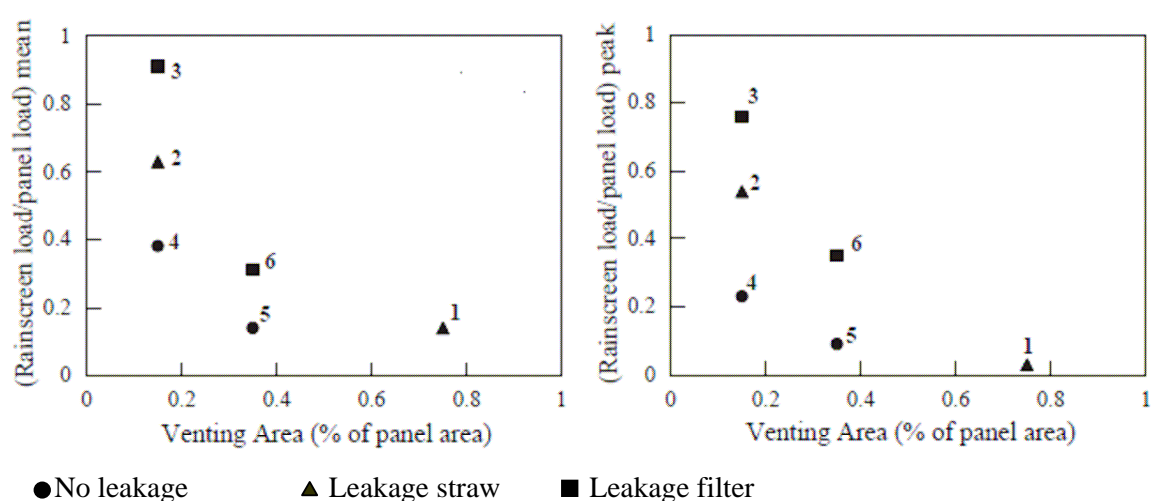
Figure 2.2 Rainscreen load reduction as a function of venting and leakage area reproduced from Kumar et al. (2003)

On the other hand, data measurements were also examined in the frequency domain in order to evaluate the PE process. Both Inculet and Davenport (1994) and Kumar, through several publications (Kumar et al. (1999), (2003) and (2008)), confirmed that low venting area which leads to poor pressure equalization, does not allow the complete transmission of low frequency pressure fluctuations to the cavity. In this case, there is a high damping of the differential pressure across the rainscreen of all frequencies. Low frequency

external fluctuations are attenuated and not completely transmitted to the cavity, while higher frequencies are completely transferred to the rainscreen.

Furthermore, Kumar observed that the venting area variation significantly affects the PER wall performance at a constant air barrier leakage rate significantly. Higher-pressure equalization ratios at lower frequencies can be obtained by increasing the venting area. However, the high frequency wind pressure fluctuations are not influenced. They are transferred to the rainscreen almost at the same rate.

Such behaviour in the high frequency region is still in the course of studies and investigations, especially that it is related to the critical damping frequency according to Ganguli and Dalgliesh (1988). At full-pressure equalization of PER wall model, the latter authors observed that only frequencies higher than 1 Hz are taken by the rainscreen. The suggested reason behind this performance was related to the spatial averaging of the gusts that may because of the high frequency pressures across the rainscreen.

By mounting the PER panels on the building façades, field experiments can describe how the wind conditions affect the rainscreen pressures, in case all the data sets are available. However, Ganguli et al (1988) did not present the data measurements to all the 24 panels that he has used, and just gave general conclusions. They realized that the strongest winds did not necessarily give rise to the largest pressure differences across wall panels. In addition, the peak pressure differences across the rain screens were associated with storms having wind speeds in the range of 14-15.5m/s.

For a PER panel located between the middle and the corner of the north wall and subject to full pressure equalization, they attributed the large sustained loads (lasting several seconds) of around 60 Pa by the rainscreen to exterior pressure gradients coming across, stating they decrease to 15 Pa when the external pressure becomes uniform. Transient loads (< 1 second) on the rainscreen of around 200 Pa were tracked under negative wind pressure. A combination of reasons was suggested referring to the limitation of the instrumentation, and the small and quick spatial variations of the external fluctuations:

the external pressure was varying rapidly, that the cavity could not respond immediately, and the equalization was not directly accomplished. At this case only, the cladding was receiving instantaneously 45% of the load.

Kumar et al. (2003) claimed that the highest-pressure coefficients C_p occur when the wind blows normally to the PER wall panel. Also, they realized that the influence of wind velocity on PE is predominant in case of leaky air barrier and can be reduced by providing larger venting area. In general, smaller percentage of long duration wind pressures is transferred to the rainscreen at lower wind velocities.

Moreover, Baskaran and Brown (1992) and Fazio and Kontopidis (1988) examined the effect of rainscreen venting on the PER when subject to a sinusoidal signal. They found similar conclusions referring to a higher cavity response when increasing the rainscreen venting area ratio, or decreasing the air barrier leakage. Note that details of the field experiments previously discussed are provided in Table 2.5.

Apart from air barrier leakage and rainscreen venting area ratios, few researchers have discussed the effect of other parameters on PER wall performance. Canada Mortgage and Housing Corporation proved in 1999 that compartmentalization of the wall cavities especially at the corners of a pressure equalized rainscreen system transmits the pressure load to the air barrier system. In addition, they realized that compartment seals also withstand pressure loads from both inside and outside, especially in the case of full compartmentalization. Also, Choi and Wang (1998) also described the air barrier rigidity role in the PE, in comparison with the curtain walls that have flexible back-panel. He could demonstrate that for the same venting area and cavity volume, and at the same frequency of pressure fluctuation, the cavity pressure of curtain wall is lower than the one of PER wall with rigid back-panels. Therefore, the flexibility of the air barrier can slow down the increase of the cavity pressure, due to the largest aerodynamic damping. According to the rainscreen venting, it has the same effect on both assemblies.

Author	year	wall / panel dimensions	Rainscreen vent openings	Rainscreen vent ratio (Ars/Aw)	Air barrier leakage	Cavity depth (m)	Theoretical modeling	Observation
Ganguli & Dalglieh	1988	3.6 m x 2.9 m precast concrete panel with 2.1 m x 1.8 m central window	3.6 m x 0.015 m slot at bottom & 2.1 m x 0.015 m slot at top	1.20%	$\dfrac{A_{rs}}{A_{ab}} > \dfrac{10}{1}$	0.0127	-	Full (PE) due to high venting to leakage ratio
Baskaran & Brown	1992	1.5m wide x 2.1m high wall *reinforced 0.1m brick veneer rainscreen *0.012m foil-covered gypsum board air barrier	head joints at the bottom of the brick veneer	0.3% 0.5% 1.1%	holes drilled in the gypsum board $\dfrac{A_{ab}}{A_w} = 0.07\% \& 0.11\%$	insulation-filled (mineral wool)	Mass balance model	$\dfrac{A_{rs}}{A_w}$ should be at least 1% to get (PE) in case of sinusoidal signal pressure
Inculet & Davenport	1994	*0.1m brick veneer rainscreen wall *steel stud air barrier	4 venting holes per subcavity (2 at top and 2 at bottom) (vent is 54mm height and 10mm wide)	up to 0.1%	$\dfrac{A_{ab}}{A_w} \approx 0.1\%$	0.33	Helmholtz resonator model	Poor (PE) due to low venting $A_{rs} \sim A_{ab}$
Brown, Rousseau & Dalgliesh	1995	3.81m wide x 4.6m high wall divided in 6 windows bays	Six louvered inserts (two per level) 0.013m wide x 0.06m high	Ars=0.01 m^2 per compartment	$\dfrac{A_{rs}}{A_{ab}} \sim \dfrac{2}{1}$	irregular shape	-	Poor (PE) due to low venting to leakage ratio
Schijndel & Schols	1998	cavity with perforated blades placed on Eindhoven university $A_w = 1.3 m^2$	Sharp-edged circular holes	$0.001 < A_{rs} < 0.01 m^2$	$A_{ab} = 0.0052 m^2$	$0.05 < V_c < 0.25 \ m^3$	Helmholtz resonator & Mass balance model	minor differences between the two models in case of harmonic input signal
Kumar & Shijndel	1999 & 2003	1 m x 1.3 m wooden panel	Sharp-edged circular holes of 3mm diameter	0.15% 0.35% 0.75%	Straw, filter & noleakage Filter & noleakage Straw	0.15	Mass balance model	At a constant leakage, (PE) improves with higher venting area

Table 2.5 Previous full-scale experiments for pressure equalized rainscreen walls

2.3.2 Wind Tunnel Experiments

Previous wind tunnel experiments showed a satisfactory agreement with the full-scale results and induced the same recommendations regarding the effectiveness of a high rainscreen venting to air barrier leakage area ratio for pressure equalization like (Irwin et al. 1984) and (Kumar et al. 2008). Both authors studied a wind tunnel model for the PER system already tested respectively in "Place Air Canada" and "Eindhoven building University" in full-scale. (Irwin et al. 1984) modified the overall building dimensions and the cavity depth (0.5mm instead of the actual 0.063mm based on a scale of 1:200) and reported the results as pressure coefficients. Kumar et al. (2008) showed the results in the same way. They agreed that a high venting to leakage ratio leads to a good pressure equalization. In general, measurements of mean, maximum and rms pressure coefficients for panel and rainscreen sections fall within the range of field data for all the configurations, except for the worst configuration, with leaky air barrier and smallest venting area.

For configurations with sufficient leakage and poor venting, lowest reduction in rainscreen load was observed for both centre and edge taps on the building model (the centre tap is located where the panel is placed). Differences in rainscreen rms pressure coefficients showed up for the lowest vent to leakage ratio configuration: field values were underestimated by the wind tunnel data, due to internal pressure variations in the field and to the reduced oncoming turbulence in the tunnel. Besides, reductions of rainscreen loads seemed higher in the wind tunnel in comparison with the field results.

Inculet and Davenport (1994) got similar conclusions with the wind tunnel testing shown in Table 2.6, in comparison with full-scale model results. The authors revealed the high importance of a large rainscreen venting area. In absence of air barrier leakage, a larger venting area leads to an increase in the critical damping frequency ϖ_d, so the rainscreen is able to capture a lower load at each frequency in the region of the vent, with the same exterior forcing pressure and volume. The same concept is applicable for equal venting area but smaller volume; where the critical frequency is increased with a smaller volume.

In case of air barrier leakage, the transfer function of the differential pressure across the ranscreen is higher than zero at low frequencies.

However, the first case presents some disagreement with Kumar's (1999) observation. Actually, Kumar considers that, in absence of leakage, increasing the rainscreen venting area does not affect the transfer function magnitudes of the cavity pressure.

Author	Scale	Panel dimensions	Rainscreen vent openings	Rainscreen vent ratio (Ars/Aw)	Air barrier porosity	Cavity depth (m)	Theoretical modeling
Inculet & Davenport (1994)	1:12	rainscreen model mounted on a face of 0.6 m cube	-	between 0.02% and 1%	between 0.02% and 0.125%	0.0055 0.0275 (model scale)	Helmholtz resonator model
Kala, Stathopoulos & Kumar (2008)	1:50	*1 m x 1.3 m scaled panel *1mm thick rainscreen	6 holes of 1mm diameter 12 holes of 0.7mm diameter	0.15% 0.35% 0.75%	No leakage & 0.13%	0.15 (full scale)	-

Table 2.6   Previous wind tunnel experiments for pressure equalized rainscreen walls

Other wind tunnel tests have also discussed the vent holes distribution and the compartmentalization of the pressure equalized rainscreen walls based on implications from buildings' pressure models experiments, i.e. the experiments realized by Davenport, Surry and Inculet in the Boundary Layer Wind Tunnel Laboratory of the University of Western Ontario. It was shown that mean and unsteady pressure gradients have extremely large values at the edges of the building face, thus, it is difficult to achieve pressure equalization near building edges. In this situation, significant residual mean pressure differences result across the rainscreen. In addition, net mean rainscreen pressures decrease with decreasing compartment size and with decreasing the mean pressure gradient.

Besides, as the pressures become progressively more positive further from the edges, Skerlj and Surry (1994) proposed to "place the vents in the rainscreen at the compartment location that experiences the most positive pressures" referring to the locations that are furthest from the building edge. By installing several rainscreen compartments at various locations on the face of a building model (1:64 length scale) of various full-scale widths

(1m, 2m, 4 m and 8m) where each compartment is vented by one hole placed at its maximum mean exterior pressure location, Skerlj and Surry realized that at zero degree wind angle, net negative or near zero pressures act on the rainscreen. Also, the values of $(C_{pe} - C_{pi})$ are around zero at the compartment edge, where the vent is located.

Later, Inculet et al. (2001) observed that pressure gradients dictate the design of venting openings distribution and the cavity compartmentalization as well. "Compartments need to be extremely small to reduce the pressure difference across a compartment to an acceptable level". Also, placing of vents at the compartment edge furthest from the building edge would suppress the forces driving water into the cavity, because of the higher positive cavity pressure in comparison with the external pressures.

2.3.3 Comparison with Theoretical Model

By applying both Model 1 and Model 2 in the numerical simulations for cavity pressure prediction in the PER systems of previous tests, it was proven that matching with the experimental results is governed by the way the key input parameters are used, and the frequency domain of the external pressures in addition to the way of formulating the models equations. For instance, in spite of using two different theoretical models, both Inculet and Davenport (1994) and Kumar et al. (1999) reached the same conclusion: the theory underestimates the mean pressure drop across the rainscreen, especially under high frequencies. Also, the discharge coefficient K should be lowered in case of the low amplitude reversing flows in comparison with its value in the steady flow, for the theory to match with the experiment, an approach that was first suggested by Holmes (1979) who adjusted K to 0.15 under high fluctuations pressures, instead of 0.63.

Inculet and Davenport (1994) used the Helmholtz resonator model to predict the PE performance of a wind tunnel model. Following the concept of adjusting K until the (rms) values of the pressure drop across the rainscreen equal those of the experiment, the discharge coefficient was lowered to 0.47 to get a match in the transfer function. It was noted also that when the rainscreen venting area becomes larger, K is adjusted to 0.19.

With the close matching between the experimental and simulated pressures, the low frequency fluctuation of pressure across the rainscreen were overestimated, while the high frequency fluctuations were underestimated. The authors attributed these discrepancies to the linearization of the damping term in the model equations.

Kumar et al. (1999) observed similar results when comparing the simulated pressure time histories with the measurements of the full-scale model of the panel installed on the technical university of Eindhoven façade at different wind speeds and air barrier leakage conditions. In spite of the agreement between the two numerical models in the differential pressures predictions across the rainscreen, Model 1 was used for the prediction of cavity pressure; due to a less number of floating point operations $1.1x10^6$ in comparison with Model 2 at $2.7x10^9$, thus it is much faster. In addition, Kumar considered that the inertial effect in Model 2 could be avoided, because the resonance is highly unlikely to occur when inspecting the undamped natural frequency expression. Therefore, with the general matching between the trends of numerical and experimental results, Kumar attributed the differences to the fact that the numerical model does not take into account the spatial non-uniformity of pressures acting on the panel, and the appropriate damping of flow (the input pressure was the average exterior pressure acting on the panel along with a damping through a single vent hole only). Regarding the pressure drop across the rainscreen, Kumar found that the simulated time histories $(P_e - P_c)$ were smoother, and some real peaks were unpredicted. Also, the amplitudes of $S(f)/\sigma^2$ were higher above 1 Hz in case of the measured rainscreen pressures. Note that, K was lowered to 0.49, but it was also noticed that in absence of air barrier leakage, a better agreement exists between numerical and experimental transfer functions when lowering K.

Other authors launched numerical simulations by using sinusoidal input signals. Baskaran and Brown (1992) showed a match between pressure difference measurements across the raincreen and the computations based on mass balance model. However, sometimes the cavity pressure was overestimated and the phase shift underestimated by Model 1, which was explained by estimating the time lag as the inverse of undamped resonant frequency,

independently from the leakage area. In addition, the value of 0.5 was used for the air barrier flow exponent.

Schijndel and Schols (1998) developed equations based on both the Helmholtz resonator model and Mass balance model, and found a satisfactory agreement between the predictions of both models. The authors explained this saying that the second-order inertial term $d^2 P_c / dt^2$ used in Helmholtz equation is small with respect to the damping term, when the vent area is large enough compared with volume as Harris (1990) pointed out. A match was observed between experimental and numerical pressure drop across the rainscreen at frequencies less than 0.1 Hz, while the simulated pressure depicted more damping for the fluctuations at more than 0.1Hz.

2.4 Design Guidelines for PER

2.4.1 Rainscreen Venting Area

The rainscreen implementation reduces the differential pressure resulting from the wind loading on buildings that causes rainwater penetration as revealed by Kumar (2000). Its venting process controls the rate of transferring the air volume necessary to equalize cavity pressure with external pressure. The percentage of the necessary venting area depends on the amount of leakage of the air barrier, as well as the volume of air within the compartment. The majority of researchers agree on a high venting to leakage area ratio. Latta (1973) suggested a venting area of 10 times the leakage area under steady wind conditions. Killip and Cheetham (1984) found that it should be between 25 and 40 times the leakage area, while the minimum ratio is 20 for NRC (1998). Morrison Hershfield Ltd (1998) explained that the effective venting area for a compartment should be the sum of 1) 5 times the estimated leakage area of the air barrier, 2) 10 times the estimated leakage area of any corner seals, and 3) 1 times the estimated leakage area of intermediate compartment seals. Inculet (1990) specified for most high-rise buildings, a ratio venting to total wall area not less than 2%, based on precast concrete or metal panel high-rise building façades. The criterion is that the differential pressure across the rainscreen is less than 1% of the mean pressure drop across the composite wall.

2.4.2 Venting Configuration (locations and dimensions)

Since the deliberate vent openings ensure a rapid equalization of the cavity pressure with the external pressure, they should be distributed over the panel face, in order to reduce the average wind load acting on the external cladding. Vents are usually located at the bottom of the wall, so they can also drain it; besides, all vents of a compartment should be placed at the same height to avoid airflow loops. Generally, they are symmetric with respect to the panel, while Morrison Hershfield Ltd (1998) proposed an asymmetrical vent holes distribution. Also, some studies suggest their placement on the side of the compartment closest to the centre of the façade. This helps raising the cavity pressure, since the vent is located where the pressure on the face is high, and pushes the water out of leakage paths. The minimum adopted diameter of venting holes is 10mm, based on Garden (1963) to eliminate capillary plugs.

2.4.3 Cavity Volume

2.4.3.1 Cavity Depth:

In general, the smaller the cavity volume, the lesser is the airflow Q necessary to equalize the pressures, and the faster is the response time of the cavity pressure. The minimum allowed cavity depth is 25mm (Garden (1963)). In 1990, Inculet established the following relation $dc \leq 10\sqrt{A_{rs}}\big/A_W$ indicating that more rainscreen venting is needed for a larger cavity.

2.4.3.2 Compartment Size:

As a rule of thumb, the compartment height should not exceed 6m (about two stories). Garden (1963) proposed the location of horizontal closures up to 9m on centres over the total wall area; and vertical enclosures should be provided at each outside corner of a building, and at 1.2m intervals for about 6m from the corners, while compartment width could be up to 6m in the central portion of the façade and about 1.2 m at building edges and parapets. The British Standards (8200) mentioned that the largest lateral dimension of air spaces within 25% of the corner or top of the enclosure should be about 1.5m, and elsewhere about 5m. Cavity compartmentalization is made using separators or

delimiters; that connect the rainscreen to the air barrier system. According to Kumar (2000), they provide compartment seals at wall corners where the seals should be designed in order to withstand 2-3 times the wind load. Besides, they ensure an adequate number of ties to transfer the lateral loads from the rainscreen to the air barrier. Multiple wall components can act as delimiters, such as metal shelf angles, rigid sheet metal and foam plastic insulation strips, as long as they can be made relatively airtight and can be installed to sustain the lateral air pressure loads.

2.4.4 Air Barrier Stiffness and Leakage

The air barrier must be supported structurally to withstand both sustained and peak wind pressures and suctions with a resulting deflection that can be accommodated within the wall assembly. In fact, the excessive flexibility of the air barrier system will result in fluctuations in the volume of the air chamber compartment, which will adversely affect the potential for rapid pressure equalization across the rainscreen.The air barrier leakage is an unavoidable matter, even present in all nominally sealed buildings. For IRC's Canadian Construction Materials Centre (CCMC), the maximum air leakage rate allowable for the air barrier system in exterior walls of low-rise buildings is $0.2 L/(s.m^2)$ at 75 Pa pressure differential. Others recommended that air permeability values would be less than $1.3 x 10^{-6} m^3/m^2/Pa$ or $Q < 0.1 Lps/m^2$

CHAPTER 3

FULL-SCALE EXPERIMENT

3.1 Test Methodology

The current full-scale experiment aims at examining the rainscreen venting area effects on the PER wall performance a under random pressures signals associated to real wind fluctuations. The majority of experiments previously done in the field were applying wind pressures on PER panel after it is installed on the building, meaning that the tests results are significantly influenced by leakage, an unavoidable problem in the cladding industry. Here, I am trying to achieve a completely sealed full-scale model, by minimizing the leakage rate, in order to reach an optimum pressure equalization performance using the design parameters of the theory. The experiment has been carried out at the Insurance Research Laboratory for Better Homes (IRLBH), which is built by the University of Western Ontario in London Airport location, and known as the "Three Little Pigs Project". The full-scale model dimensions were dictated by the general design guidelines for PER walls, as well as the in-situ conditions of the facility. I decided to build a PER wall panel with one compartment combining the good performance with the ability to sustain the maximum loads pressures.

3.1.1 Model

A 2.6 m length by 2 m height rectangular rig is built bounded by two steel I-section columns. The PER wall as shown in Fig 3.1 consists of three components: 1) 0.00635m aluminum rainscreen panel, 2) wooden air barrier wall, 3) air space (cavity) between them. The rainscreen is firmly bolted at edges on both columns, while the back of the rig (air barrier) is movable to allow for cavity depth variations in future tests. The rig dimensions were dominated by the principle basics of previous pressure equalization studies, and the size of tools and equipments available in the facility. In addition, the intent was to use a full-scale model panel that matches with the typical dimensions in

industry, and allows different test configurations in terms of vent area and location to be explored.

3.1.1a) Rainscreen

The rainscreen panel is constructed from aluminum due to its stiffness and affordable cost. It is chosen with a standard length of 2.6 m since it will be installed between two columns of 2.2m clear span. It has 6.35 mm thickness as most common cladding panels. According to the height, the value of 2m is chosen in order to have room for two 0.71m height pressure boxes, which will be mounted later at top and bottom of the rainscreen. Therefore, two aluminum rainscreen panels (2.6m length by 1m height) were sealed
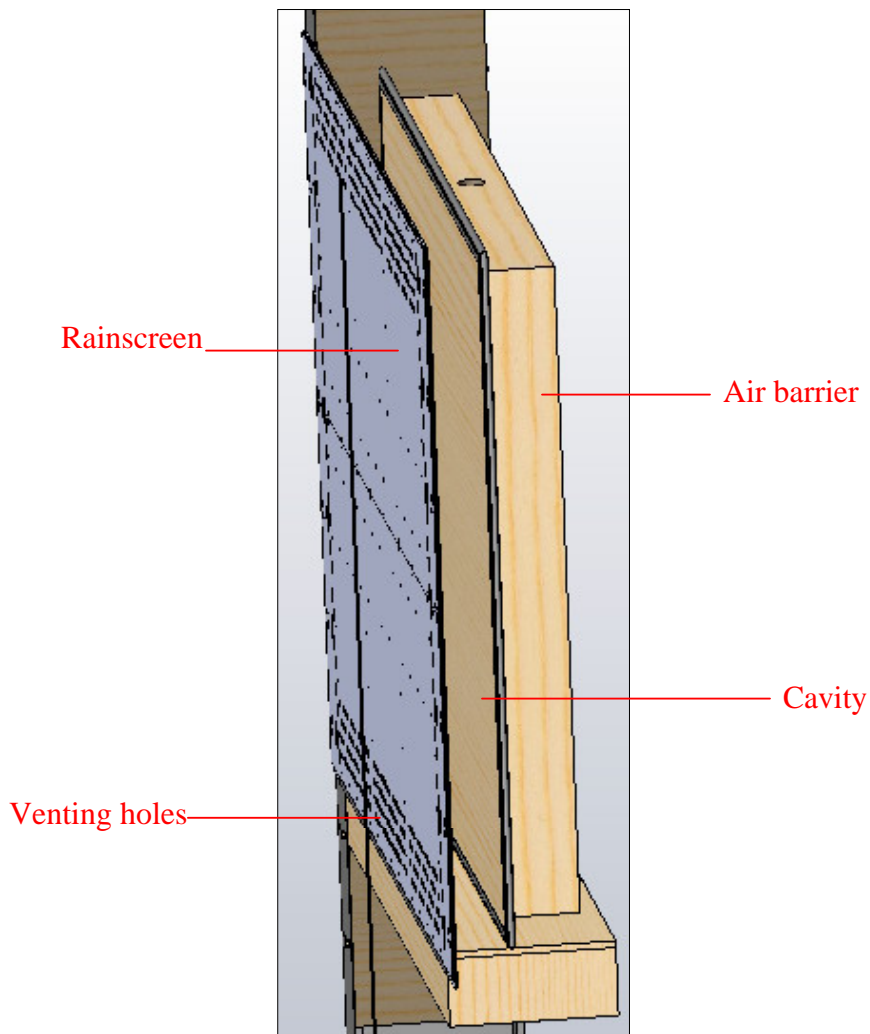
Figure 3.1 Pressure equalized rainscreen panel model (side view)

together using glue with an aluminum 5 cm wide plate to give the finalized rainscreen setup. Taking into account that the rainscreen plate is fixed at both edges, the working section of the rig is considered as 2.2m length by 2m height.

The rainscreen is perforated showing deliberate vent openings for the venting requirement for pressure equalization; it includes 304 20mm diameter holes in total, divided symmetrically between top and bottom, and forming 1.99% of the total area of the panel. Actually, the plan in this project is to test the PE performance of the model for a range of rainscreen venting area ratios going up to 2%. This venting percentage is chosen based on recommendations proposed by Baskaran and Brown (1992) who said that the ratio (A_{rs}/A_{w}) should lie in the range of 1 to 1.5%, and Inculet (1990) who
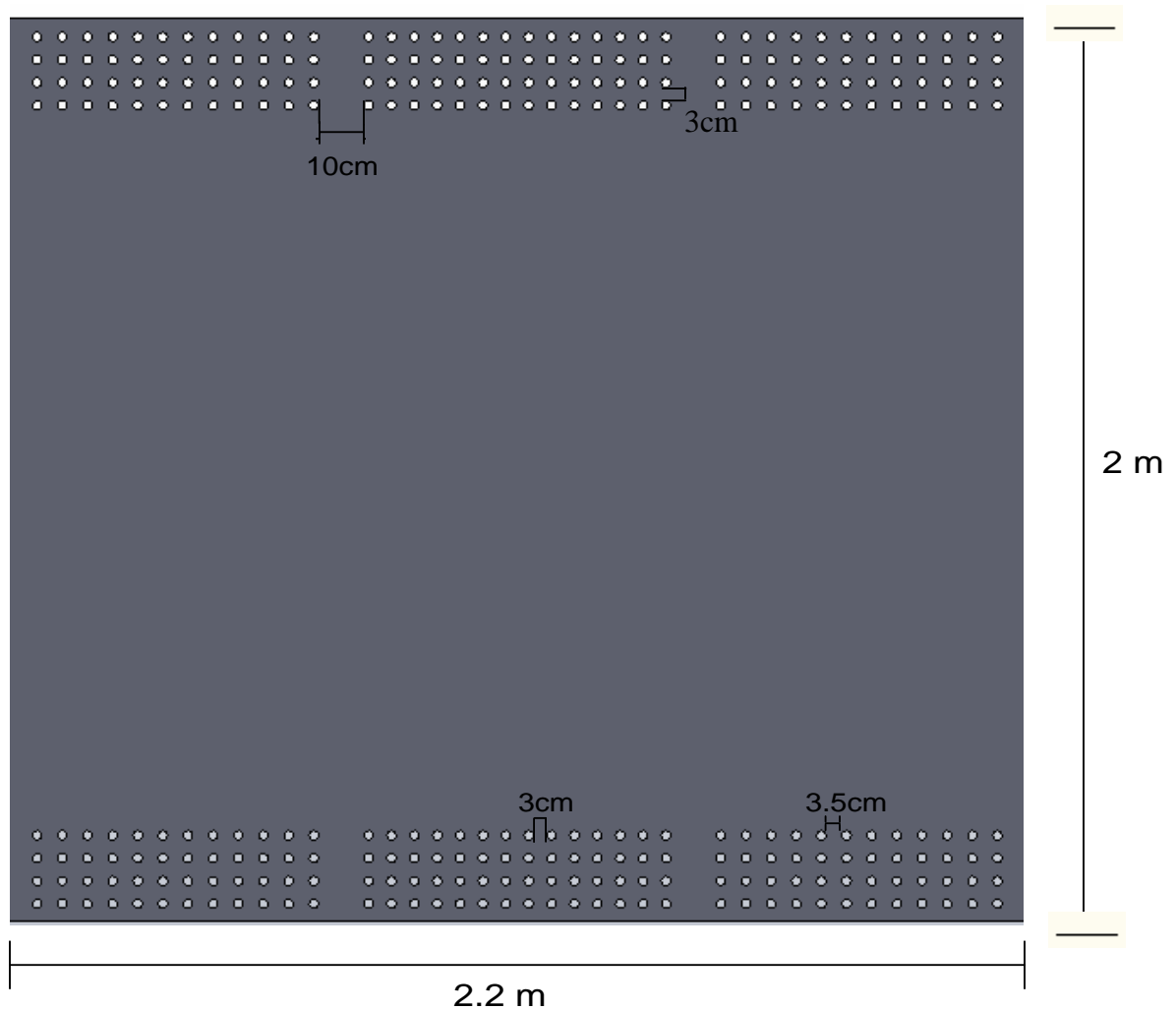
Figure 3.2 Distribution of 20mm venting holes on the aluminum rainscreen

settled the minimum venting ratio of 0.1% for re-sealed high-rise buildings; and 2% for high-rise buildings.

The bottom (top) of the rainscreen shows 152 holes distributed into 3 groups, which will allow the application of 3 different external pressure signals varying horizontally. The lower (upper row at the top) row at the bottom is 3cm distant from the lower (upper) edge of the panel. The holes are horizontally spaced by 3cm at the middle (14 holes per row), and by 3.5 cm at both sides (12 holes per row) as shown in Fig.3.2. The two pressure boxes made of wood and mounted respectively at top and bottom in front of the venting holes ensure the rainscreen rigidity.
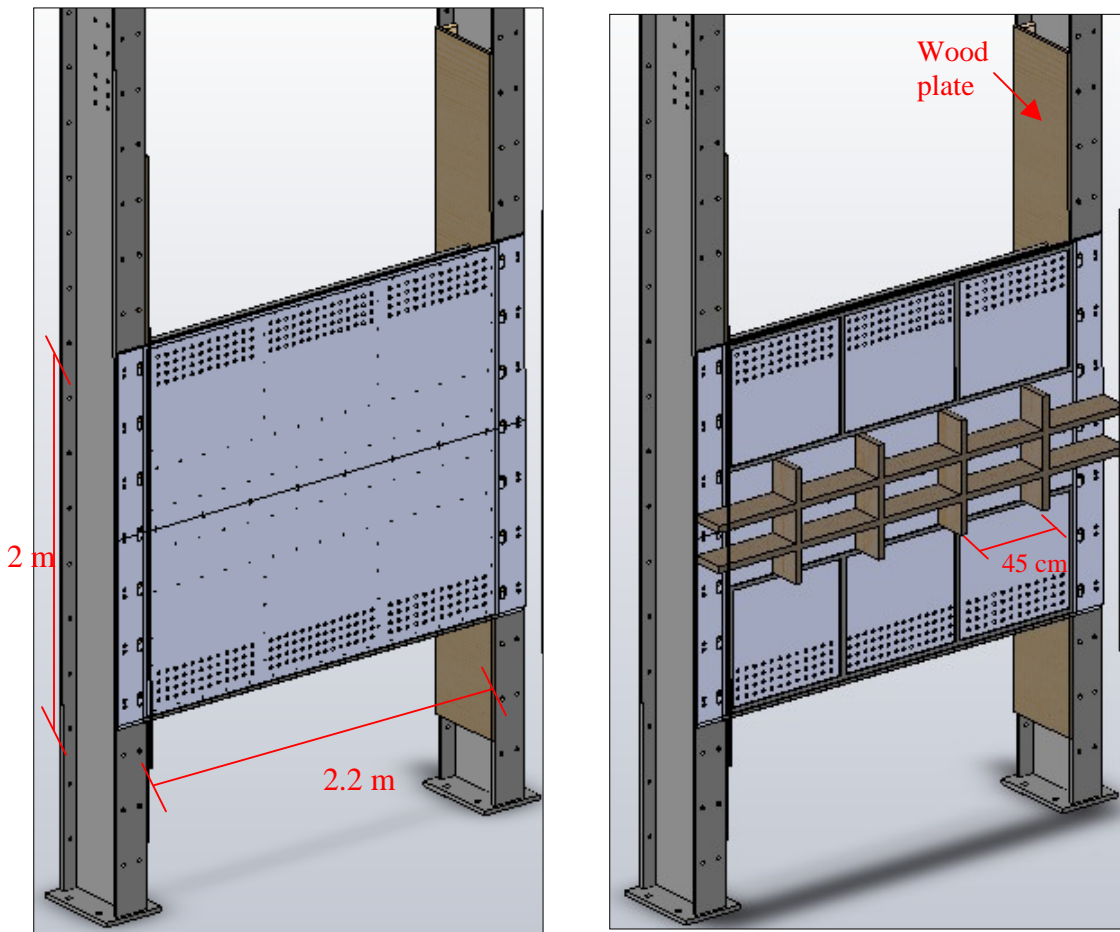
a) 2.6 x 2 m aluminum rainscreen. The small black points indicate the screws used later for fixing the foam seal and wood studs.

b) Placement of foam seal underneath each PLA box. The horizontal studs are equally spaced by 20 cm.
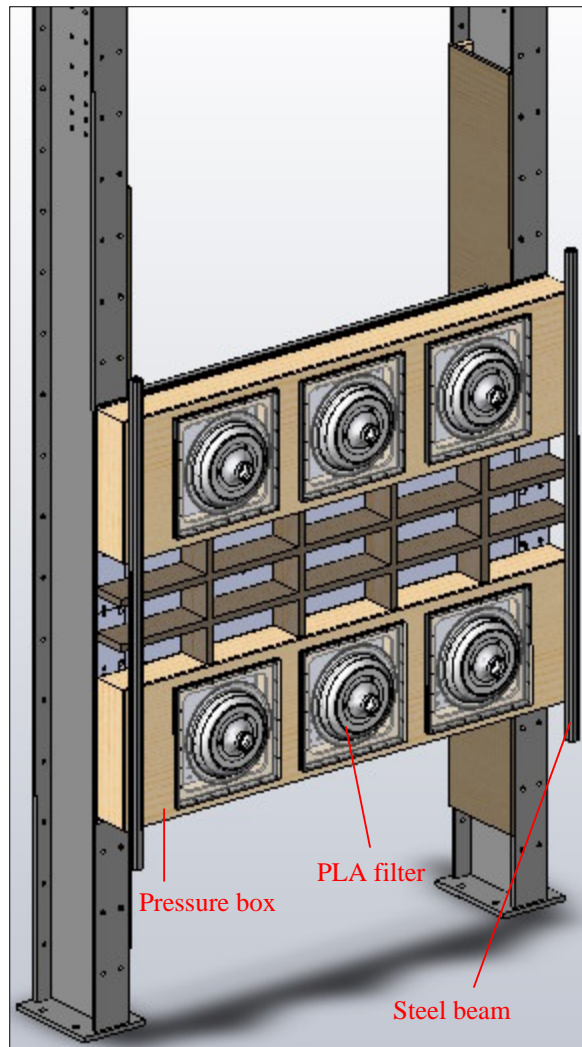
c) Filters connect the PLAs to the pressure boxes in order to apply wind load towards the vent openings.

Figure 3.3 Rainscreen model

They have a dual role of housing the PLA filters which form part of the Pressure Loading Actuator system, detailed in section 3.1.2; and stiffening the rainscreen, as they are glued and screwed to the aluminum, and strengthened at both edges by 3 x 5 cm² cross section steel beams. Also, four 3.5 x 18 cm spruce wood studs are placed vertically at 45 cm equal spacing between the two pressure boxes, screwed from top and bottom for deflection prohibition of the front panel; crossing with two horizontal studs spaced by 20cm. Figure 3.3 shows the model of the rainscreen as designed in Solid Works 2010.

3.1.1b) Air Barrier

The goal of this experiment is to achieve a perfectly sealed model. The easiest way to reduce any leakage at the sides was to fix a wooden plate between the flanges of each column to close the PER wall at the edges, and support the air barrier assembly. The air barrier is a 2.2 x 2 m² spruce wooden wall, stiffened with six 3 by 18 cm studs, at 36cm distance. Figure 3.4 reveals that the top and bottom of the rig are sealed with 50 x18 cm rectangular section wooden boxes that are glued and screwed to the front aluminum panel. The air barrier is contoured by a rubber frame that allows its sliding for the change of the cavity depth. It is also supported by two horizontal 12 x 14 cm steel I-beams connected to the columns at both sides, using threaded holes and small I-beams connectors as in Fig.3.6.
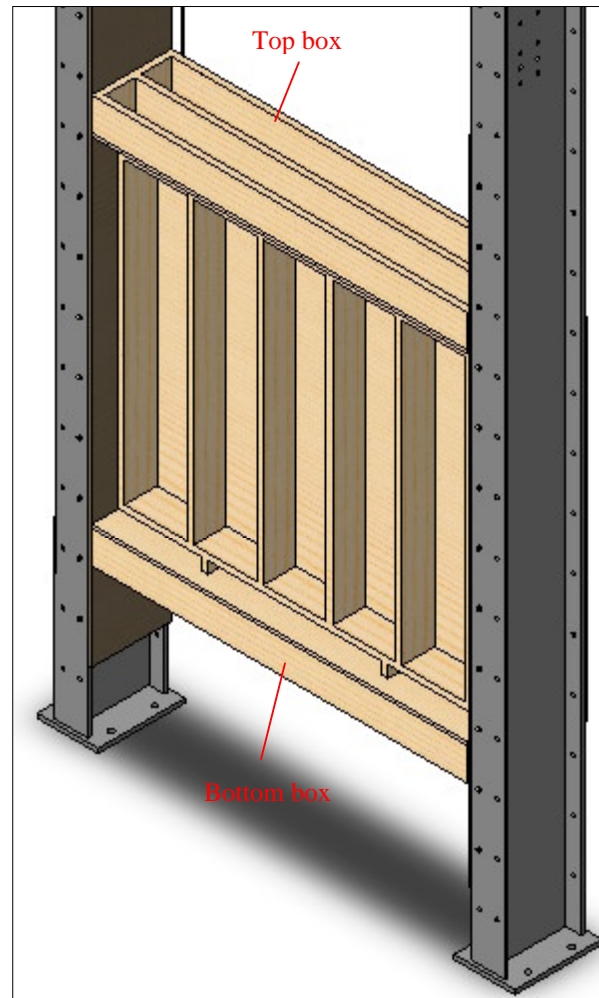
Figure 3.4 Air barrier assembly

The rubber frame just stands and seals itself to the plywood; and some screws are used in order to support the wood, so that it will not snap out of the rubber. The air space between rainscreen and air barrier is set at 25 mm as the minimum cavity depth as per Garden (1963).

3.1.2 Equipment

In order to apply realistic wind loads to the PER wall panel, we used PLAs; these machines are able to follow a pressure trace accurately and in a reliable way, thus, they generate the target exterior pressure signal. The number of PLAs associated with each configuration, is determined based on PLA performance curves of model R6PP3110M, as well as the required pressure amplitude. As a rule of thumb, a PLA unit blows air on a certain structure through an air bag (air box) installed on this structure, as mentioned by Kopp et al. (2010). The purpose of the current experiment is to apply three different pressure signals varying horizontally in addition to the unique pressure signal; for this reason, two wooden boxes 20 cm thickness x 71 cm height are mounted respectively at the bottom and top of the rainscreen, where every pressure box is divided by three adjacent air boxes built separate and covering 3 groups of venting holes. Each air box is connected to a PLA through a circular plastic filter (of 35 cm diameter) that connects to the PLA hose and diffuses the airflow inside the box. Also, four additional PLA tube filters (9 cm diameter) are included in case there is a need for extra PLAs. Note that these filters are closed with 0.0762m plastic caps when not required. The PLA filters are built within rectangular 60 x 60 cm removable Lexan window that covers the airbox, and allows an easy access to the venting holes to change the venting configuration. The Lexan windows are sealed to the pressure boxes with foam seal and screws.

Experimental runs were launched using a graphical user interface (GUI) program that provides target pressures to the PLA system and allows visualizing the data acquired by the electronic devices of the Data Acquisition System (DAQ). The cavity pressure is measured by mounting 12 pressure transducers at the back of the air barrier wall. The pressure taps are distributed over the total area of the plywood wall to ensure a full

coverage of the cavity pressure, Figure 3.5.b. Measurements are recorded with the DAQ formed by a National Instrument NI PXI-1042 computer device and SCXI 1004 Modules chassis; these are connected to a Triple-output 30V, 3A Digital Display DC power supply. The whole system allows reading the voltage measured by eighteen HOSKIN pressure transducers, of a range of (−1)… (+1) PSI, connected to the SCXI Modules; and then voltage values are converted to pressure.

The pressure signal achieved by the PLAs is read using six pressure transducers of the same type, that are placed on the six air boxes at top and bottom of the rainscreen, and each is linked to its corresponding PLA. In some cases, where the air box does not allow enough room for the placement of the pressure tap on one side, the pressure transducer is installed on the other side closely to another pressure transducer associated to an adjacent air bag, as shown in Fig.3.5a.
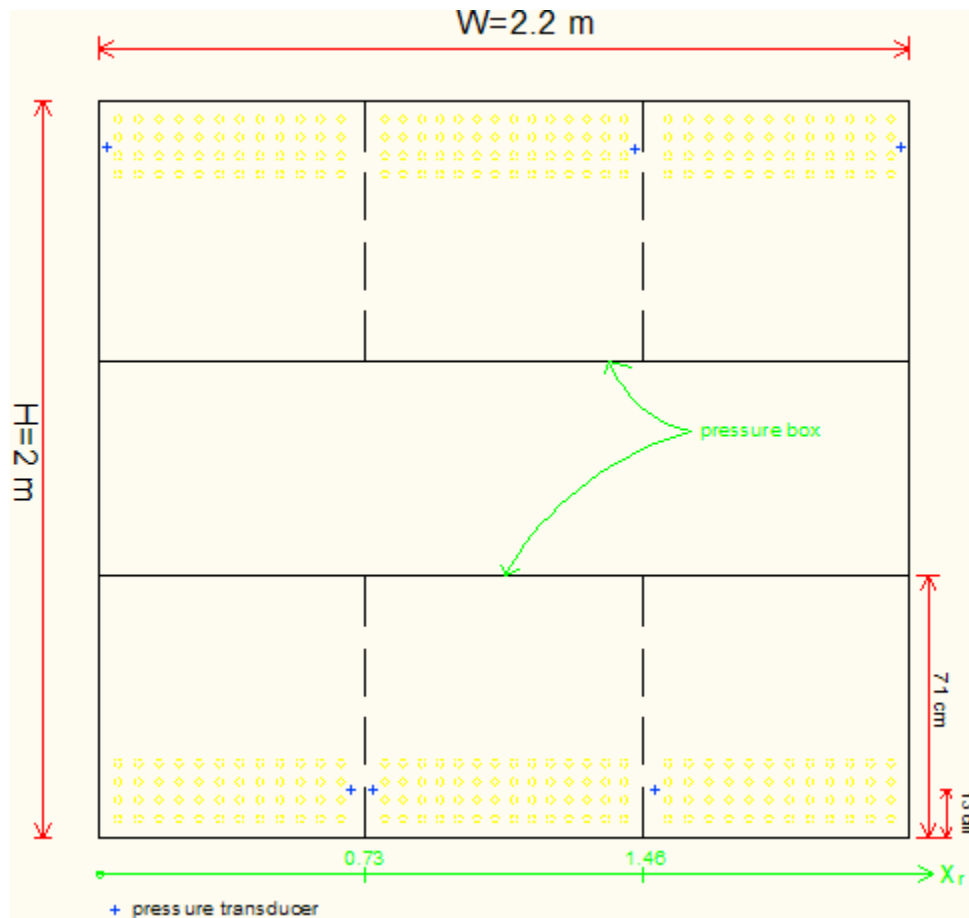
a) Pressure transducers distribution on the pressure boxes

The data are examined using Matlab 7.1 software that shows the instantaneous values of the demand and achieved external pressures, in addition to the cavity pressure time series. Note that, a small time lag (in order of few seconds) exists between the PLA system and the DAQ. Therefore, measurements acquired by the front pressure transducers (related to the PLA systems) and those reading the cavity pressures (related to the DAQ) sometimes give a misleading interpretation on the real time lag between the applied pressure and the cavity, by not having the same time duration signal. For this reason, some pressure transducers were sometimes removed from the back of the panel and installed on the working pressure boxes in order to read the applied external and cavity pressures with the same system.
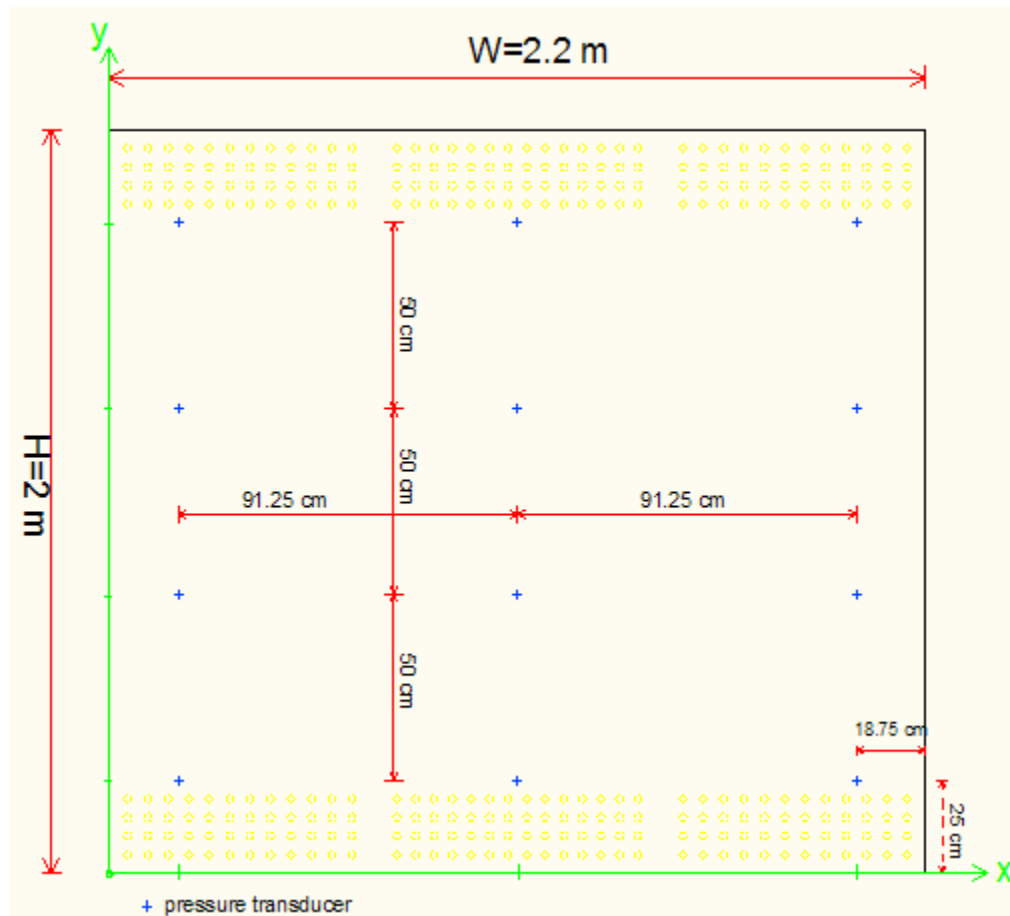
b) Pressure transducers distributions on the air barrier

Figure 3.5 Pressure transducer locations

Below, Figure 3.6 shows the rig as built in the facility after the installing all components.

a) Front view

b) Back view
Figure 3.6 PER wall panel

3.2 Testing Configurations

3.2.1 Exterior Pressure Signals

In order to examine the wind pressure drop across pressure equalized rainscreen walls built around a structure, it has been deemed substantial to use real wind pressure traces. The exterior pressure signals applied to the rainscreen panel in this test are associated with random pressures fluctuations measured on a pressure model building in the wind tunnel at the University of Western Ontario and discussed by Inculet (2001). The basic pressure model represents a rectangular building of 60m full-scale height, 40 m width and 20 m depth; of a 1:200 length scale; exposed to a zero degree wind angle and located in an open country exposure. The data are sampled at 500 Hz during two minutes, the velocity scale is 0.28, and the full-scale velocity at 10m is V_{10m} =20m/s. All pressure coefficients C_p are collected as referenced to z_{ref} =1.52 m and then re-referenced to the building roof height for conversion to full-scale data.
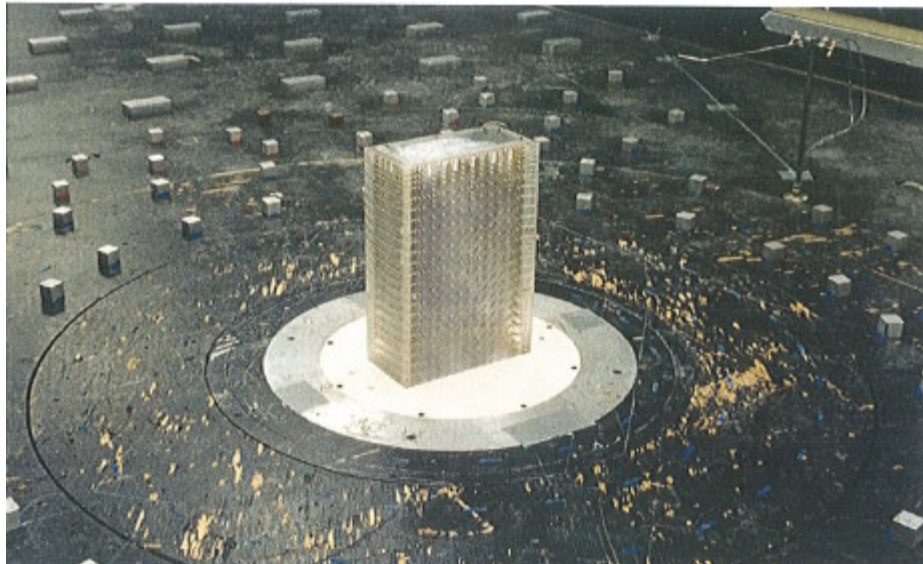
Figure 3.7 Pressure model of a high building in the wind tunnel (Inculet 2001)

Each of the two building faces (wide and narrow) was tested separately in the wind tunnel, exposed a normal wind flow and pressures coefficients were acquired at all taps.

For the present full-scale experiment, the external pressure signals applied to the PER panel correspond to pressures acquired at specific taps for both the wide and narrow faces (each being windward face). For each face, four pressure traces of five minutes equivalent full-scale duration are extracted from the data: 1) one random signal P associated to a middle tap; that will be applied simultaneously to all pressure boxes of the panel; and 2) three pressure signals P_1, P_2, P_3 corresponding to three edge taps located at the left of the face. These will be applied simultaneously at the three adjacent pressure boxes at the bottom of the panel in order to examine the differential pressure across the rainscreen under an external pressure gradient.

The four pressure taps used are located at the same position of $y_m/H_m = 0.76$ (where y_m designates the vertical coordinate from the bottom of the building model). This height is chosen as being proximate to the location of the maximum pressure distribution in the middle of the face; also the corresponding edge taps pressure values are not extremely small.

In fact, the middle pressure tap is located at 1.45 cm vertical distance (model scale) above the maximum mean pressure coefficient tap in the wind tunnel model, where $\overline{C_p}$ max is equal to 0.368 at $y_m/H_m = 0.75$ equivalent to 0.75 value in full-scale. Figure 3.8 shows the mean pressure coefficient distribution data for the wide face at $y_m/H_m = 0.76$, representing the taps used in the experiment. Also, it indicates the equivalent full-scale horizontal distance in meters originating from the left side of the PER model, i.e. the tap corresponding to the external pressure (P_1) is associated with the first air box (0.73m length) mounted on the rainscreen from the left; the second tap (P_2) refers to the second airbox (0.73m $< x_r <$ 1.46m), and the third tap (P3) is assumed to be located within the third pressure box.

At the testing stage, the signals were converted to full-scale and given to the PLAs as pressure values instead of pressure coefficients. However, the pressure transducers were

not able to read accurately the signals because the pressure values were within the range of $\pm 0.6\,kPa$, which corresponds to the margin of sensitivity of the transducers. Also, the pressures were too small for the PLAs to reproduce the signals.

For this reason, the data were converted again and pressure values were raised by doubling the wind speed at the height of the building, which gives a full-scale velocity of 53.6m/s, velocity scale of 0.14 and a frequency scale of 28. Thus, for a five minutes trace signal, the full-scale frequency becomes 18 Hz. Finally the signals are filtered at 7 Hz as being the frequency limit of the PLA.
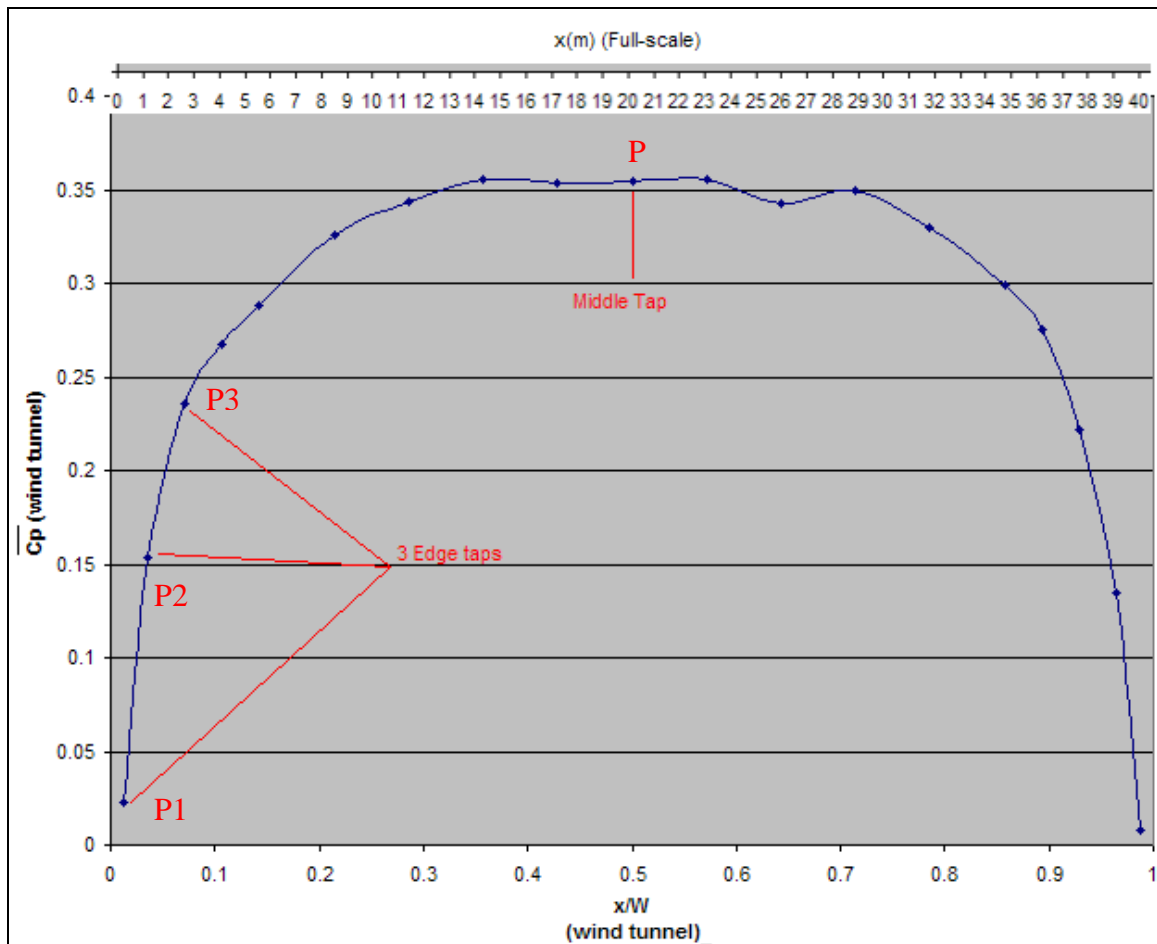
Figure 3.8 Mean pressure distribution for the windward wide face at $y_m/H_m = 0.76$ under zero degree wind angle

The PLAs generate the signals with a sampling frequency of 100 Hz; thus the data acquired with the DAQ system are also acquired at 100 Hz. The matching between demand pressure and achieved pressure (performed by the PLA) usually showed a high correlation factor of around 0.93 for all the demand traces as in Fig. 3.9.
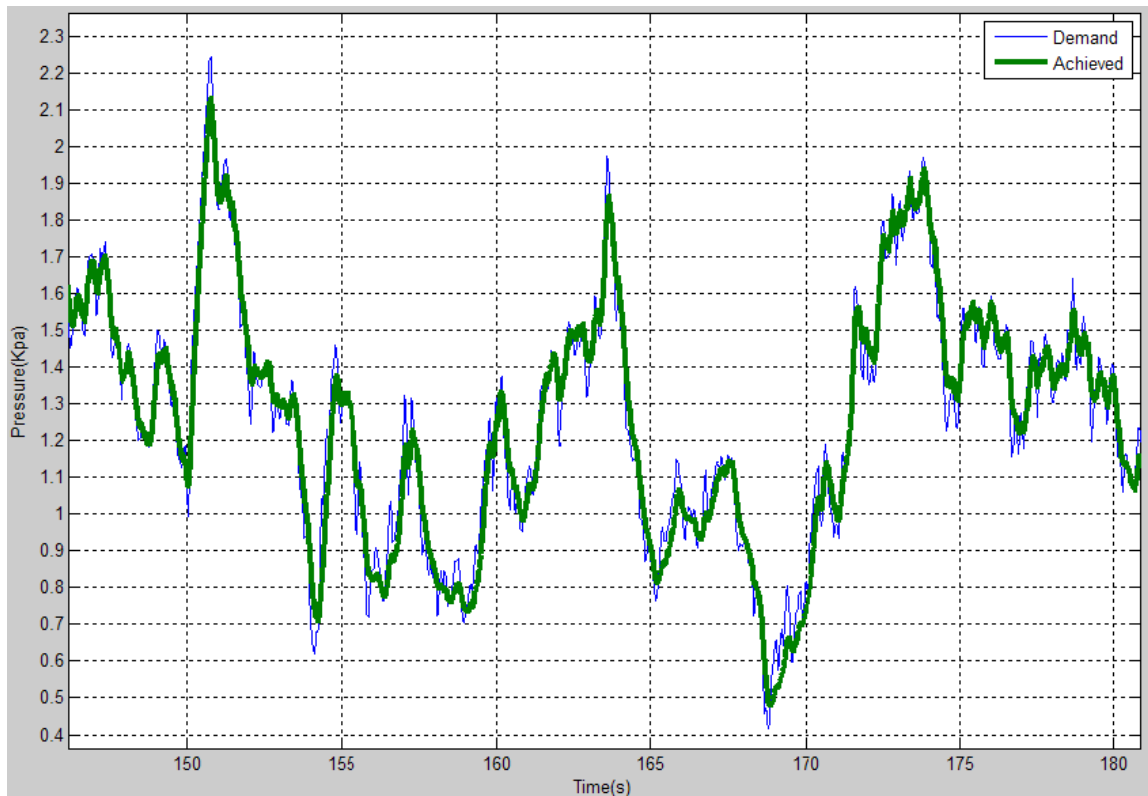
Figure 3.9 PLA pressure trace for the middle tap of the wide face

The test configurations are performed using traces associated to both wide (40 x 60 m² – full-scale) and narrow face 20 x 60 m² – full-scale size) of the building model. The fluctuations of the middle tap vary in the range of + 0.3…+2.8kPa for the wide face, and +0.37…+2.69 kPa for the narrow face; while the edge taps traces reveal suction and are in general in the range of   -0.08 …+2.24kPa for the wide, and –0.27…+2.38kPa for the narrow face.

3.2.2 Panel Setup Configurations

The differential pressure across the rainscreen due to the applied pressure traces is examined by varying two parameters: 1) the rainscreen venting area ratio A_V and 2) the location of vent holes. This is done by redistributing the deliberate openings at a certain venting area between top and bottom of the rainscreen.

The cavity depth was set constant at 25mm as the minimum required space in a pressure equalized rainscreen system. 0.0207m pliable vinyl plugs diameter were used to provide changes in the aluminum rainscreen venting area: each time the movable Lexan windows were pulled out in order to plug or unplug the 20mm holes under the pressure boxes, and then moved back to their location by fastening with set screws. For venting cases, the aim was to perform tests within a wide range of venting to wall area ratios starting from the lowest (equivalent to one hole in the rainnscreen) to the maximum limit obtained with 304 vent holes. However, pressure equalization between the exterior and the cavity at d_c =25mm was reached for 15 vent holes where $A_V = 0.11\%$; and it stabilized for 36 vent holes ($A_V = 0.27\%$), thus it was decided to stop the tests configurations at this stage. Table 3.1 shows the different test configurations based on the ratio of rainscreen venting area (A_{rs}) to the total wall area (A_w). Each run was performed twice; by applying the pressure signals associated to both wide and narrow faces.

Also, Appendix A (section A.1) shows the drawings of the different test cases and the distribution of plugged and unplugged vent holes at top and bottom of the rainscreen.

Configuration	Number of holes	Venting percentage $A_V = A_{rs}/A_w (\%)$	Holes Layout	Face	Tap Signal	Cavity depth dc (mm)
a	1	0.007	bottom	w	middle	25
				n	middle	25
b	3	0.022	bottom	w	middle	25
					edge	25
				n	middle	25
					edge	25
c	4	0.03	bottom	w	middle	25
					edge	25
				n	middle	25
					edge	25
d	15	0.11	bottom	w	middle	25
					edge	25
				n	middle	25
					edge	25
e	36	0.27	bottom	w	middle	25
					edge	25
				n	middle	25
					edge	25
f	4	0.03	top and bottom	w	middle	25
				n	middle	25
g	15	0.11	top and bottom	w	middle	25
					edge	25
				n	middle	25
					edge	25

Bottom: the holes are located at bottom of the rainscreen

Top and bottom: the holes are distributed between top and bottom of the rainscreen

w: wide face   n: narrow face   middle: middle tap   edge: 3 edge taps

Table 3.1 Test configurations

CHAPTER 4

FULL-SCALE EXPERIMENTAL RESULTS

4.1 Introduction

Experimental results of the test configurations, described in Table 3.1, are discussed in this chapter, and the cavity pressure measurements for both the applied single and three pressure signals are examined. For each case, the data are represented in the frequency domain, which helps to assess the pressure equalization process. Also, a comparison is established between the results based on the applied external pressures originally referring to the wide and narrow faces of the wind tunnel model.

4.2 Basic Statistics of Measured Cavity Pressures for a Single Applied Pressure

4.2.1 Pressure Gradient inside the Cavity

A sample of the measured exterior pressure and cavity pressure time series running for five minutes duration is presented in Figs. 4.1 and 4.2; corresponding to a single applied pressure signal of 53.6 m/s full-scale velocity. The data refer to two different venting configurations, revealing the pressure equalization process in each case as a function of the differential pressure across the rainscreen ($P_e - P_c$). Figure 4.1 referring to $A_V = 0.022\%$ shows that the pressure inside the cavity is following the external signal without reaching the peaks. The largest loads sustained by the rainscreen are in the range of 150 to 200 Pa on average, lasting sometimes up to 20 seconds. Also, shorter duration peaks of 250 Pa in suction and 300 Pa in pressure are identified for periods of five seconds. Thus, for both wide and narrow faces, the load is not completely transmitted to the cavity. The full-pressure equalization between cavity and external pressures occurs when the PER has $A_V = 0.11\%$ as shown in Fig. 4.2. In this case, the differential load across the rainscreen is around zero, the peaks of the cavity pressure response coincide with those of the applied signal.
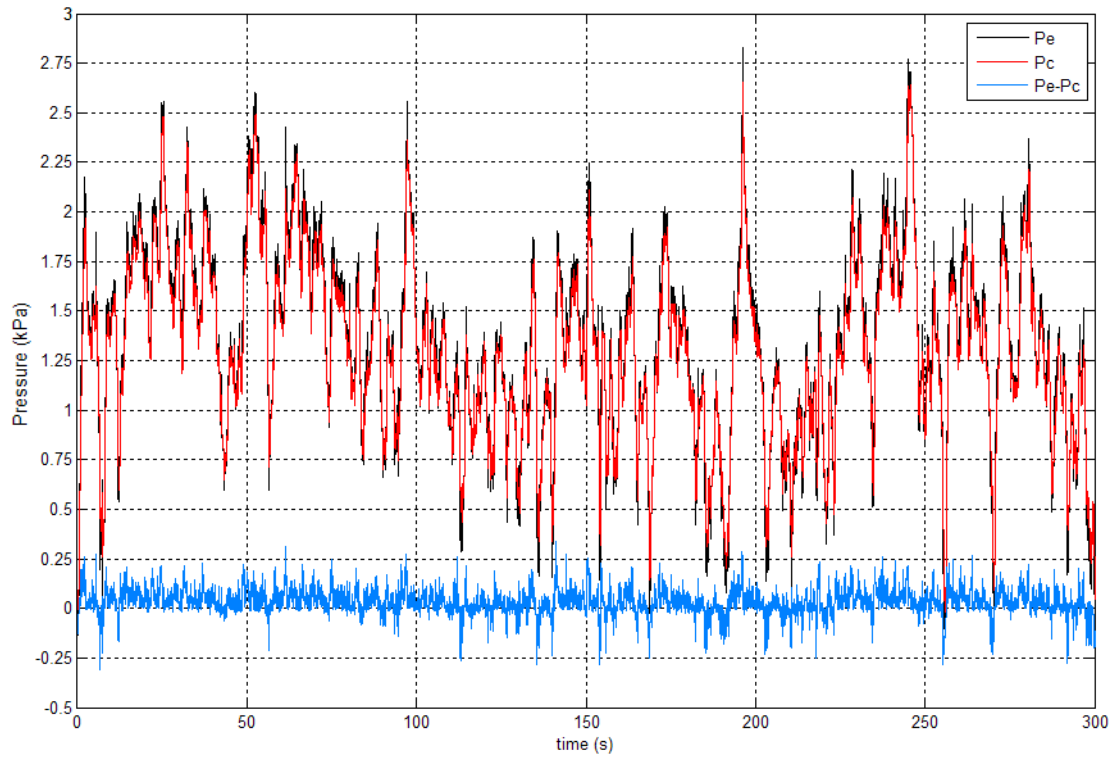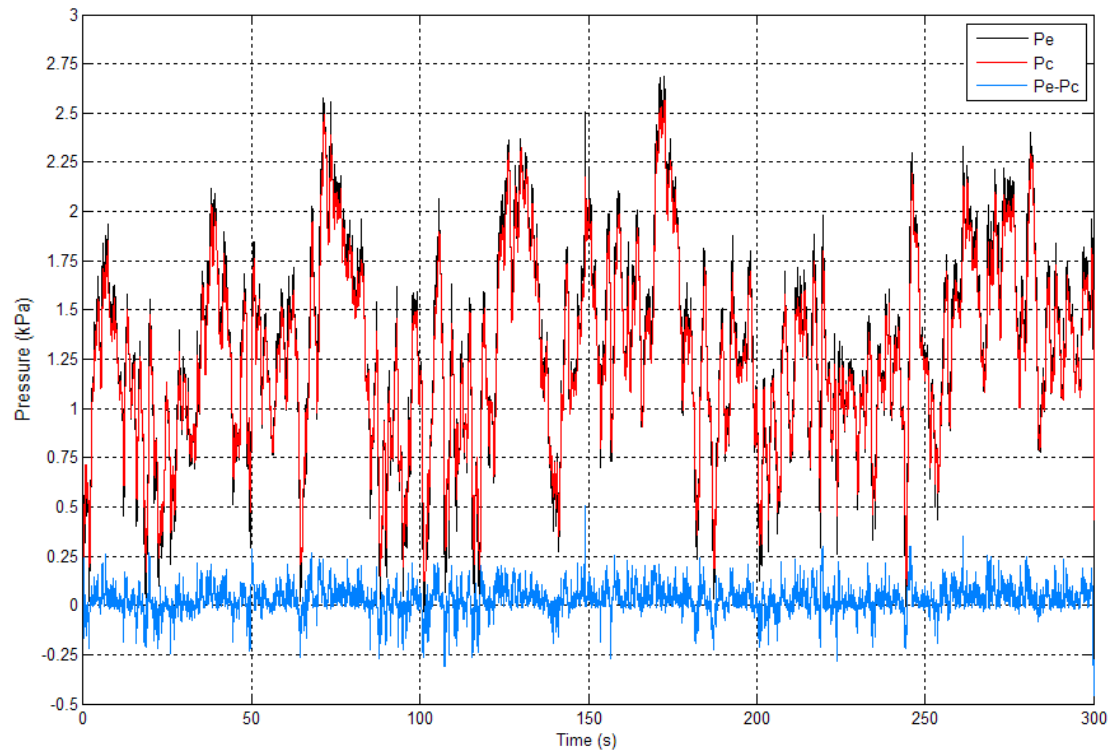
Figure 4.1 Time series pressures for configuration b for a) wide face and b) narrow face
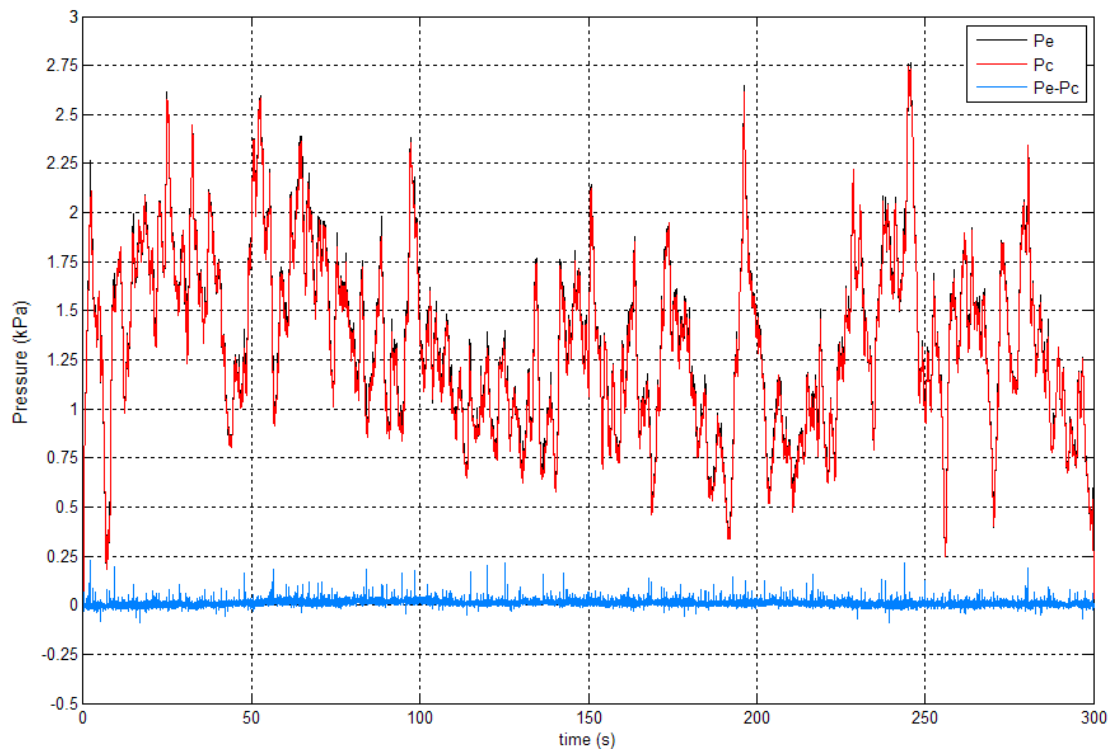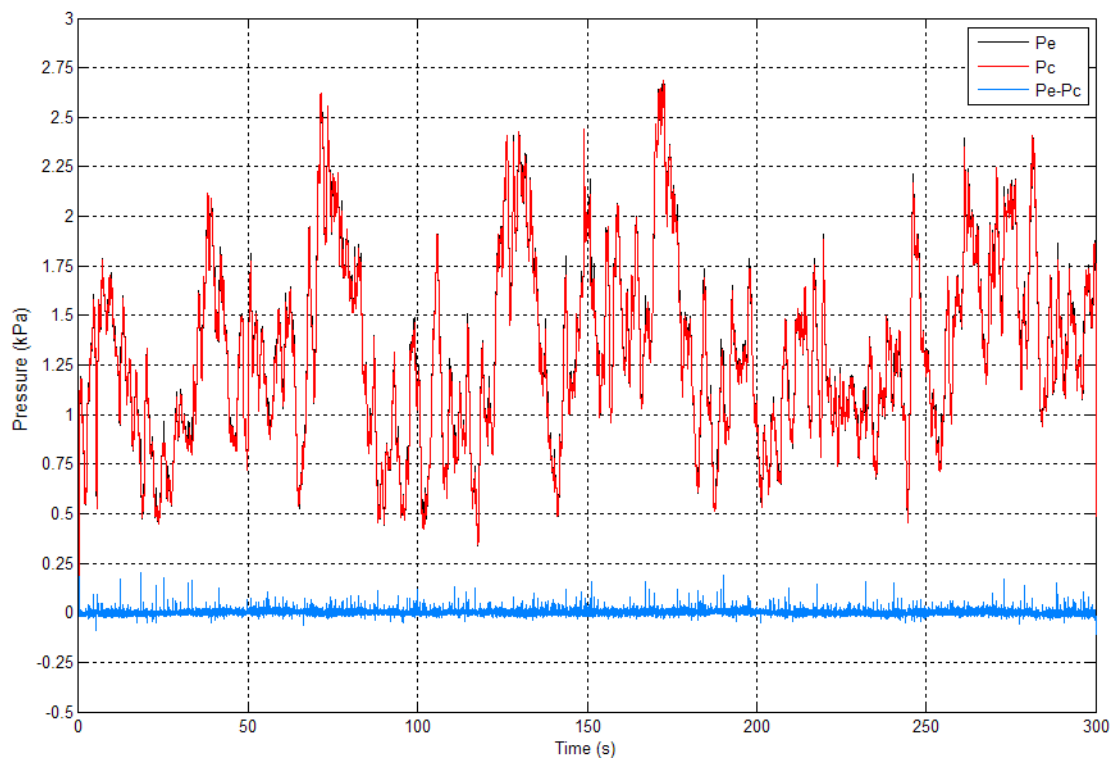
Figure 4.2 Time series pressures for configuration d for a) wide face and b) narrow face

$\overline{P/Pt}$	x/W				$\overline{P/Pt}$	x/W		
y /H	0.085	0.5	0.91		y /H	0.085	0.5	0.91
0.125	1.006	1.005	1.004		0.125	1.005	1.006	0.999
0.375	-	1.000	1.002		0.375	-	1.000	1.001
0.625	-	1.008	-		0.625	-	1.006	-
0.875	1.005	1.002	1.002		0.875	1.004	1.001	1.002

a) Wide face   b) Narrow face

Table 4.1 Mean normalized pressure values inside the cavity for the single signal pressure for configuration b, $A_V = 0.022\%$

Very small residual net pressures are observed through the signal $P_e - P_c$, that reach 10Pa at maximum when comparing to the value recorded by Ganguli and Dalglieh (1988) of 15Pa at full-pressure equalization. Actually, these are attributed to experimental errors. Also, the instantaneous spikes available correspond to those produced by the PLAs when generating the signal.

In terms of the cavity pressure variation inside the PER panel, a first glance at the pressure transducers measurements placed at the back of air barrier reveals that there is neither a horizontal nor vertical pressure gradient inside the cavity in all of the test configurations, at 25mm cavity depth setup for both the wide and narrow face. As an example, Table 4.1 shows the mean instantaneous normalized pressures represented by the ratio $\overline{P/Pt}$ for every pressure transducer location; where P presents the instantaneous pressure, and Pt is the instantaneous pressure measured at the bottom pressure transducer located at $x/W = 0.5$ and $y/H = 0.375$. The reader can refer to Fig 3.5 for coordinates system for the air barrier pressure transducers.

The data clearly demonstrate that the pressure at each location is almost constant with respect to the reference pressure transducer reading. Furthermore, there is no significant difference when comparing the results corresponding to both the wide and narrow face external pressures. In fact, the latter random signals show the same statistical values after conversion to full-scale.

Wide face external signal: $(\overline{P}_e = 1.32; \hat{P}_e = 2.8; \tilde{P}_e = 0.43 Kpa)$

Narrow face external signal: $(\overline{P}_e = 1.30; \hat{P}_e = 2.7; \tilde{P}_e = 0.45 Kpa)$.

This is due to the fact that both signals are recorded each at a middle pressure tap located at $x_m / W_m = 0.5$ and $y_m / H_m = 0.76$, when applying separately a normal wind pressure on the wide and narrow faces of the building pressure model discussed in Inculet (2001). Also, the analysis of wind tunnel measurements indicates similar pressure coefficient distributions at this position for both faces, which explains the analogy between the full-scale pressure signals.

4.2.2 Measurements of Cavity to Exterior Pressure Ratio P_c / P_e

To get a closer view of the pressure statistics Figure 4.3 represents the mean ($\overline{P}_c / \overline{P}_e$); peak ($\hat{P}_c / \hat{P}_e$) and rms ($\tilde{P}_c / \tilde{P}_e$) cavity to exterior pressures ratios for both the wide and narrow face cases, as a function of the rainscreen area venting ratios. The curves describe the cavity pressure behavior for the five basic cases (configurations a, b, c, d and e in chapter 3) when the venting holes are located at the bottom of the rainscreen; while the extra points refer to configurations (f and g) where the holes are distributed between top and bottom. The cavity pressure ratios show a similar behaviour with only slight differences, when comparing the wide and narrow face cases, since the two corresponding external signals are applied to the same PER wall panel area. The three curves present the same rising trend with the rainscreen venting area ratio A_V; but the mean pressure ratio seems slightly higher: this is probably due to the fact that steady pressure is effectively transferred to the cavity, while unsteady fluctuations are resisted by the aerodynamic damping of the vent openings; especially at low venting rates ($A_V < 0.11\%$).

The experimental measurements show that, generally, the equalization between cavity and external pressures improves as the rainscreen venting area gets bigger at a constant cavity depth (d_c =25mm); as proved by previous full-scale and wind tunnel experiments (i.e. Inculet and Davenport (1994) and Kumar et al. (2003)).
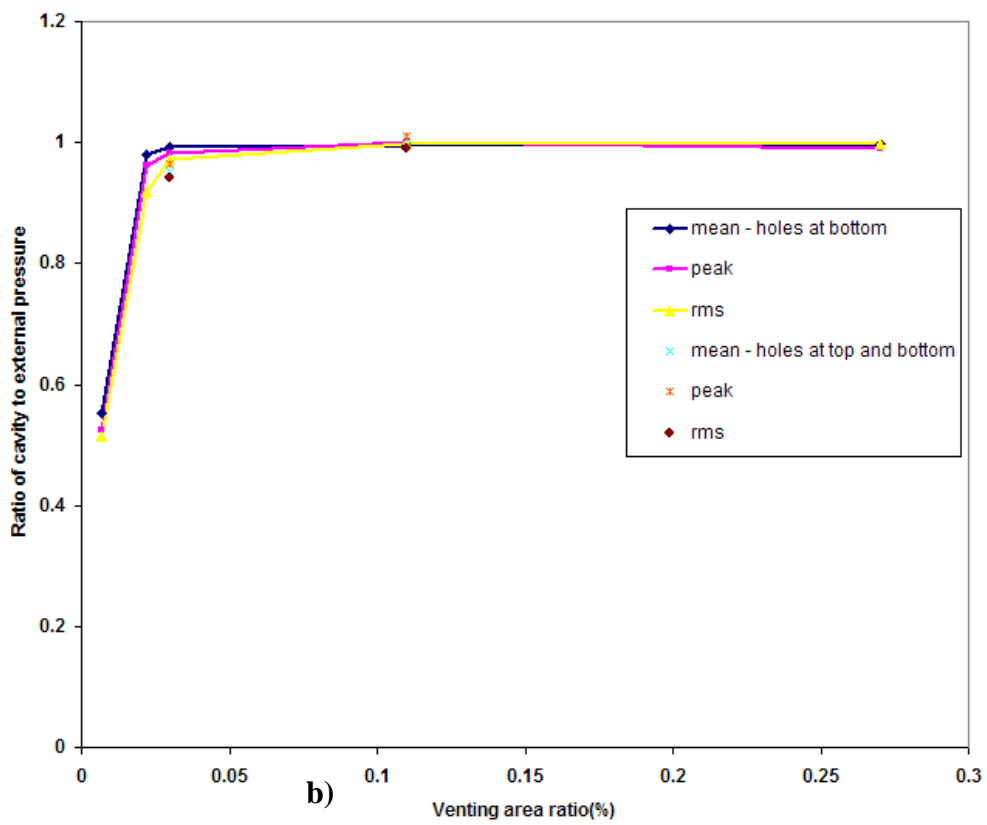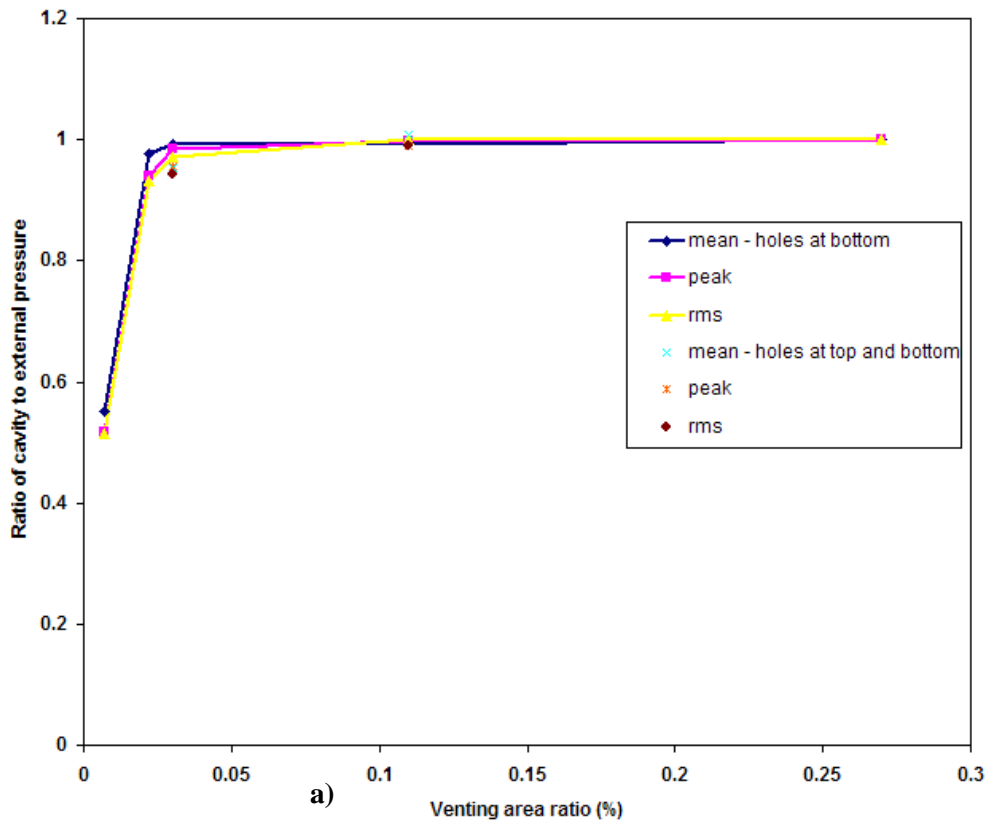
Figure 4.3 Basic statistics for a single applied pressure signal for a) wide face, and b) narrow face

More precisely, the shape of the curves reminds of Fig 2.2 showing the rainscreen load reduction as a function of venting and leakage area and observed in Kumar et al. (2003). By using a wider range of venting area ratio ($0.15\% < A_V < 0.75\%$), Kumar confirmed that the wind load absorbed by the rainscreen gets smaller with a larger venting area, thus the pressure inside the cavity increases; which is perfectly seen in the current experiment.

Since the present PER wall panel is assumed built perfectly sealed, the air barrier should be impermeable without exhibiting paths for flow losses. Therefore, in the case of venting (i.e. a single opening) the cavity pressure will develop and increase trying to reach the external pressure fluctuations in the vicinity of the opening, based on the concept of Holmes (1979) for the internal pressure behaviour in the case of a single windward opening wall of a low-rise building without leakage. Thus, in this case, we can say that the panel requires only a small venting area to have good pressure equalization, a thought that was already proven by Kumar (1999). However, the massive mean pressure drop across the rainscreen revealed in Fig 4.3(a and b) at the lowest venting area; where only 55% of the mean external pressure is transmitted to the cavity is an indication of a presence of a certain mean flow that is increasing the damping associated with the flow through the venting opening and, hence, negatively influence the cavity dynamic response. This mean pressure drop is reduced significantly at higher rainscreen venting area ratios: $\overline{P_c}/\overline{P_e} = 0.97$ at $A_V = 0.022\%$ and $\overline{P_c}/\overline{P_e} = 0.99$ at $A_V = 0.03\%$. Also, the rig assembly was untouched during all configurations; only Lexan windows were removed each time from the front pressure boxes, to change the vent holes area. In addition, the test associated with $A_V = 0.007\%$ was not performed at the beginning of the experiment; it is ranked middle with respect to other configurations. Therefore, it is unlikely for leakage, if it does exist, to be the main cause for the observed mean pressure drop, although it may be a contributor. Certainly, there is a kind of process that is happening in the way the external pressure is transmitted through a single opening in the rainscreen, and that may be causing pressure losses in the air box. A possible explanation might be that

the air flow volume first blown into a single 71cm height by 73cm wide air box is not fully transmitted to the cavity. The PER model performance gets better as the rainscreen venting area ratio increases until reaching the full pressure equalization $(\overline{P_c}/\overline{P_e} = \hat{P_c}/\hat{P_e} = \tilde{P_c}/\tilde{P_e} = 1)$ at $A_V = 0.11\%$; which explains the flatness of the curves from 0.11% to 0.27% rainscreen venting ratio, for both the wide and narrow face cases.

The effect of vent openings location on the pressure equalization process of the panel is also examined for some configurations. At $A_V = 0.03\%$, the data show a drop in the mean, peak and rms ratios referring to a reduction in the cavity pressure in the order of 3%; when the four vent holes are symmetrically redistributed as two holes under the bottom and top middle airboxes (configuration (f) in chapter 3). This change can be either attributed to the physical behaviour of the air inside the cavity, mainly triggered by the vent hole location, or to the PLA performance.

In contrary to the experimental results, an increase in the cavity pressure was expected when the holes were at the top and bottom, since the external pressure will travel just half the distance within the box. However, it seems that the pressure equalization is better when the vent openings are distributed along the width of the PER panel. On the other hand, since the 2 PLAs placed at the top and bottom are generating the same signal with high correlation, the cavity pressure response variation cannot be due to a technical process or cross flow between the PLAs. Also, the two venting configurations did not show any pressure gradient inside the cavity. So at low rainscreen venting area ratios, the cavity response behaviour is only affected by the layout of the vent openings, and it is higher when they are placed at the bottom of the rainscreen, as if they are forming a discontinuous slot.

At $A_V = 0.11\%$, the change in the location of the 15 holes does not seem to have as much effect. Although the number of PLAs gets doubled (six instead of three), the mean cavity response pressure seems slightly higher with respect to the external

pressure in comparison with the bottom venting holes location for both wide and narrow face cases. This is probably due to the fact that full-pressure equalization is reached in the basic configuration, so varying in the vent openings location would not affect the cavity response pressure.

When comparing wide and narrow face results, slight differences are observed mainly due to the performance of the PLAs. The reasonable increase in the peak cavity to external pressure ratio, highlighted in the narrow face at $A_V = 0.11\%$ (15 holes top and bottom), is not shown in the wide face case. The reason behind such behaviour is that the achieved external peak pressure value is slightly higher than the real peak value, so the peak ratio value $\hat{P}_c / \hat{P}_e$ referring to a higher peak cavity pressure collapses with that of the vent areas basic location (15 holes at bottom). Similarly, in the narrow face case, $\hat{P}_c / \hat{P}_e$ appears above $\overline{P}_c / \overline{P}_e$ at four holes top and bottom configuration because the achieved $\hat{P}_e$ is 0.9% less than the peak demand pressure.

The change in the vent holes locations within one compartment and for a constant venting area ratio has not been examined before. Previous experiments used different layout configurations: venting slot at the bottom of the rainscreen in Ganguli and Dalgliesh (1988), and holes spread all along the rainscreen in Kumar et al. (2003). Inculet (1990) placed two holes at top and two holes at bottom, but the poor pressure equalization performance observed in the model was attributed to the low venting rainscreen to air barrier leakage area ratio, not to the distribution of the vent holes.

Figure 4.4 shows the peak factor g of the cavity pressure measurements given by $\hat{P}_c = \overline{P}_c + g\tilde{P}_c$. The computed values are observed in the range of 2.7 to 3.2, and as the rainscreen venting area gets larger, the peak factor increases.
The narrow face case does not show a straight increase from 0.007% to 0.03% area venting ratio as the wide face signal curve does: this is due to the lower peak factor at $A_V = 0.03\%$ (g=2.8 in the narrow face) in comparison with (g=2.9 in the wide face).

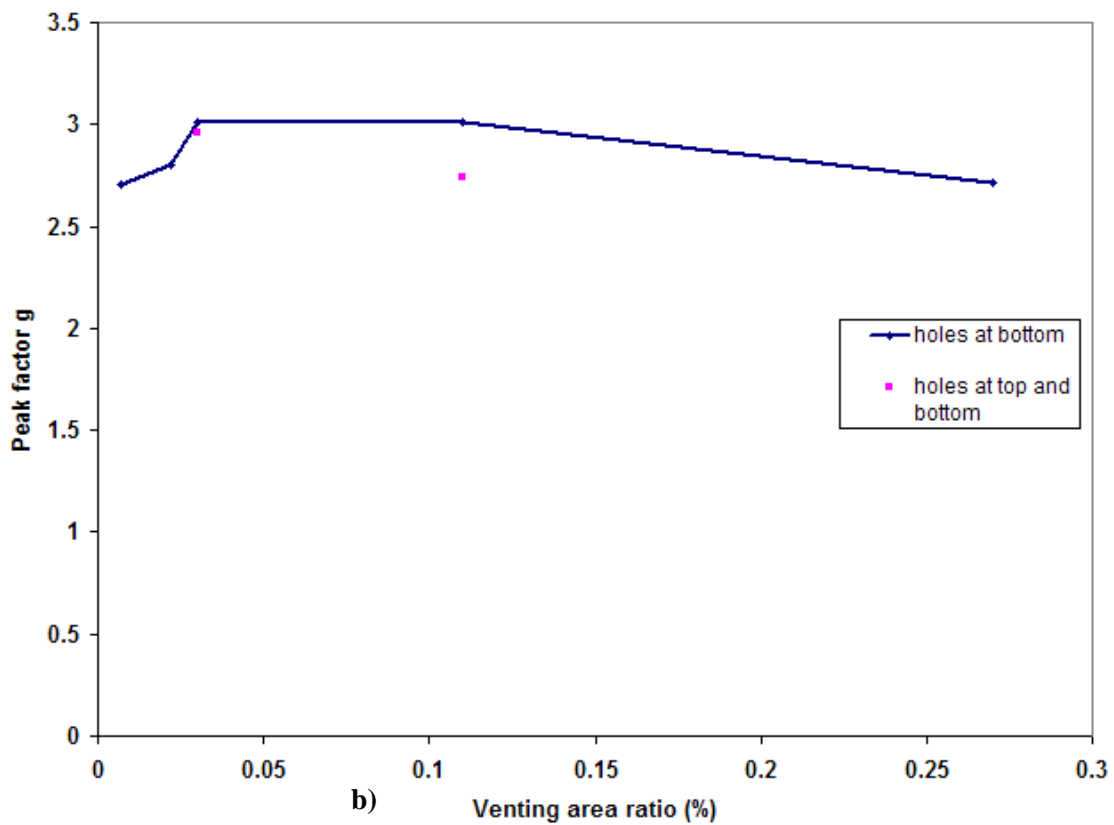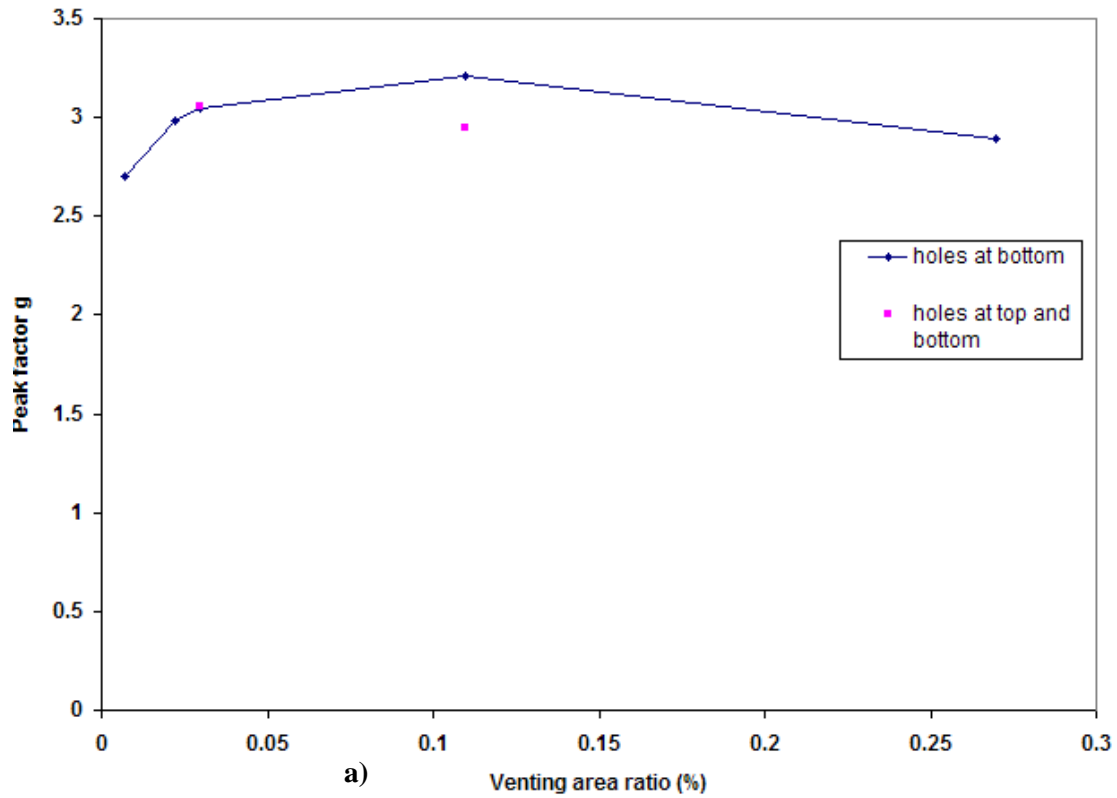**Figure 4.4** Peak factor for a single applied pressure signal for a) wide face, and b) narrow face

At $A_v = 0.27\%$, the difference $\hat{P}_c - \overline{P}_c$ between the peak and mean cavity pressure is similar to that of $A_v = 0.11\%$, but the rms value is larger, which explains a smaller peak factor value, that leads to a decreasing behaviour after $A_v = 0.11\%$.

The extra points referring to the vent holes redistribution are also marked on the graph. Since the mean cavity pressure increases at a venting area ratio of 0.11% as shown in Fig. 4.3, the peak factor value decreases in comparison with the initial venting location at the bottom. According to the lower venting area, the redistribution does not have any significant effect on the peak factor, since the drop in the mean and peak cavity pressures are compensated by the increase of the rms cavity pressures.

4.2.3 Analysis of the Experimental Results in the Frequency Domain

The effect of rainscreen venting to panel area ratio $A_v\%$ on the pressure equalization process can be practically verified by the spectral analysis through the transfer functions and phase angles between the external and cavity pressures signals. Figure 4.5 depicts the external and cavity pressures of the basic venting configurations, with respect to the rainscreen area-venting ratio, in the frequency domain for both the wide and narrow faces. The ordinates represent the normalized product of frequency and spectral density function with respect to the corresponding variances (σ^2), while the horizontal axis shows the frequencies. The spike existing at $f = 2.14 Hz$ is equivalent to $60 Hz$ electrical noise frequency in the wind tunnel data. Also, meaningless harmonics are shown for frequencies higher than 7 Hz in all spectral plots, since the PLA cannot generate frequencies above 7 Hz, so this makes the data beyond this value unreadable. The measurements show in general that as the rainscreen venting area gets larger, the pressure cavity spectra becomes closer to the external pressure, which is clearly seen in terms of the transfer functions shown in Figs 4.6a and 4.7a. As the venting area increases, higher frequency fluctuations are increasingly equalized with the applied fluctuations. The same behaviour can be seen in the phase angle in Figs 4.6b and 4.7b.
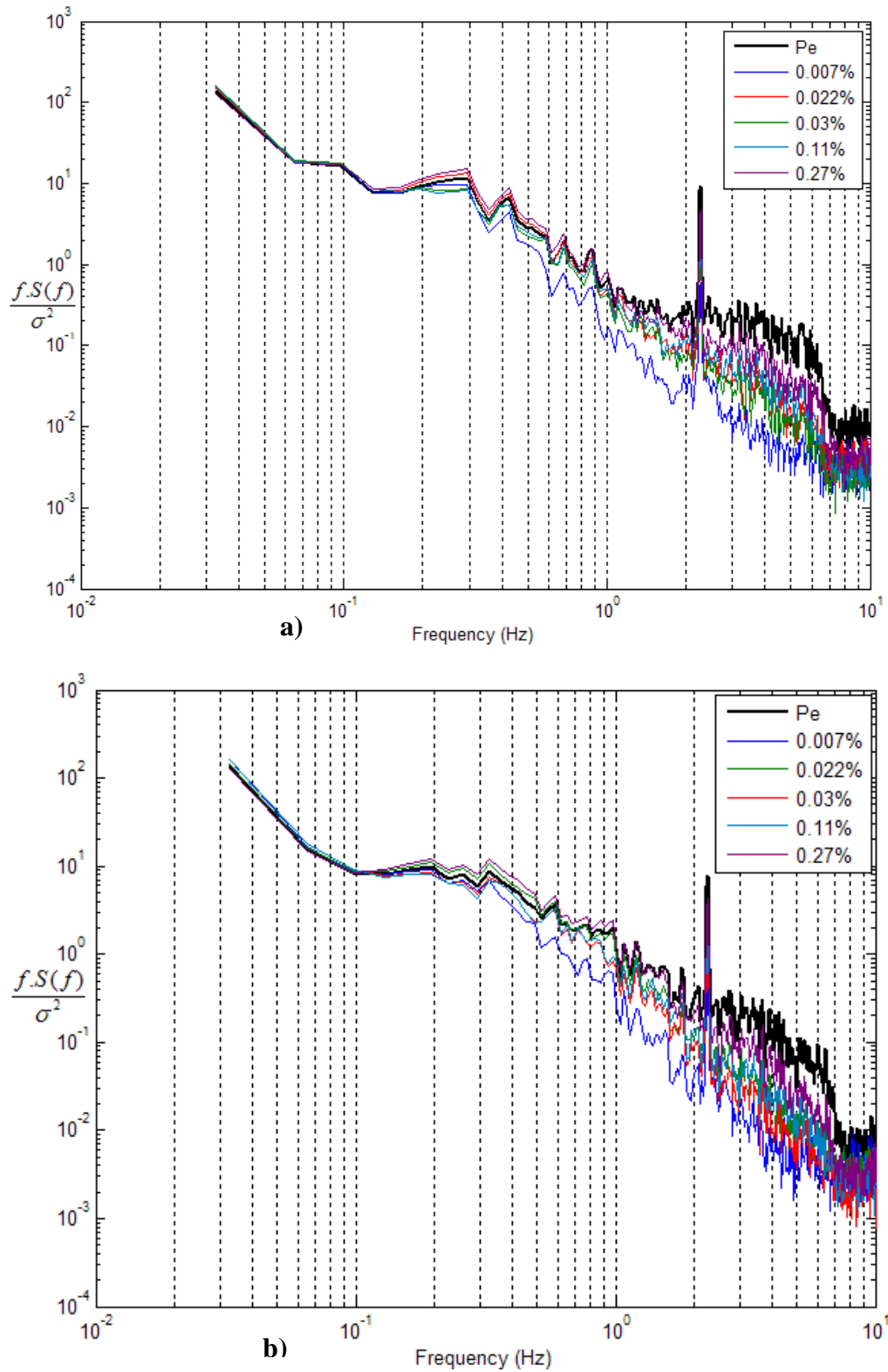
Figure 4.5 Spectral density functions for cavity pressures varying with area venting ratio % for a) wide face, and b) narrow face

Furthermore, it is remarkable that for each venting rate, there is a certain frequency above which the attenuation of the external pressure fluctuations occurs, and this frequency gets higher as the venting area ratio increases.

Inculet and Davenport (1994) referred to such frequency as the critical damping frequency ϖ_d which allows lower frequencies to pass fairly effectively into the cavity. Also, they confirmed that an increase in venting area for constant volume results in, a higher critical damping frequency, which is perfectly observed in the present transfer functions. To illustrate, Figure 4.6a shows that the transfer function starts rolling off at 0.6 Hz at $A_V = 0.022\%$, while the damping frequency seems around $6 Hz$ for the highest venting ratio. In this case, only frequencies higher than 6Hz are taken by the rainscreen. In addition, this value is close enough from the frequency limit of the PLA ($7 Hz$), which means that the majority of external fluctuations are transmitted to the cavity and full pressure equalization occurs.

Moreover, we may say that the influence of the venting area increase is found to be more pronounced in the low frequency regions, at low venting areas when $A_V < 0.11\%$: As the rainscreen venting area ratio gets higher, the critical damping frequency increases meaning that a wide range of lower external frequencies fluctuations get transferred to the cavity, but the attenuation of high frequencies still available. This behaviour agrees with Kumar's observation, who claimed in 1998 that the pressure equalization process seems to be indifferent in the high frequency region, irrespective of the different wall characteristics.

The transfer function associated to the lowest venting area ratio of $A_V = 0.007\%$ reflects again the pressure drop already revealed in the statistical results. Clearly, the damping has a huge impact on the low and high external pressure frequencies as well. Even the curve is much more smoother with respect to the other venting area ratios.
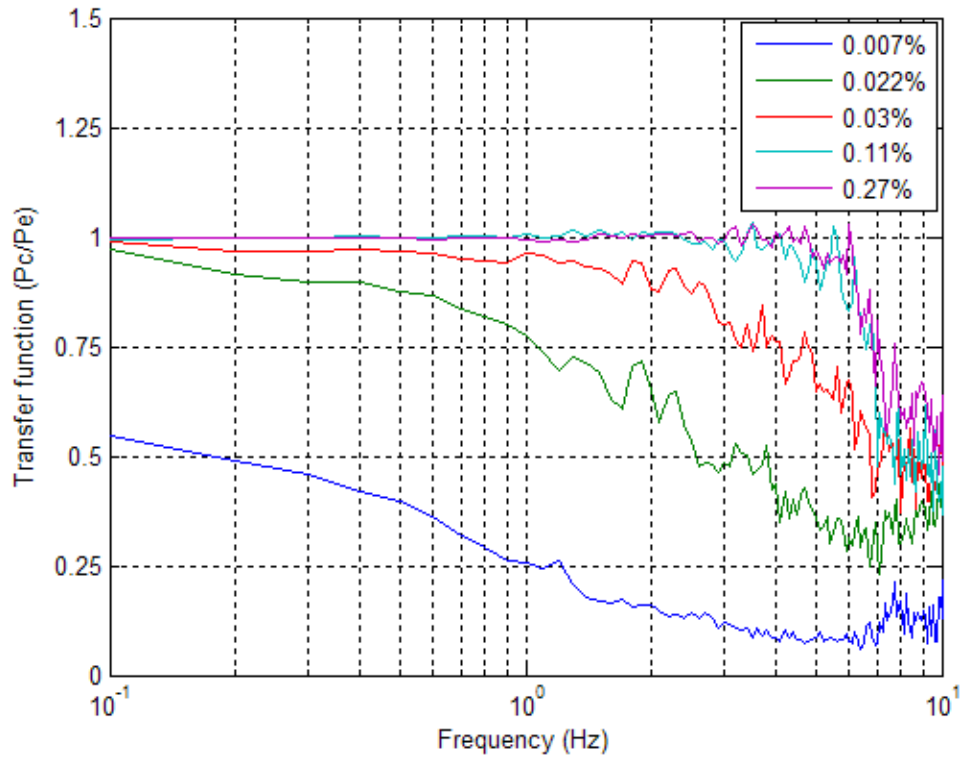
a)
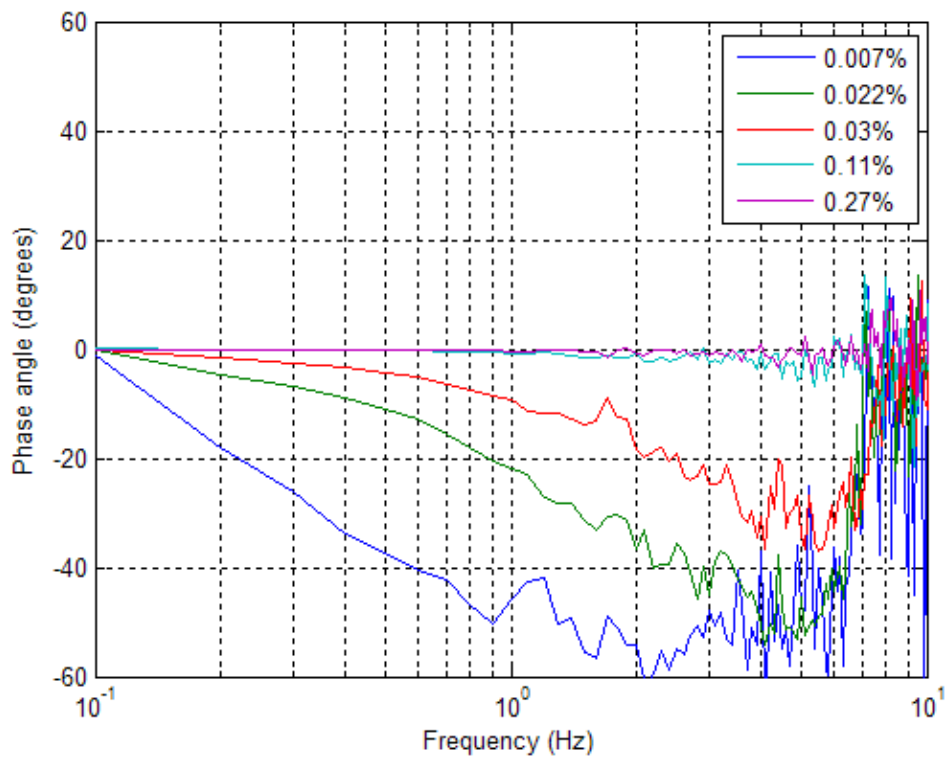
b)

Figure 4.6 Transfer function (a) and phase angle (b) variation with venting area ratios % (wide face)
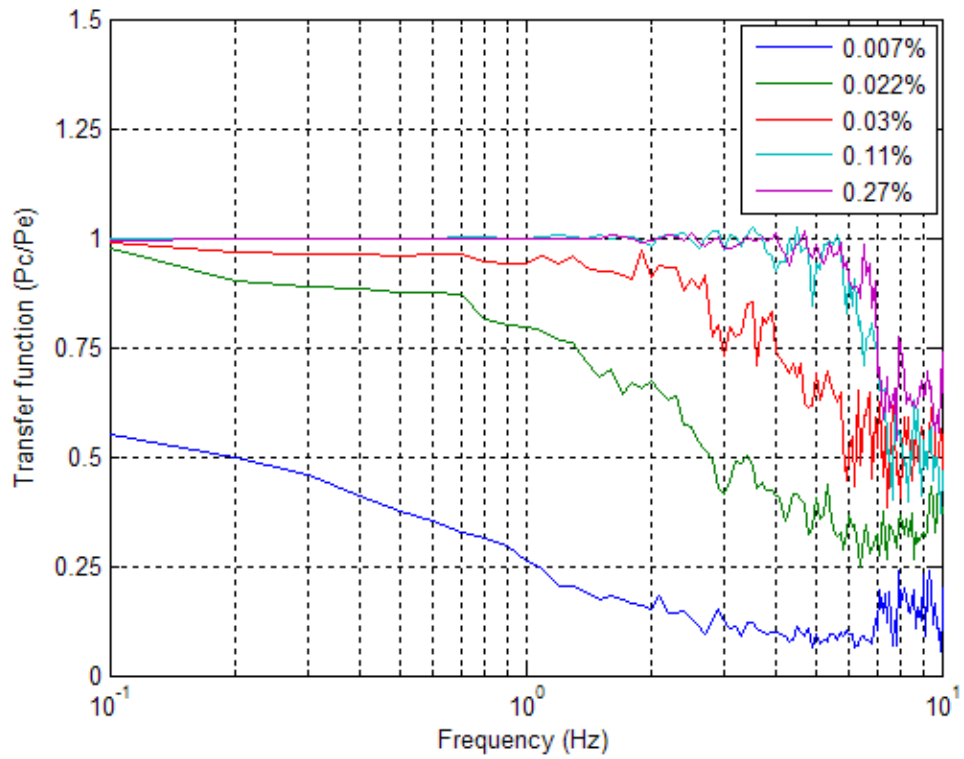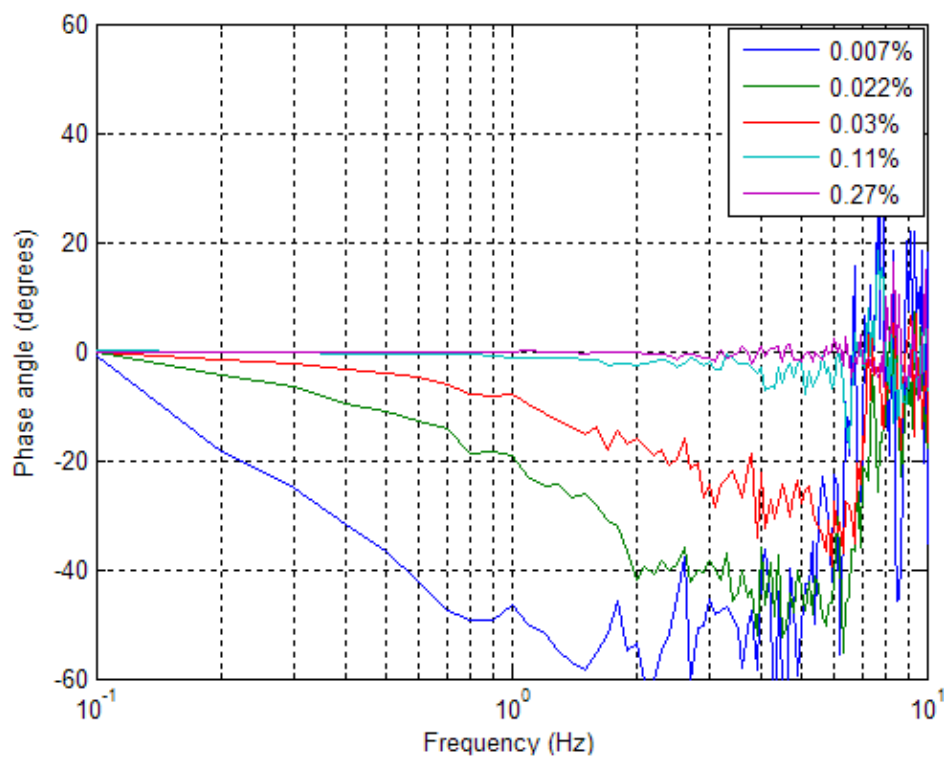
Figure 4.7 Transfer function (a) and phase angle (b) variation with venting area ratios % (narrow face)

In terms of phase angle, the effect of the rainscreen venting area is well identified as shown in Figs 4.6b and 4.7b. As the rainscreen venting rate increases, which will allow the external signal to spread more through the vent openings and makes the cavity response pressure prompt to develop faster. The pressure inside the cavity then rises more rapidly to reach the external pressure within a smaller time lag τ, which is proved by the reduction of the phase angle between the external and the cavity pressures. The data clearly show that both signals are out of phase at low rainscreen venting area ratios. As A_V gets higher, the magnitude of the phase angle gets smaller; the associated curves seem straight linear at low frequencies. At higher frequencies, there is a rapid change in the shift that gets faster as the frequencies increase, corresponding to the dropping fluctuations in the transfer function.

No significant difference is recorded when comparing the normalized spectral densities, transfer functions and phase angles for the wide and narrow faces, which reflects the similarity of the cavity to external pressures ratios previously seen. It is only noted that the phase angle curve associated to 0.11% venting area ratio is closer to that of 0.27% at high frequencies in the wide face case.

Figure 4.8 describes the differences in the external fluctuations transmission into the cavity when the vent openings location is changed for the same venting area ratio. The measurements demonstrate that the vent openings distribution at the bottom of the rainscreen has an advantage to their layout between top and bottom; especially at low venting area ratio. At $A_V = 0.03\%$, higher external frequencies fluctuations are transmitted to the cavity, which causes a reduction in the phase angle. At $A_V = 0.11\%$, the transfer functions have almost similar magnitudes, which is influenced in the statistical pressure ratios, but the phase lag is significantly smaller especially at high frequencies, when the holes are located at bottom.
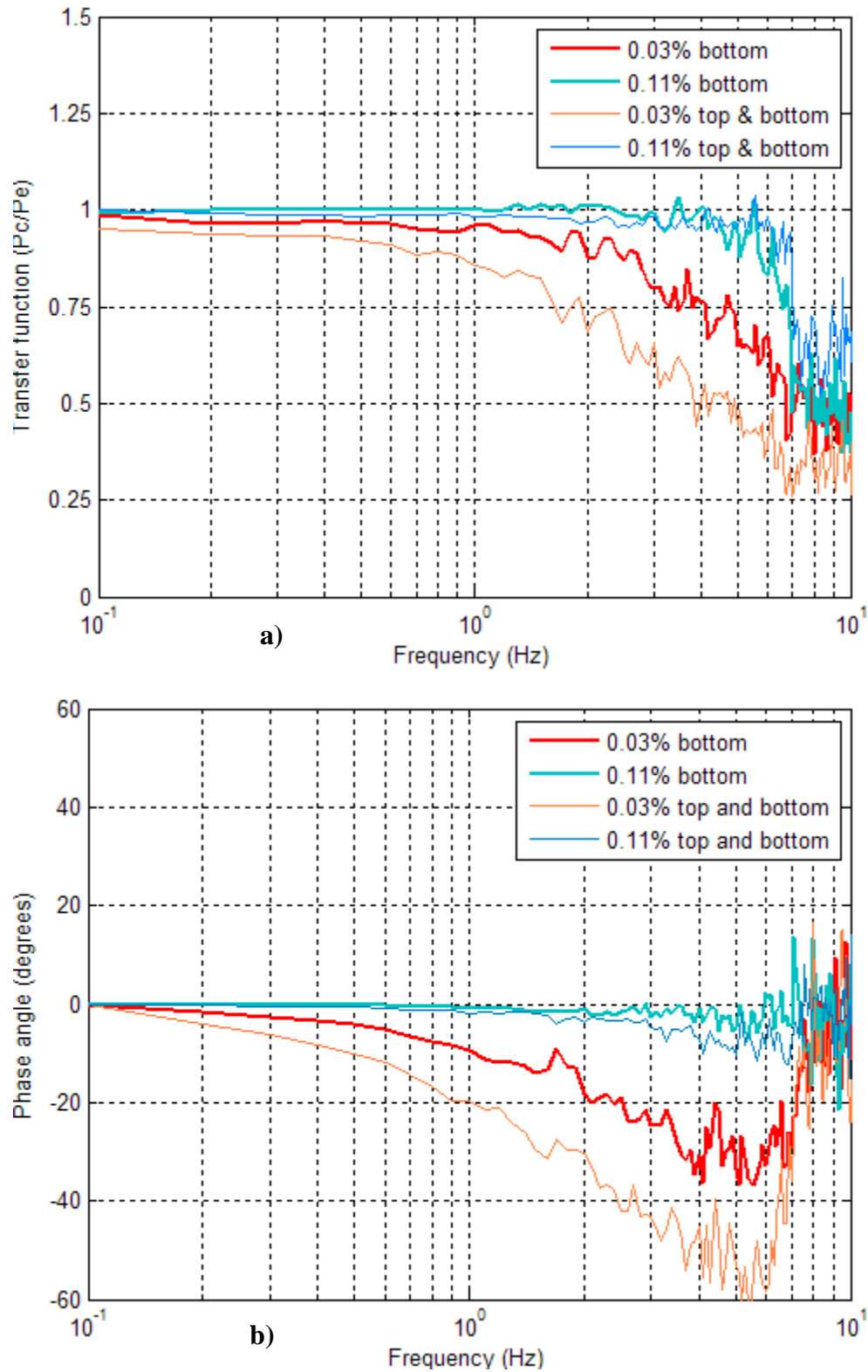
Figure 4.8 Transfer function (a) and phase angle (b) variation with venting location (wide face)

Finally, all the figures showing the spectral analysis do not indicate any resonance inside the cavity; which Holmes (2001) and Kumar (1999) previously confirmed for the case of small volumes. Table 4.2 represents the values of undamped natural frequencies calculated by the formulae provided by both authors.

Venting Area ratio	Number of holes	Holmes (1979)	Kumar (1999)
0.007 %	1	19.0	21.2
0.022 %	3	33.7	27.8
0.03 %	4	38.9	30.0
0.11 %	15	75.0	41.0
0.27 %	36	116.7	51.0

Table 4.2 Undamped natural frequencies $f(Hz)$ at $d_c = 25\text{mm}$

As Inculet and Davenport (1994) proved, the natural frequency gets higher as the rainscreen-venting ratio increases at constant cavity depths. Also, the smaller value of 19 Hz associated to the lowest venting area in the current experiment, does not even show in the tail of the spectral density function. Therefore, the cavity frequency is not excited by the external pressures fluctuations, and signal resonance will never occur.

4.3 Basic Statistics of Measured Cavity Pressures for Three Different Applied Signals

4.3.1 Pressure Gradient inside the Cavity

Table 4.3 presents the statistical values of the three edge taps pressure signals, which are extracted from the wide and narrow faces external pressure measurements of the pressure model in the wind tunnel. These signals are applied simultaneously to the three pressure air boxes at the bottom of the rainscreen. The thought in this part of the project is to examine the cavity pressure responding to the pressure gradient applied across the rainscreen, rather than comparing it to each of the three signals. For this reason, it was chosen to estimate the area averaged pressure P_a calculated over the three equal area pressure air boxes, to check its impact on the cavity pressure, in comparison with the single applied pressure case. P_1, P_2 and P_3 refer respectively to

the edge, middle and third air box exterior signal applied to the rainscreen from the left.

	Wide face				Narrow face			
	P_1	P_2	P_3	P_a	P_1	P_2	P_3	P_a
mean	0.06	0.47	0.73	0.42	0.16	0.65	0.928	0.58
peak	1.74	2.15	2.24	2.04	1.38	2	2.38	1.92
rms	0.28	0.33	0.36	0.32	0.28	0.32	0.35	0.31

Table 4.3 Statistical values for the three applied pressure signals

Obviously, P_1 reveals the lowest statistics since it corresponds to the pressure measured at the tap located at the edge of the building face in the pressure model of the wind tunnel test (Section 3.2.1), followed by the two adjacent taps signals P_2 and P_3. In fact, for a windward face subject to zero wind incidence angle, the pressure increases as going further from the edge to the centre of the face.

Despite the exterior pressure gradient applied on the PER panel due to three different applied signals, the pressure response inside the cavity does not exceed 2% variation in x and y directions for both the wide and narrow faces, similarly to the single applied signal case, as proved in Table 4.1.

$\overline{P/Pt}$	x/W				$\overline{P/Pt}$	x/W		
y/H	0.085	0.5	0.91		y/H	0.085	0.5	0.91
0.125	1.011	1.001	0.998		0.125	1.001	1.002	0.995
0.375	-	1.000	1.017		0.375	-	1.000	0.988
0.625	-	1.013	-		0.625	-	1.005	-
0.875	1.005	1.021	1.003		0.875	1.000	1.002	0.992

a) Wide face   b) Narrow face

Table 4.4 Mean instantaneous normalized pressures inside the cavity for the three applied signals (Configuration b) $A_V = 0.022\%$

Table 4.4 shows the mean instantaneous normalized pressure values of the cavity for the lowest rainscreen venting area ratio, with respect to a pressure transducer reference located at $x/W = 0.5$ and $y/H = 0.375$ at the back of the air barrier. For other venting configurations, the cavity shows the same behaviour.

67

Figures 4.9 and 4.10 reveal a snapshot of 15 seconds for the time series of the applied and cavity pressures signals for two rainscreen venting configurations. The data show the averaged exterior pressure signal $P_e = P_a$ as well as the pressure difference ($P_e - P_c$) across the rainscreen.
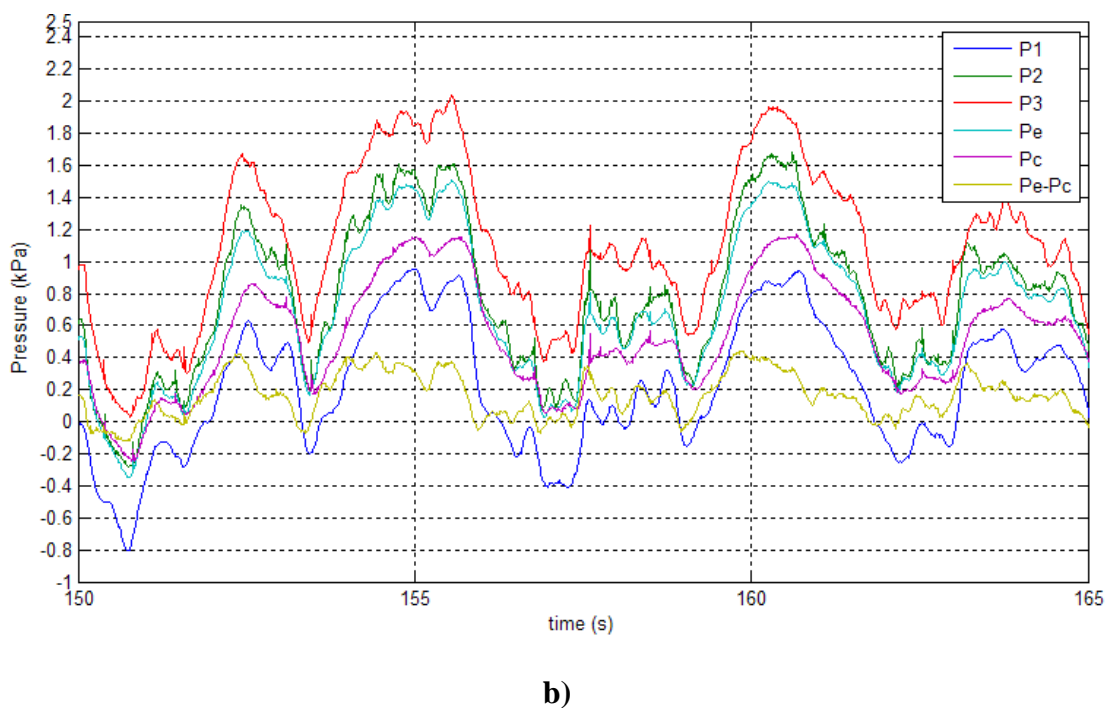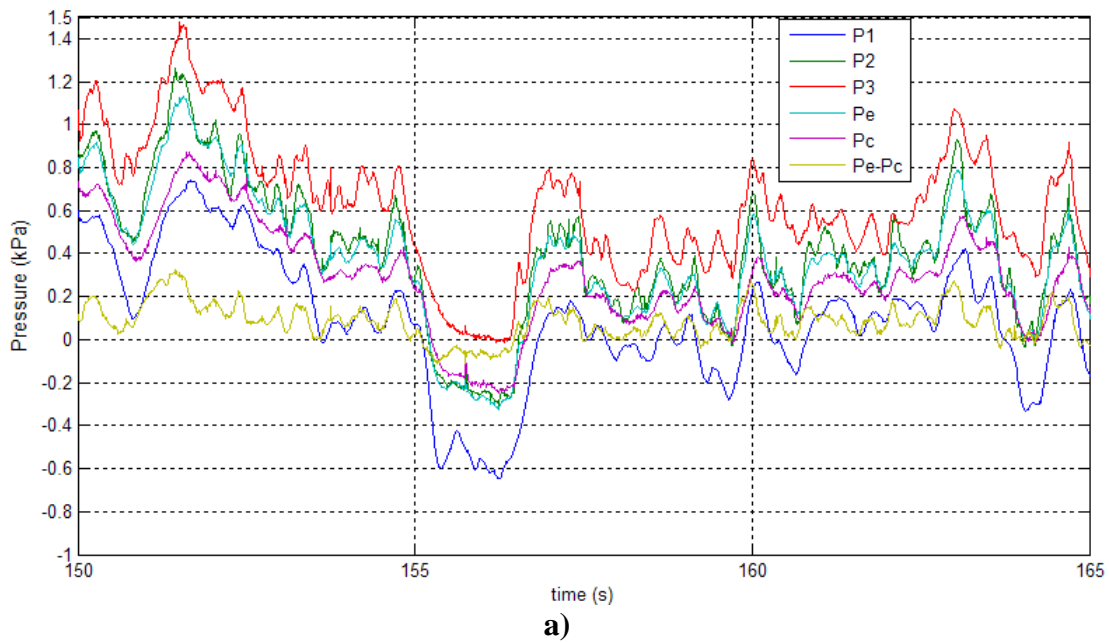

a)

b)

Figure 4.9 Time series pressures for configuration b for a) wide face and b) narrow face
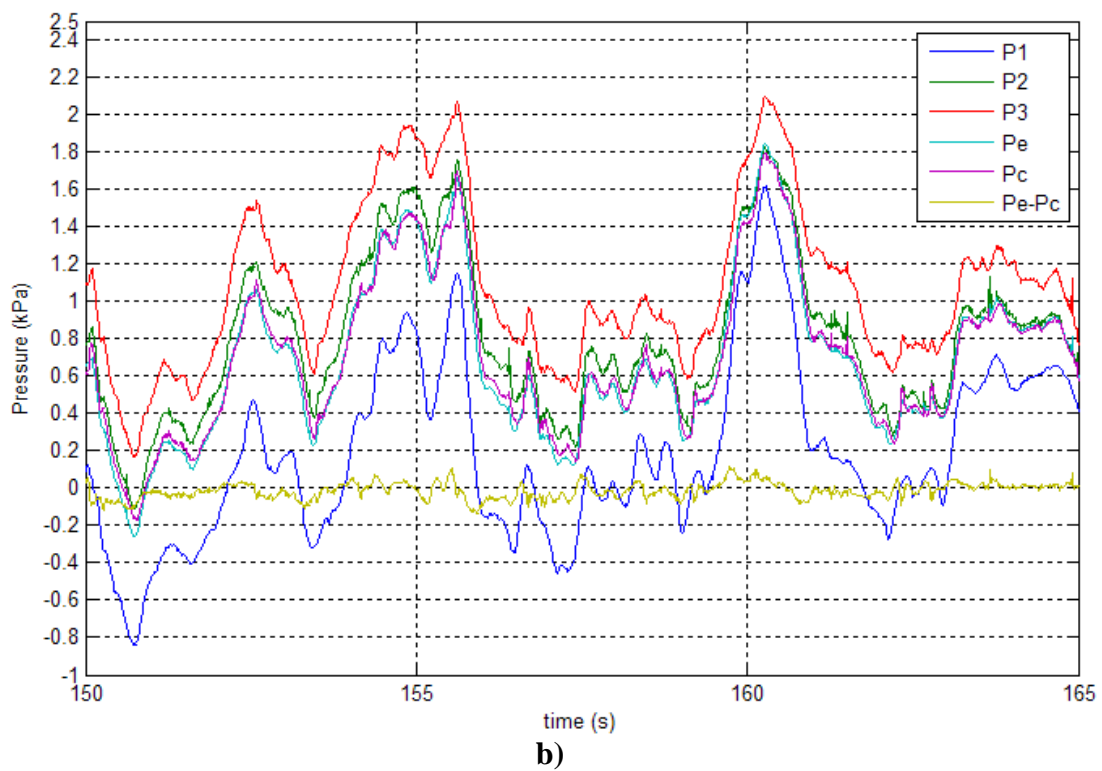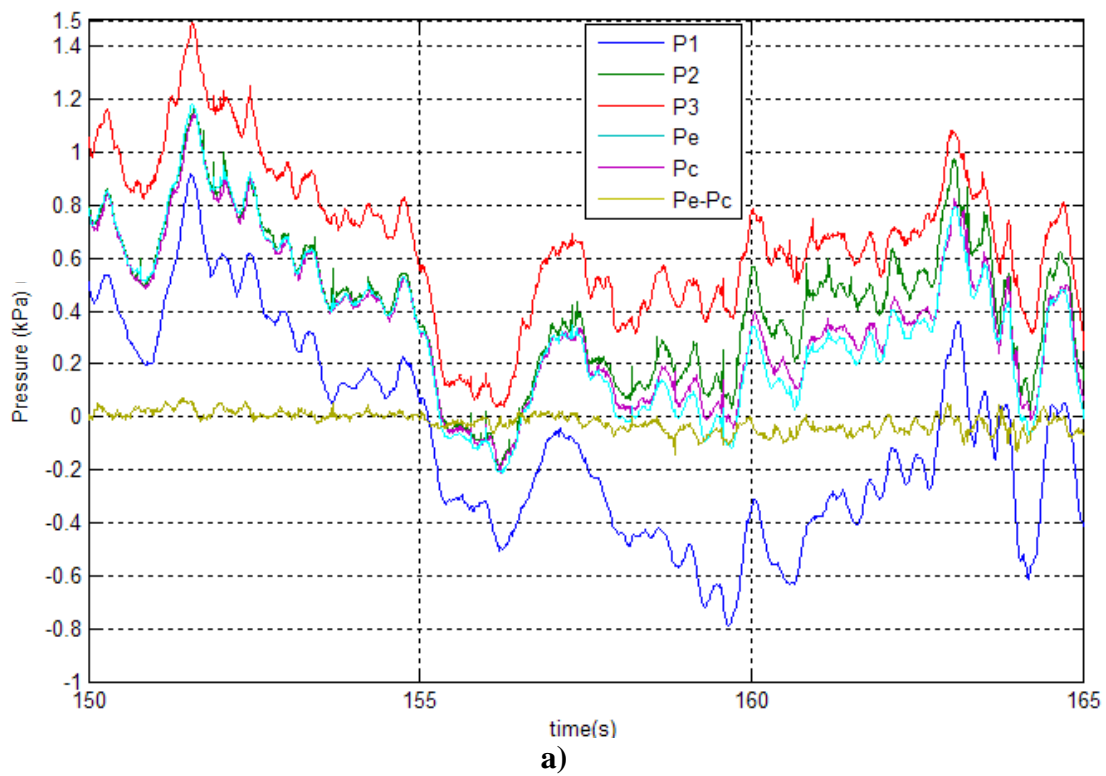
Figure 4.10 Time series pressures for configuration d for a) wide face and b) narrow face

As the measurements indicate, the area-averaged pressure P_e is practically following the middle tap signal P_2 since the external pressure gradually increases from P_1 to P_3, for both the wide and narrow faces; the three signals being applied to a similar box area. The lowest rainscreen venting area $A_V = 0.022\%$ indicates poor pressure equalization between the cavity and area-averaged exterior pressures, in comparison with $A_V = 0.11\%$. The cavity pressure signal P_c is visibly smoother than the external pressure as shown in Fig 4.9, signifying that the external high frequency fluctuations are indeed transmitted to the rainscreen. Moreover, P_c is following P_e with a small phase shift without reaching the positive peak fluctuations, while sometimes it shows slightly higher magnitudes under negative pressure

The wide face cavity response pressure performance seems slightly better: the largest differential pressure peaks sustained by the rainscreen are 650 Pa in pressure and 170 Pa in suction, in comparison with 780 Pa and 270 Pa for the narrow face, as recorded data indicate. These values are indeed higher than those previously observed under a uniform pressure signal in section 4.2.1, due to the existing gradient pressure, as proved Ganguli and Dalgliesh (1988). The peaks last for no longer than 2 seconds and they are correlated with those of the three pressures signals. The differential pressure signal $P_e - P_c$ identifies this difference since it has larger amplitude in Fig 4.9b with 400 Pa peak value.

When the rainscreen venting area becomes 0.11% the majority of external pressure fluctuations are transmitted to the cavity as shown in Fig 4.10. P_c tends in general to collapse with P_e, and the differential pressure across the rainscreen is reduced to around zero, which indicates satisfactory pressure equalization for both the wide and narrow faces. However, a look at the time series especially in Fig 4.10a demonstrates that at certain moments the cavity response pressure is not capturing the minimum peaks of the exterior area-averaged pressure signal P_e, although both signals are generally in phase.

4.3.2 Measurements of Cavity to Exterior Pressure Ratio P_c/P_e

Figure 4.11 describes the pressure equalization process with respect to the rainscreen venting area, in terms of the cavity to area-averaged exterior pressures ratio. For both the wide and narrow faces cases, the pressure equalization between the cavity and the exterior improves as the rainscreen venting becomes larger. Note that the curves refer to the basic venting holes where three, four, 15 and 36 are respectively distributed under the three bottom pressure boxes of the rainscreen; while the marked points show the pressure behaviour when the 15 holes are redistributed between top and bottom. The data in both Figs 4.11a and b reflect the fact that the most satisfactory pressure equalization performance occurs in terms of mean pressure since the mean pressure ratio curve is the highest. When comparing the two faces cases, the mean ratio $\overline{P}_c/\overline{P}_e$ presents similar values: only 75% of the mean external load is transmitted into the cavity at the lowest venting area, and the percentage increases until reaching the full-pressure equalization between the mean external area-averaged and cavity flows at $A_V = 0.11\%$, where the curve keeps flat until $A_V = 0.27\%$. The rms ratio values $\tilde{P}_c/\tilde{P}_e$ also collapse with the mean ratios at $A_V = 0.022\%$ presenting an ascendant trend when the venting gets higher for both faces. However, the cavity response pressure equalizes faster with the area-averaged pressure in terms of peaks when the three signals refer to the wide face. This trend can be seen with the higher values of the peak ratio $\hat{P}_c/\hat{P}_e$ observed in Fig 4.11a for all rainscreen venting configurations. Note that the cavity response was able to catch up with the external pressure peak leading to a peak ratio equal to unity at $A_V = 0.11\%$ in the wide face case.

When comparing these statistical values to those of the cases referring to a single applied pressure signal (Figs 4.3a and b), the reader can make several observations: When the PER wall panel is subject to a single pressure signal applied through pressure boxes, the three statistical (mean, rms and peak) pressure ratios collapse similarly for both faces.
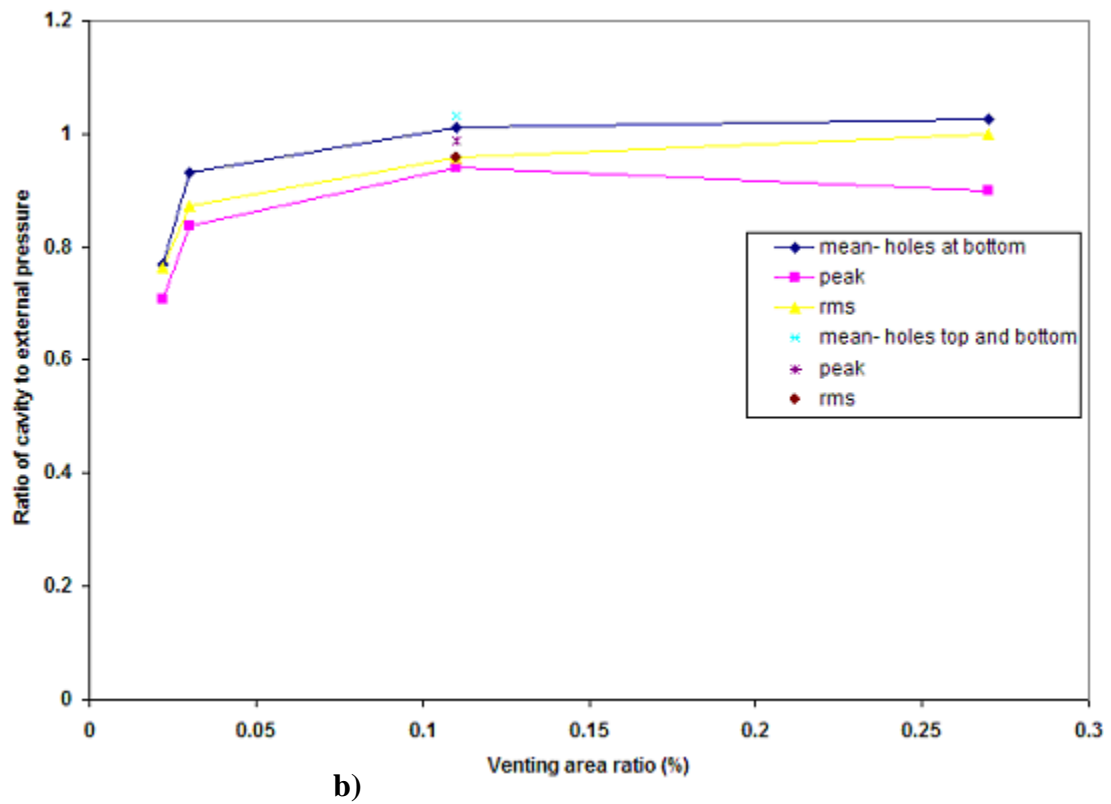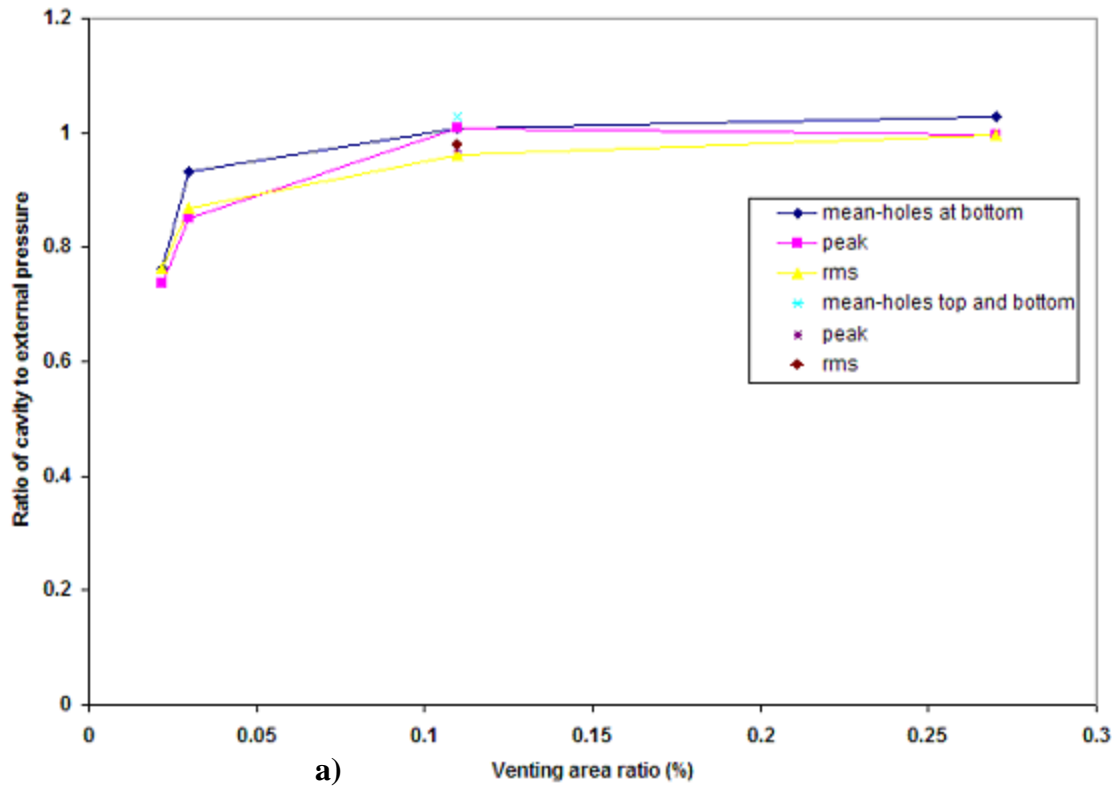
Figure 4.11 Basic statistics for three applied pressure signals for a) wide face, and b) narrow face

Thus, the cavity response is able to reproduce all external pressure statistics in the same way, for all venting configurations.

In case three different pressure signals are simultaneously applied to the model through three equal area pressure air boxes, the pressure equalization process is slower (i.e. for three vent holes in the rainscreen $\overline{P}_c / \overline{P}_e$ =0.75 in Figs 4.11.a and b, while it is equal to 0.95 when a single pressure is applied in Figs.4.3.a and b). This is due to the existence of pressure gradient across the three boxes, which will practically lead to a smaller time lag between the area-averaged external pressure and the pressure cavity response, causing a lower degree of pressure equalization.

On the other hand, similarly to the single signal case, the redistribution of the 15 vent holes between top and bottom of the rainscreen slightly improves the cavity pressure response, under a pressure gradient. In case the external signals refer to the narrow face, the mean cavity to external averaged pressure ratio is raised in conjunction with the peak and rms values; while the wide face case has only the mean ratio increased. These differences are due to the way the six PLAs are generating the three different signals in each case and to the repeatability and accuracy errors already observed.

Figure 4.12 shows the peak factor when three different signals are applied to the rainscreen. The curves provide an interpretation of the statistical values shown in Figs 4.11a and b; indicating an increasing behaviour as the rainscreen vent area gets larger, The peak factors present higher values when compared to the single applied pressure signal case, which is result of the pressure gradient as Inculet (2001) stated. For example, at $A_V = 0.11\%$ g=3.88 instead of 3.2 in Figs 4.4a and b. The main explanation is that the mean of the area-averaged pressure issued from the three edge signals is much lower that the windward signal mean pressure value. Regarding the vent holes location effect, there is an agreement between both cases: the redistribution of the vent holes between top and bottom causes a drop of the peak factor.
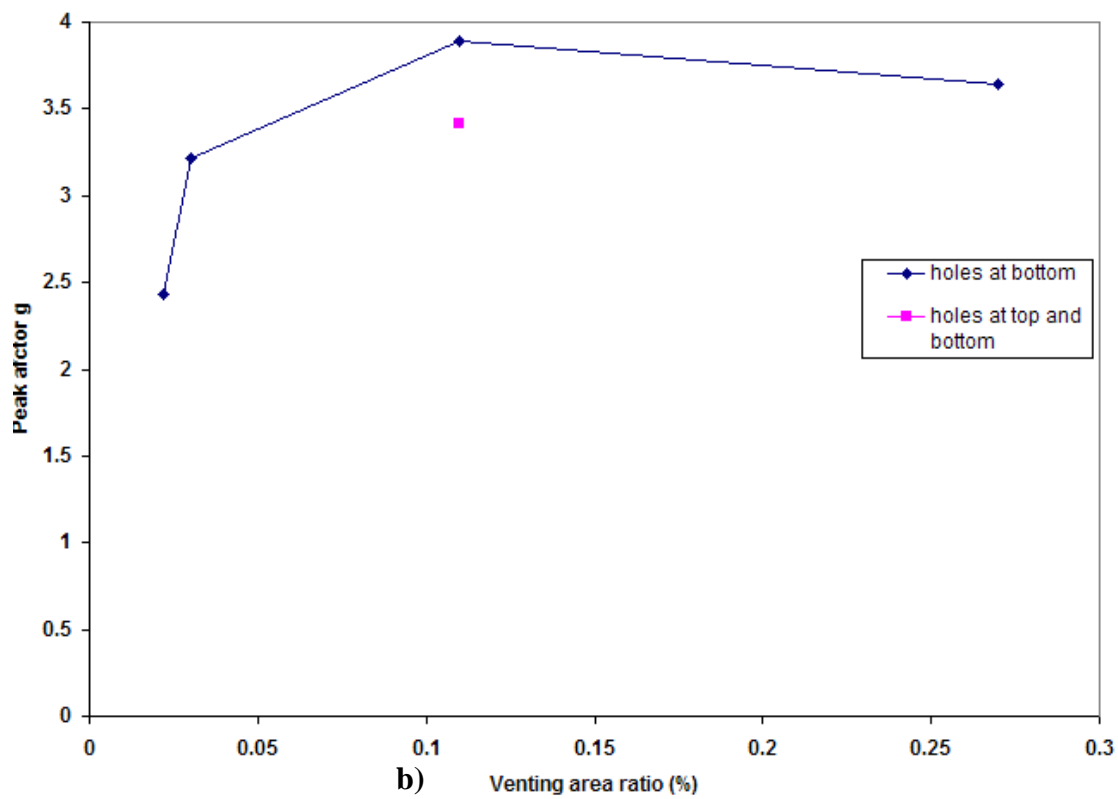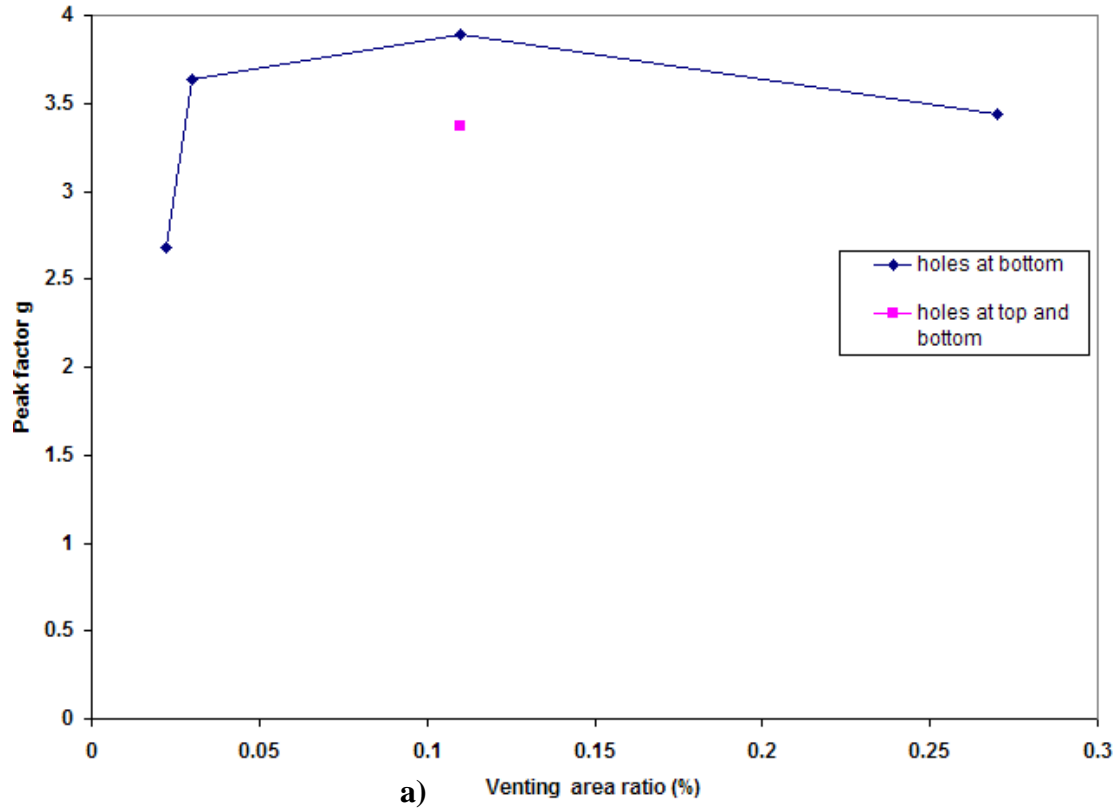
Figure 4.12 Peak factor for three applied pressure signals for a) wide face, and b) narrow face

4.3.3 Analysis of the Experimental Results in the Frequency Domain

Figure 4.13 shows the normalized spectral density functions of the cavity pressure when three different signals are applied to the PER panel. Spikes at 60 Hz equivalent wind tunnel electronic noise frequency are always identified. The behaviour of the cavity with respect to the exterior pressure varies consistently in the frequency domain with respect to the venting area as shown in Figs 4.14 and 4.15. The transfer functions display the area-averaged pressure amount transmitted to the cavity, that obviously increases, as the rainscreen venting area ratio gets higher. Similarly to the single signal case, the critical damping frequency increases as A_V gets larger allowing a wider range of low external frequencies to get transferred behind the rainscreen. The full equalization between the cavity pressure and $P_e = P_a$ appears at $A_V = 0.27\%$, while it is reached at a lower venting area of $A_V = 0.11\%$ under a single pressure signal. In fact, the transfer functions and phase angles corresponding to these two venting configurations almost collapse in the case of a uniform pressure, while in this case they both show more attenuation.

In addition, when a single pressure is applied to the rainscreen, the transfer functions corresponding to low venting configurations, apart from the one hole case, originate from a value close to one; in contrast with the current plots; that indicate a pressure drop and start to roll off at lower frequencies i.e. $4Hz$ instead of $6Hz$ at $A_V = 0.27\%$. Therefore, when the PER panel is subject to a pressure gradient, the cavity pressure equalizes with the external pressure at a smaller degree for the same rainscreen venting area ratio. On the other hand, it is noticed that slower pressure equalization is established when the three external pressure signals are extracted from the narrow face.
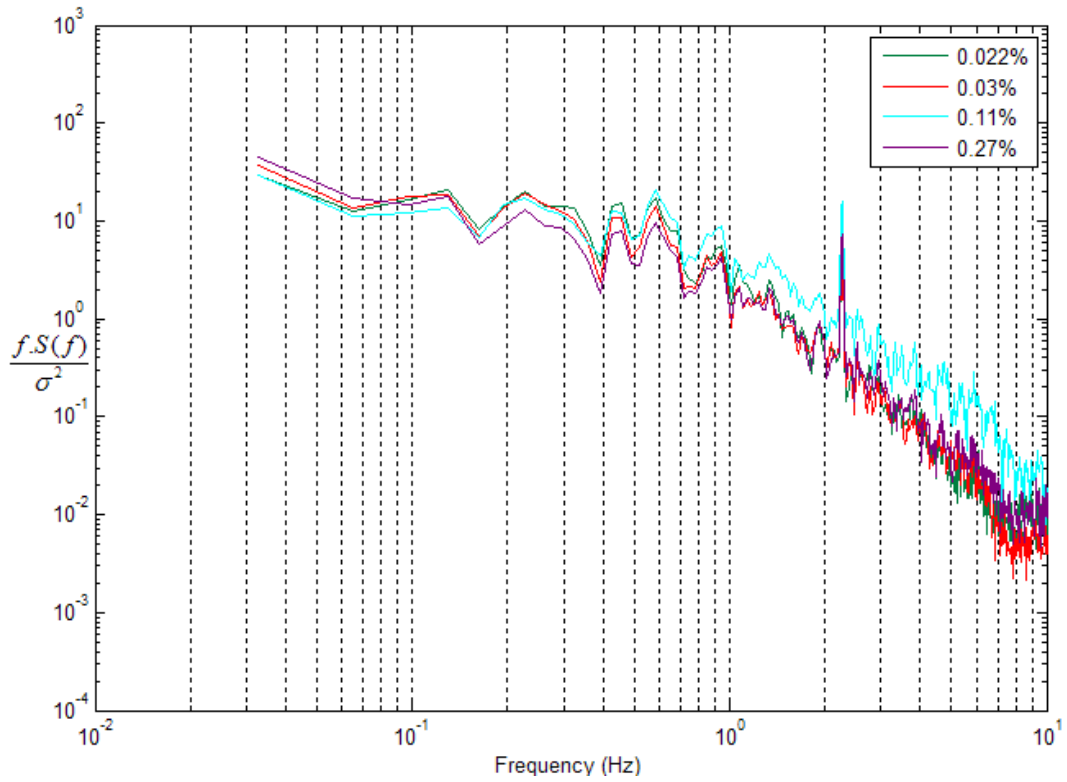
a)
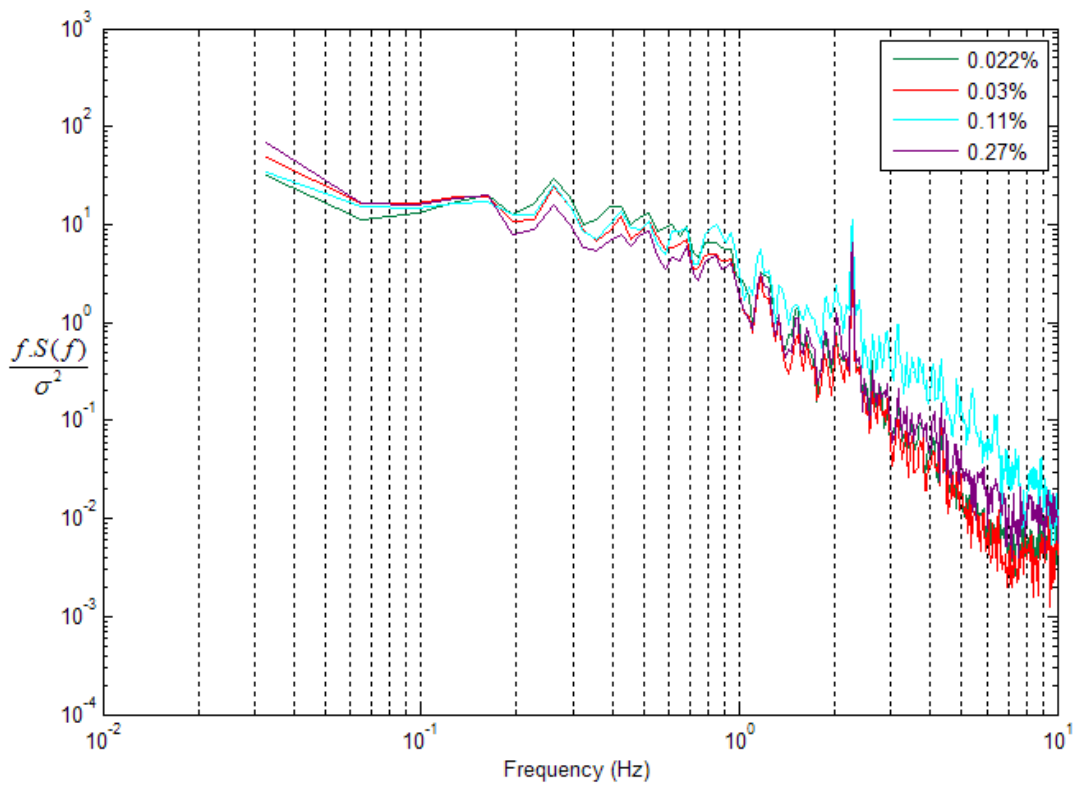
b)

Figure 4.13 spectral density functions for cavity pressures for a) wide, and b) narrow face
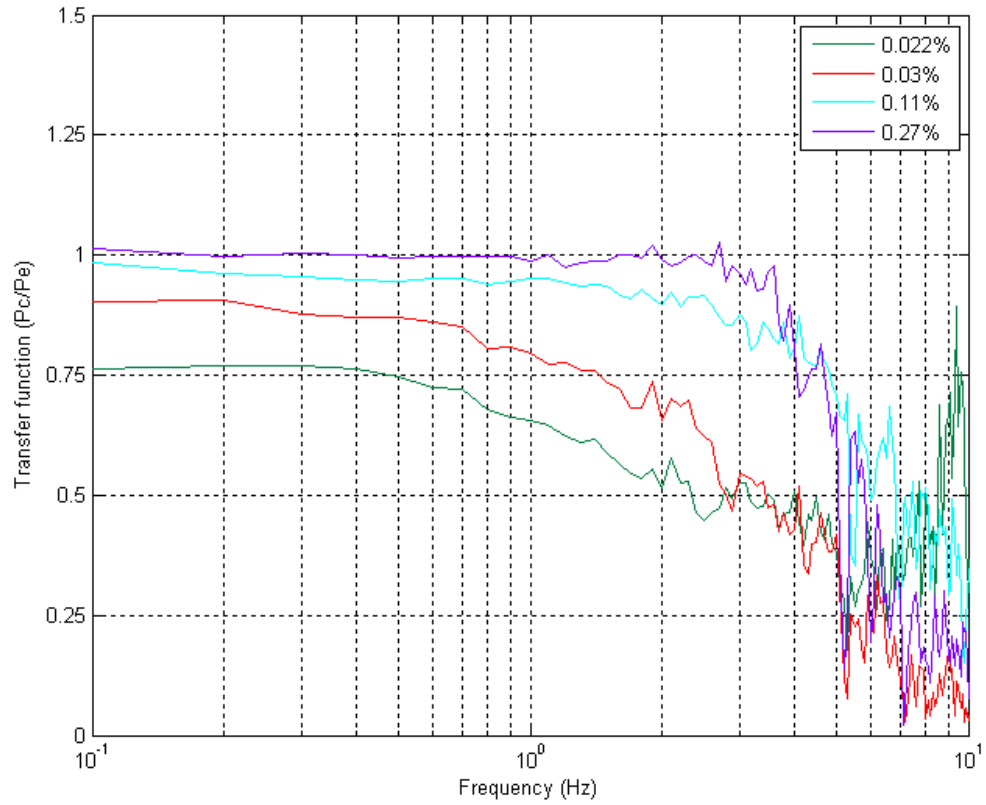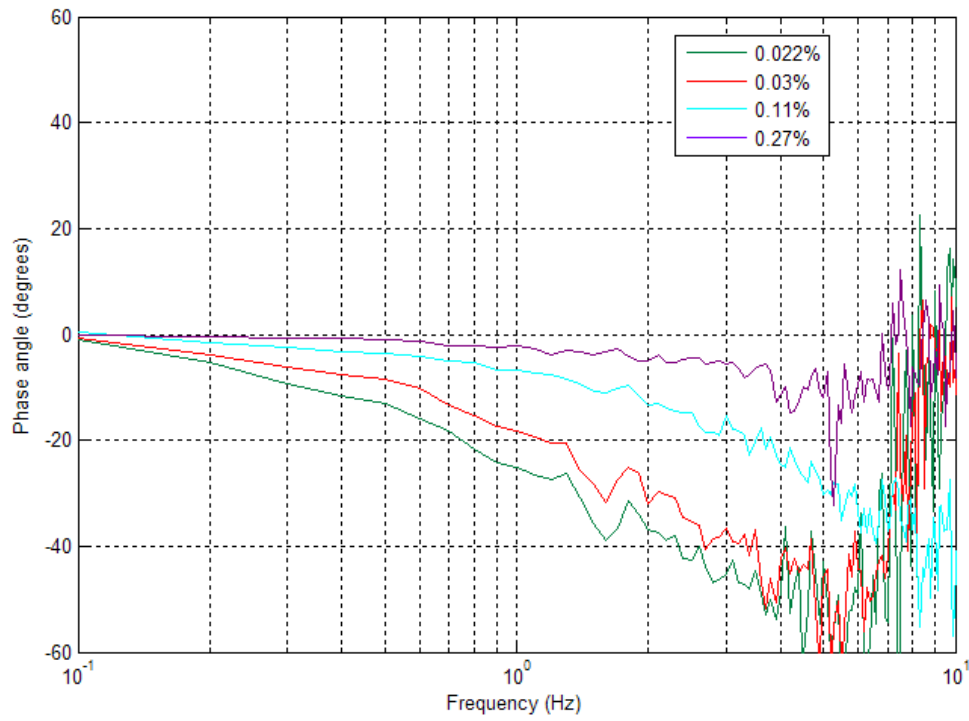
Figure 4.14 Transfer function (a) and phase angle (b) variation with venting area ratios (wide face)
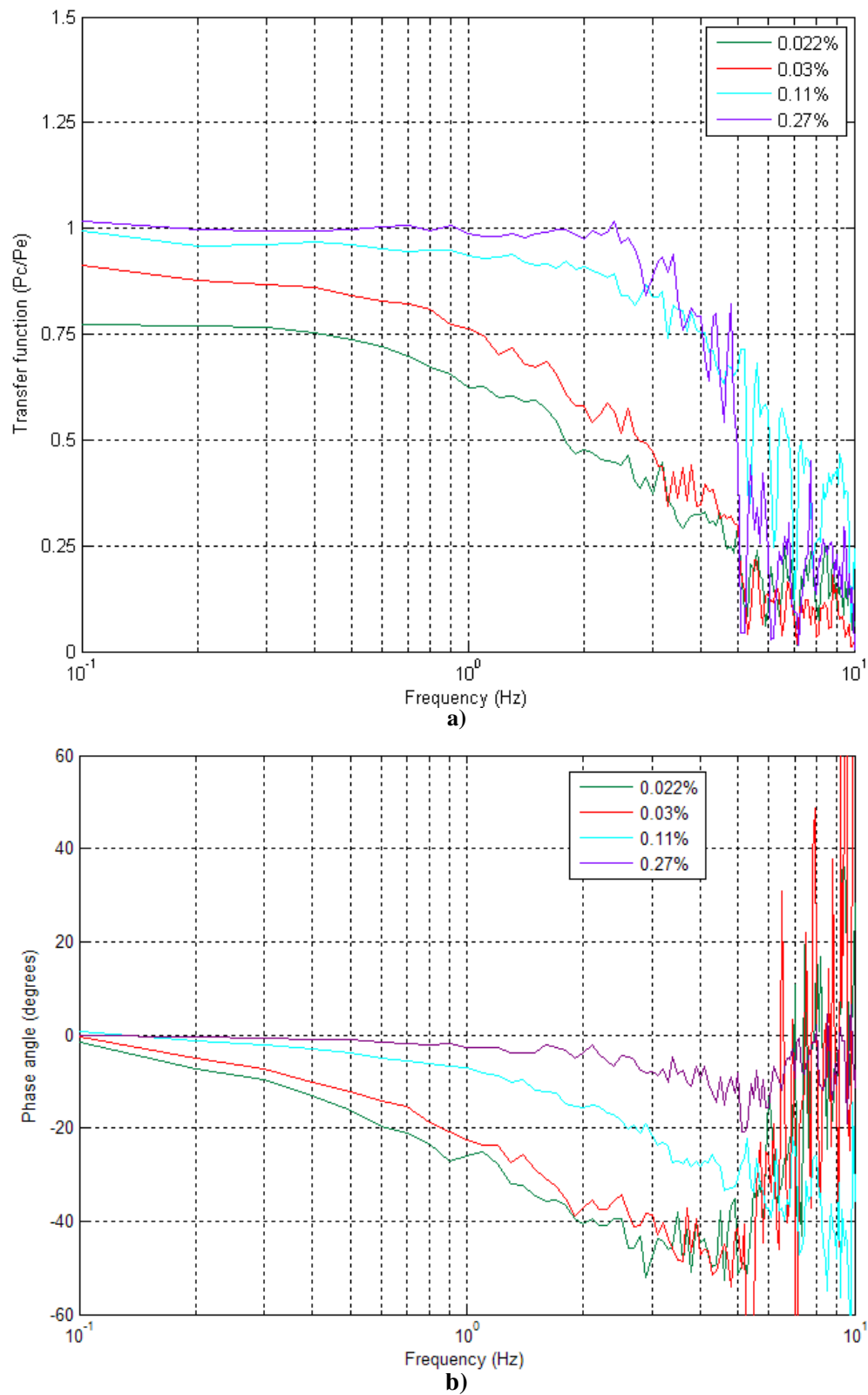
Figure 4.15 Transfer function (a) and phase angle (b) variation with venting area ratios (narrow face)
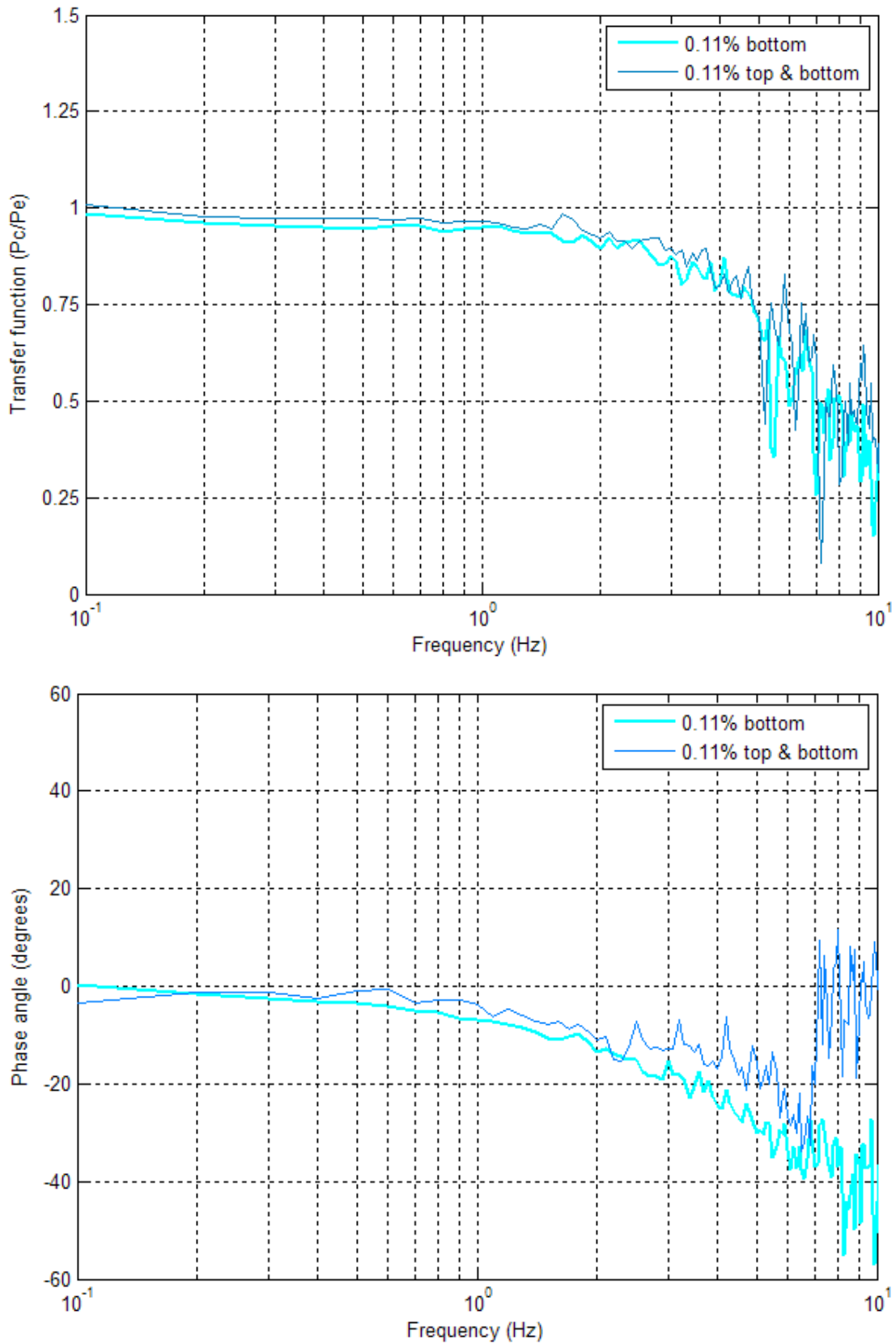
Figure 4.16 Transfer function (a) phase angle (b) variation with venting location (wide face)

The phase angle plots are presented in Figs 4.14b and 4.15b. As pressure equalization improves, the phase angle is reduced. However at high raincsreen vent area ratios, the phase angle does not keep the value of zero all the time: the cavity and area-averaged pressures are out of phase in the high frequencies regions, which proves again that, under a pressure gradient, the cavity has less ability in responding to the external pressures.

The effect of vent openings location is described in Fig 4.16. The redistribution of 15 vent holes between top and bottom on the rainscreen does not have a significant impact on the pressure equalization process. The transfer function magnitudes are slightly increased but the damping occurs at the same frequency. Also, the phase angle is slightly reduced at high frequencies

4.3.4 Comparison of Wide and Narrow Face Results

Measurements previously revealed in the statistical values and transfer functions have shown some differences in the cavity pressure behaviour between the wide and narrow face cases. Apparently, façade characteristics and wind flow behaviour do have an effect on the degree of pressure equalization, especially at lower frequencies. When the three applied signals were extracted from the three edge taps of the windward wide face, the pressure equalization for our PER model was faster and there was better transmission of low frequencies fluctuations at all venting configurations. For example when comparing Figs 4.14a and 4.15a, the transfer functions show that at the lowest venting area where $A_V = 0.022\%$, 75% of external pressure fluctuations are transmitted to the cavity at frequencies lower than $0.5Hz$ in the case of the wide face, while at higher frequencies this percentage start to decrease. However, when the three applied signals correspond to a part of the three edge taps exterior pressures of the windward narrow face, only frequencies below $0.4Hz$ are 75% transferred to the cavity. Similarly, at high rainscreen venting area ratios, the transfer functions show a faster decay in the case of the narrow face. This is probably attributed to the actual difference in the three signals of the two faces that results in different pressure gradient although the full-scale applied signals represent only a part

over five minutes equivalent time period from the original data duration. Moreover, the differential pressures $P_e - P_c$ observed across the rainscreen are higher when it comes to the narrow face external signals. To illustrate, the corresponding mean values associated to $A_V = 0.022\%$ are respectively 100 Pa in Fig 4.9a and 120 Pa in Fig 4.9b.

In light of the above, it was necessary to quantify numerically the resultant horizontal gradient pressure available on the PER panel, which is caused by the applied pressure signals issued from each face, in order to justify correctly the cavity pressure behaviour. Inculet (2001) suggested an instantaneous horizontal component pressure gradient coefficient $H_g = \dfrac{\partial C_p}{\partial (x_m / W_m)}$ where x_m is the horizontal coordinate measured from the left edge of the building, aiming to examine the pressure gradients mostly observed at the edges of the facades between the different taps locations on a pressure model in the wind tunnel. In this case, a positive value of H_g indicates that the pressure is increasing from left to right across the face.

By applying this expression on the current PER model compartment, the mean horizontal pressure gradient $\overline{H}_g$ is calculated between the three adjacent pressure air boxes locations, that are subject to three different external signals, where W_m refers in this case to the width W of the rainscreen. The results prove that applied pressure signals associated with the narrow face, result in higher-pressure gradient across the rainscreen: $\overline{H}_g = 0.32$ with respect to $\overline{H}_g = 0.26$ for the wide face case. These values refer to the pressure gradient established between the edge and the second adjacent pressure air box, from the left of the rainscreen. They are, respectively, equivalent in full-scale using a mean velocity of 53.6 m/s to 585Pa pressure change per metre and 700Pa per metre, meaning a difference of about 18% between the wide and narrow faces. The pressure gradients between the second and third pressure boxes exhibit the same behaviour, but with smaller magnitudes, since the pressure gradient is reduced as we go further from the edge of the building façade.

Therefore, this should explain the higher-pressure loads sustained by the rainscreen in case of the narrow face. It is also in agreement with Skerlj and Surry (1994) who observed through a wind tunnel experiment that, higher mean pressure gradients applied to a PER compartment, produces higher mean residual net pressures on the rainscreen.

4.4 Summary

Cavity pressure measurements using a PER compartment model have been examined under both a uniform pressure and a horizontal pressure gradient. The results indicate the major role of the rainscreen venting to wall area ratio in the improvement of equalization process between the external and cavity pressures. The transfer functions revealed an increase in the critical damping frequency, and the phase angle between external and cavity pressures was reduced, as the rainscreen venting area was increasing.

In the case of a uniform applied pressure, the lowest rainscreen venting area ratio $A_V = 0.007\%$ resulted in the poorest pressure equalization between the external and cavity pressures. A great pressure loss occurred across the rainscreen: a mean pressure drop of 55% of the external pressure was observed.

The application of a horizontal pressure gradient leads to a lower degree of pressure equalization according to the experimental results. The best performance was obtained for $A_V = 0.27\%$ when the PER model was subject to three different signals, while a full pressure equalization occurred for $A_V = 0.11\%$ under a uniform pressure. Moreover, when applying three different signals extracted from the narrow face wind tunnel pressure model, the rainscreen panel experienced higher net pressures because the mean horizontal gradient pressure coefficient was 18% higher that the value associated with the wide face.

In terms of the venting area location, placing the vent holes at the bottom of the rainscreen seems to enhance the pressure equalization, in comparison with their

distribution between top and bottom. Such effect was clearly identified for low rainscreen venting area ratios. However, the vent openings layout did not have a significant effect on the performance of the PER model for high rainscreen venting area ratios.

The next chapter will present the numerical predictions of the PER model's cavity pressure response. This will allow checking whether the theoretical model is able to reproduce exactly the effect of the considered wall parameters on the model performance, under both uniform and gradient external pressures.

CHAPTER 5

NUMERICAL RESULTS

5.1 Introduction

This chapter establishes a comparison of the measurements and numerical predictions of the cavity pressure measurements in order to check the efficiency of the theory in predicting full-scale results in the future. In addition, the impact of cavity volume change on the pressure equalization is observed by predicting numerically the cavity pressure for a range of depths varying between 25 and 300mm under an external single pressure signal and pressure gradient.

5.2 Numerical Model

The numerical predictions of cavity pressures are computed based on Helmholtz resonator theory model. This model (known as Model 2 in chapter 2) has been chosen since the related equations involve damping and inertial terms for all openings, which is assumed to predict more realistically the cavity response pressure. Moreover, it is able to consider: 1) the external pressure fluctuations across each opening, 2) any number of venting holes and, 3) the leakage characteristics of the air barrier. For this reason, a Matlab program that was originally developed for internal pressure computations in low-rise buildings by Oh et al (2007) is transformed and used in order to estimate the cavity pressures in this project. The algorithm of the computer program is clarified in Appendix B Section B1. In addition to constant coefficients, the program is fed with the external pressure data matrix issued from the full-scale experiment, where each column represents the applied signal across an opening, as measured by the pressure transducers. In case of leakage, the leakage holes have a smaller diameter than the vents, and they are added to the external pressure data matrix input, as having zero pressure values.

Values chosen for the equations coefficients and parameters that are used in the computational program are defined below for the vent and leakage holes as well.

a) Flow Exponent n

The value of the flow coefficient n usually varies from 0.5 to 1 according to Table 2.3. Whenever n became higher than 0.5 in the numerical simulations, no significant variation was noticed in the cavity response pressure at a certain venting configuration by keeping the other parameters constant, and the basic statistics (mean, max, min and rms) were the same. For this reason, it was decided to use $n=0.5$ for the rainscreen which has openings with little depth.

When leakage exists, leakage holes are assumed to come out from the air barrier, which will have then its own flow exponent. In this case, $n=0.7$ according to Shaw (1981). With the numerical trials, it was noticed that if n becomes larger than 0.7, the mean of the predicted cavity pressure increases, and the peak decreases which makes the matching between experimental and numerical results harder, so n was kept 0.7. Moreover, based on wind tunnel tests conducted on PER models, Inculet and Davenport (1994) found that the venting in a rainscreen results in orifice flow giving $n=0.5$; while the leakage path through the air barrier is likely to exhibit more viscous type flow with $n=0.7$.

b) Effective Length l_e

The effective length used in the numerical simulations is chosen to be $l_e = l_0 + 0.89\sqrt{a}$ as proposed by Holmes (1979) in Table 2.4. This expression involves the effect of the orifice length l_0 which varies in the reality with the nature of the flow.

l_0 for the leakage hole is assumed to be long and wide enough to let the flow come back and forth, however it is smaller for the vent opening. For this reason, the value of l_0 for the vent opening is set equal to the thickness of the rainscreen that is 0.00635m, while it is slightly bigger for the leakage hole present in the air barrier

suggested to be 0.0075m close to the air barrier assembly thickness, a refers to the area of the opening.

c) Discharge Coefficient K

It is always difficult to assess the exact value of the discharge coefficient for a flow through the vent opening in the rainscreen. In fact, this flow may be affected by a mean flow stemming from unavoidable leakage of the air barrier, or cross flows behind the rainscreen with venting holes exposed to different exterior pressures. Furthermore, pressure losses might come from the way the flow rate is transmitted through the opening. Holmes (1979) specified the earliest values; he found that a value in the range of 0.6 to 0.65 corresponds to a steady flow, while 0.15 refers to highly fluctuating and reversing flow conditions. The presence of any leakage in the air barrier introduces also a second unknown into the theory. The leakage coefficient for the air barrier, like the discharge coefficient for the rainscreen, could take on a different value in fluctuating flows than in steady flows. However to simplify the problem, it was decided to use the steady flow value $K = 0.6$ for the air barrier, since mean velocities will be high through the small leakage path, as described by Inculet (1996). Simulations have not shown any difference when using K as 0.5 or 0.6, however when it became smaller, the predicted mean, peak and rms of the cavity pressure were raised, which yielded a poor matching with the experimental values.

In light of this discussion, the rainscreen may have a different value of discharge coefficient for each configuration depending on the flow behaviour; setting constant the flow exponent n and the effective length l_e for both the rainscreen and air barriers. The concept is to adjust the value of K until the theoretical rms of the pressure drop across the rainscreen matches the experimental value.

In the present case, the numerical value of K is first determined based on the single applied external pressure signal and then applied for the three different external pressure signals case. It was necessary, though, to quantify any existing leakage in the air barrier assembly, to include leakage holes in the numerical model for better matching with the experimental results.

Leakage openings were assumed to be small enough in the order of 2mm circular hole, where one leak represents 1% of one 20mm vent hole area. The estimation of the expected area of leakage holes in the air barrier A_{ab} is made by numerical trials. The first approximation is given as

$$\frac{A_{ab}}{A_{rs}} = \frac{K_{rainscreen}.\Delta p_{rainscreen}^{n1}}{K_{airbarrier}.\Delta p_{airbarrier}^{n2}} \tag{4.1}$$

using the experimental pressure drop values across the rainscreen corresponding to each case, and considering that the flow entering into the cavity through the vent holes is equal to the flow coming out of the air barrier from the leaks. When applied to the lowest venting area configuration of $A_V = 0.007\%$, A_{ab} is equivalent to 24 leakage holes; and becomes 6 leakage holes at $A_V = 0.022\%$. The expected amount of leakage decreases, as the venting area becomes higher, since the differential pressure across the rainscreen decreases while keeping constant the coefficients used in this formula as $n = 0.5$; $K = 0.15$ for the rainscreen and $n = 0.7$; $K = 0.6$ for the air barrier. By including 24 leakage holes in the numerical computer model, and using the same coefficients values, the predicted cavity pressure did not match the experimental signal for $A_V = 0.007\%$. For this reason, the number of leaks had to be increased in order to obtain the actual cavity pressure.

Figure 5.1 shows the time series of the external pressure, experimental and numerical cavity signals, over a short period, in the case of a wide face. The experimental cavity pressure seems much smoother than the applied pressure meaning that high frequency external fluctuations are indeed transmitted to the rainscreen. On the other hand, the most reasonable predicted cavity pressure signal corresponds to 37 leakage holes of 2mm diameter, instead of 24. Clearly, it is following the external pressure in reproducing the majority of fluctuations, which are not present in the real signal signifying that the matching in the spectral analysis will not be satisfactory.
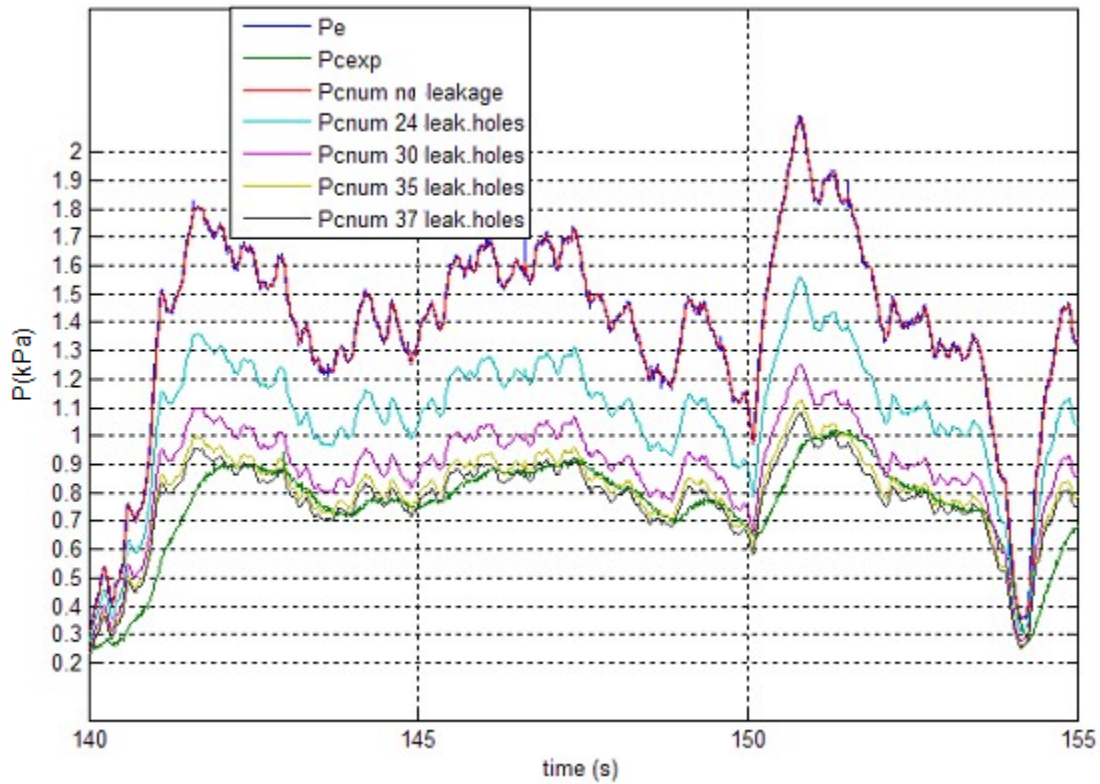
Figure 5.1 Cavity pressure prediction with respect to leakage holes for the single applied signal for wide face ($A_v = 0.007\%$)
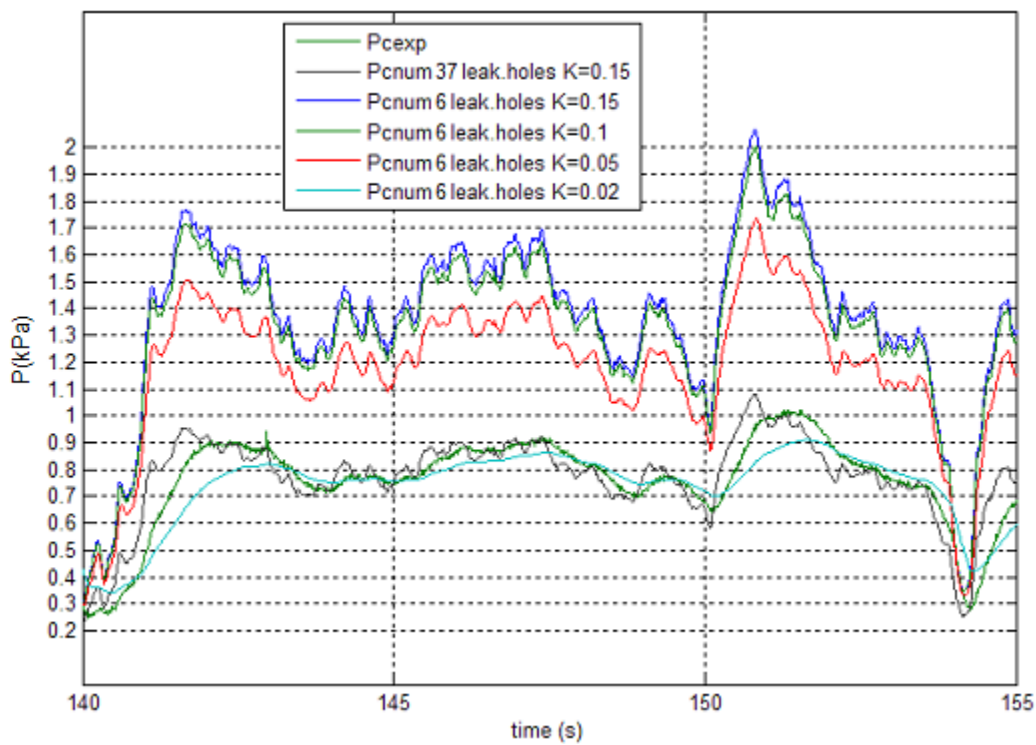
Figure 5.2 Cavity prediction pressure with respect to the Discharge coefficient
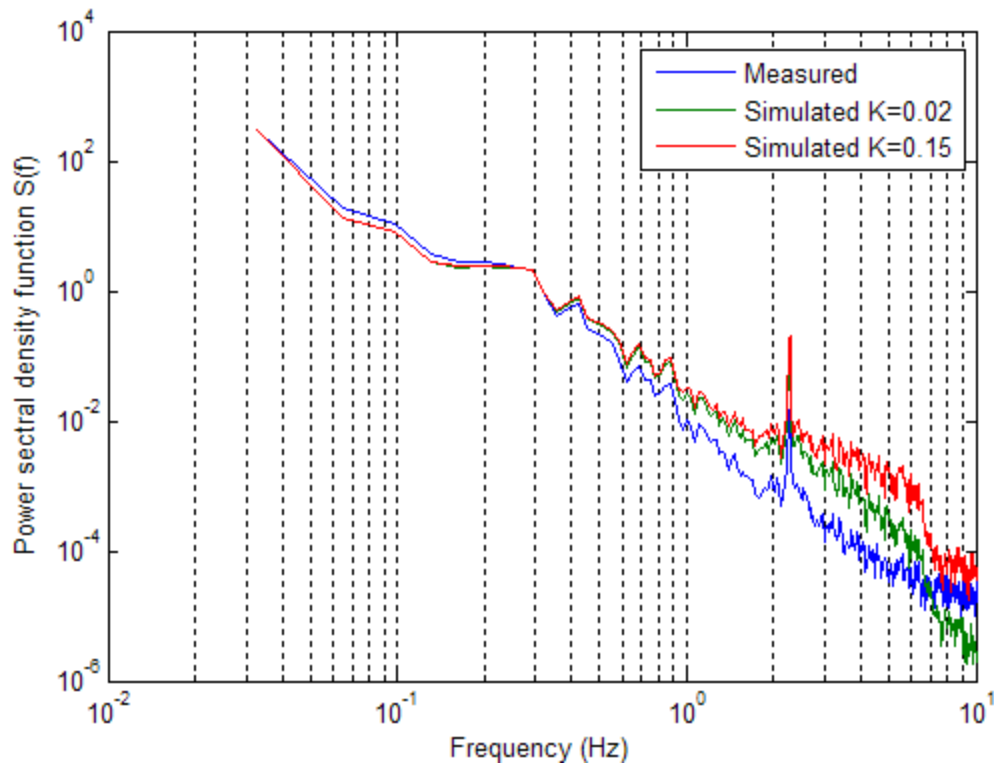
Figure 5.3 Power spectral density function for the cavity pressure for the single applied signal for wide face ($A_V = 0.007\%$)

By trying a lower number of leaks (six leakage holes) and adjusting the value of K until obtaining similar ratio pressure statistics; the numerical model was able to give better prediction in the frequency domain as seen in Figs 5.2 and 5.3. In this case, K is lowered to 0.02, which induces a greater value of loss coefficient $C_L = 1/K^2$. In fact, according to the MDE equations, as the value of the discharge coefficient decreases, the damping term increases, which implies a lower cavity pressure. Also, it can be inferred that the mean pressure drop encountered in this case is not mainly due to leakage in the air barrier. As assumed in chapter 4 section 4.2.2, the flow rate is subject to significant losses while it is transferred through the vent hole of the rainscreen.

Inculet and Davenport (1994) have reached such an extremely low value for the discharge coefficient: they have obtained values for K ranging from 0.01 to 0.56 to get good agreement with experimental transfer functions, in the absence of leakage in

the air barrier, for a wind tunnel PER model of a venting to wall area ratio $0.02\% < A_{rs}/A_w < 0.125\%$. The cavity depth was varied from 0.0055 to 0.0275 m in model scale (length scale is 1:12).

Table 5.1 presents the numerical values for the discharge coefficient K for the rainscreen for all venting configurations when a single pressure signal is applied to the PER model referring to a wide face signal. The numerical simulations show that at low venting areas ($A_V = 0.022\%$ and $A_V = 0.03\%$), the agreement between statistical values of experimental and predicted cavity pressures can be attained by two combinations: either a high number of air barrier leakage holes (37) in conjunction with a relatively high value of discharge coefficient ($K=0.15$) which normally applies to the fluctuating reversing flows and unidirectional oscillating flow conditions; or a lower number of leakage holes (6) with a lower value of $K = 0.03$. These two combinations lead to similar results in the frequency domain, as we will see later, in contrast with the lowest venting area ratio case $A_V = 0.007\%$.

Trial numerical simulations that were performed to obtain the optimum matching are also shown in terms of numerical to experimental statistical ratios. For high rainscreen venting area ratios ($A_V \geq 0.11\%$), the inclusion of leakage holes in the model does not affect the predicted cavity pressure. Thus, similar agreement is obtained with or without taking into consideration the air barrier leakage area. Statistical ratios of the numerical to experimental results indeed show a satisfactory matching at $K=0.65$; a value associated with steady flow conditions. Moreover, the numerical model always provides less matching with the experimental minimum values of the cavity pressure among the other statistical values for all venting area ratios.

Although the two leakage amounts lead to the same numerical prediction, it was assumed that the PER assembly has a constant amount of six leakage holes, since it

provided the best match at $A_v = 0.007\%$. Thus, Table 5.1 the optimum values for flow exponent and discharge coefficient taken marked in bold for each configuration.

Number of holes	Venting Area ratio (%)	Rainscreen		Numerical / Experimental cavity pressure				Leakage holes (2mm)	Air barrier	
		n	K	mean	max	min	rms		n	K
1	0.007	0.5	0.65	1.81	1.93	1.39	1.83	None	-	-
		0.5	0.15	1.81	1.94	1.47	1.83	None	-	-
		0.5	0.15	1.01	0.93	1.13	1.00	37	**0.7**	**0.6**
		0.5	0.15	1.77	1.87	1.42	1.79	6	0.7	0.6
		0.5	**0.02**	**1.00**	**0.90**	**1.02**	**0.98**	**6**	**0.7**	**0.6**
3	0.022	0.5	0.65	1.02	1.04	9.26	1.03	None	-	-
		0.5	0.15	1.02	1.05	9.26	1.03	None	-	-
		0.5	0.65	1.07	1.05	0.73	1.06	37	0.7	0.6
		0.5	0.45	1.06	1.05	0.73	1.06	37	0.7	0.6
		0.5	0.30	1.04	1.03	0.73	1.03	37	0.7	0.6
		0.5	**0.15**	**0.98**	**0.95**	**0.66**	**0.97**	**37**	**0.7**	**0.6**
		0.5	0.12	0.94	0.89	0.66	0.29	37	0.7	0.6
		0.5	0.1	0.89	0.82	0.63	0.25	37	0.7	0.6
		0.5	0.15	1.07	1.08	0.83	1.08	6	0.7	0.6
		0.5	0.10	1.06	1.07	0.77	1.06	6	0.7	0.6
		0.5	0.06	1.05	1.04	0.70	1.03	6	0.7	0.6
		0.5	**0.03**	**0.99**	**0.97**	**0.60**	**0.98**	**6**	**0.7**	**0.6**
		0.5	0.02	0.95	0.89	0.56	0.90	6	0.7	0.6
4 (at bottom)	0.03	**0.5**	**0.15**	**0.99**	**0.97**	**0.84**	**1.01**	**37**	**0.7**	**0.6**
		0.5	**0.03**	**1.00**	**0.98**	**1.05**	**0.95**	**6**	**0.7**	**0.6**
4 (top & bottom)	0.03	**0.5**	**0.15**	**1.02**	**1.00**	**1.60**	**0.97**	**37**	**0.7**	**0.6**
15 at bottom	0.11	**0.5**	**0.15**	**1.01**	**1.00**	**1.61**	**1.01**	**37 or 6**	0.7	0.6
		0.5	0.65	1.01	1.00	1.61	1.01	None	-	-
15 (top & bottom)	0.11	0.5	0.65	1.18	1.01	1.71	1.09	None	-	-
		0.5	**0.15**	**1.18**	**1.00**	**1.70**	**1.08**	**37 or 6**	0.7	0.6
36	0.27	**0.5**	**0.15**	**1.00**	**1.00**	**1.10**	**1.10**	**37or 6**	0.7	0.6
		0.5	0.65	1.00	1.00	1.10	1.00	None	-	-

Table 5.1 Ratio of numerical and experimental cavity pressure for the single signal, wide face
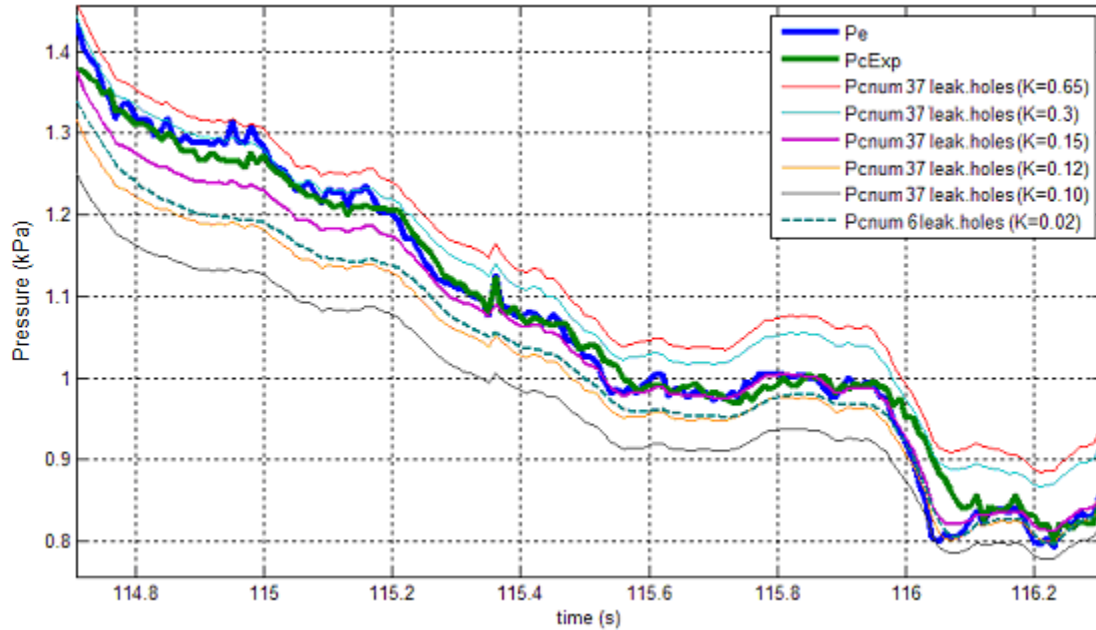
Figure 5.4 Cavity pressure for a single applied pressure signal for a wide face
($A_V = 0.022\%$)

Figure 5.4 depicts the cavity time series signal with respect to the discharge coefficient at a 37-leakage holes amount for the configuration $A_V = 0.022\%$. However, at $K = 0.15$ supposed to be the optimum value, the measured cavity pressure does not perfectly collapse with the simulated signal. It is either underestimated or overestimated; this will certainly lead to discrepancies in the transfer functions plots.

The narrow face case, being subject to the same single external pressure has similar values for discharge coefficient in the simulations in all configurations.

The numerical values for the other parameters used in the computations are listed below:

$\rho_a = 1.227 kg / m^3$: air density

$\mu = 1.5 * 10^{-5} N.\sec/ m^2$: kinetic viscosity of the air

$\gamma = 1.4$: ratio of specific heat of air

$$p_0 = 10^5 Pa \qquad \text{: atmospheric static pressure}$$

$$K_A = \gamma P_0 = 141999 Pa \qquad \text{: bulk of modulus}$$

$d = 20mm$ for vent opening, 2mm for leakage hole   :diameter of orifice

5.3 Results and Discussion

5.3.1 Single Applied Pressure Signal

Figure 5.5 presents a comparison between measured and simulated statistics, corresponding to the cavity to external pressure ratio for the basic venting configurations for the wide face case.
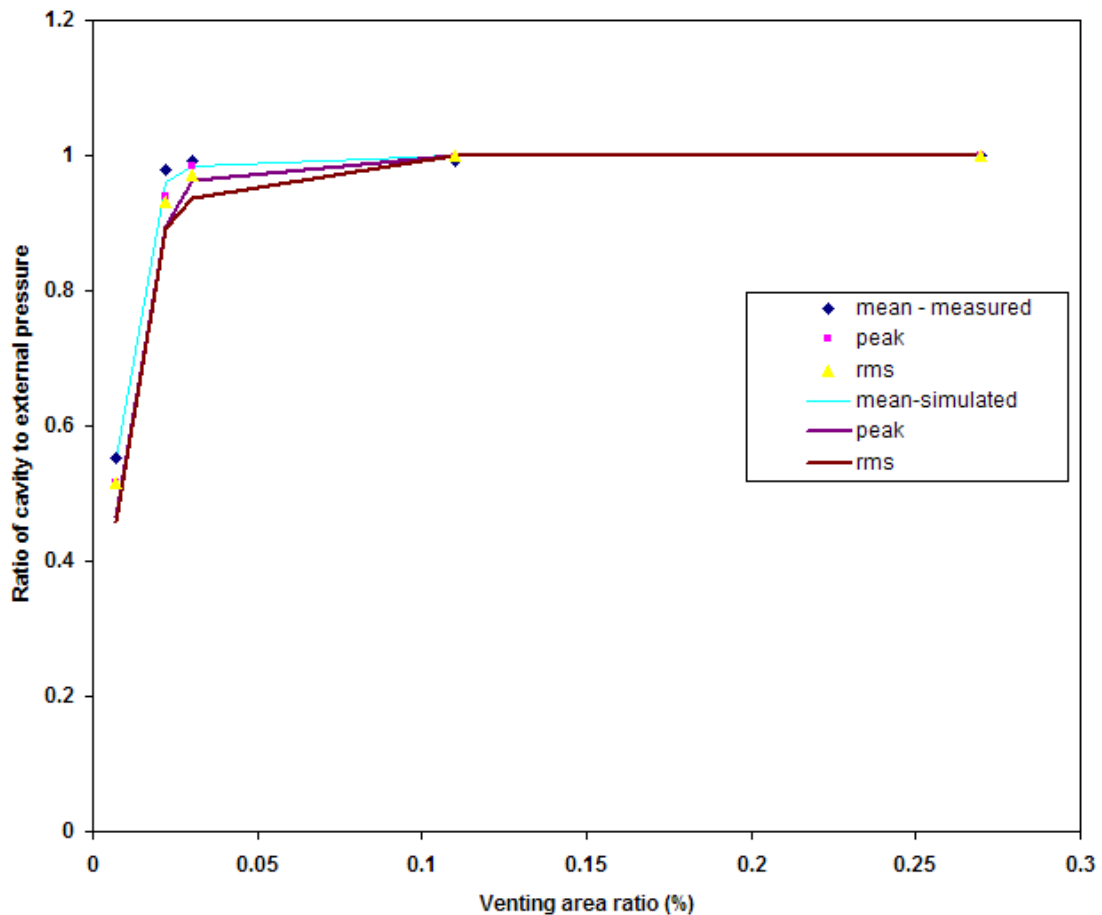

Figure 5.5 Basic statistics for the basic venting configurations for the wide face

Statistics of the simulated cavity pressure are clearly lower than those of the full-scale data at low area venting ratios, which is in agreement with the findings of Inculet (1990) and Kumar (1999). The mean values are slightly different, while peaks and rms are significantly underestimated. The matching between simulations and measurements improves at higher venting area ratios. At $A_V \geq 0.11\%$, a good match is shown, and reflected in the power spectral density functions collapse observed in Fig 5.6b. Similarly, Kumar found that the simulated spectral density function slightly under predicted when he tested a PER model panel was tested at $A_V = 0.11\%$. However, in his case the differences were bigger due to the large cavity depth (0.15m) and different leakage characteristics. At $A_V = 0.022\%$ Fig 5.6 indicates that the magnitudes of the spectral density for the cavity pressure are higher in case of simulations.

Discrepancies between simulated and measured data are also described in terms of transfer functions for the cavity over the external pressure with respect to the venting area ratio. Solid line curves refer to the experimental results while numerical simulations are presented by dashed-line. At first, Figure 5.7 shows for low rainscreen venting area ratios the predicted transfer functions based on the two input data combinations already included in the numerical model. The matching of experimental with measured transfer functions in the frequency domain appears almost similar in both cases, which means that airflow losses due to high leakage through the air barrier (37 leakage holes with $K = 0.15$) are theoretically balanced with high damping losses through the rainscreen (6 leakage holes with K=0.03).

Figure 4.8 describes the matching between measured and simulated transfer functions for all rainscreen-venting configurations. At low-venting ratios, the numerical model overpredicts the measurements with a fairly good match at low frequencies; the transfer functions corresponding to the simulated cavity pressures have in general a similar trend to those of the experimental signals. However, they start to roll-off at higher frequencies; in comparison with the actual experiments transfer functions that roll-off much earlier.
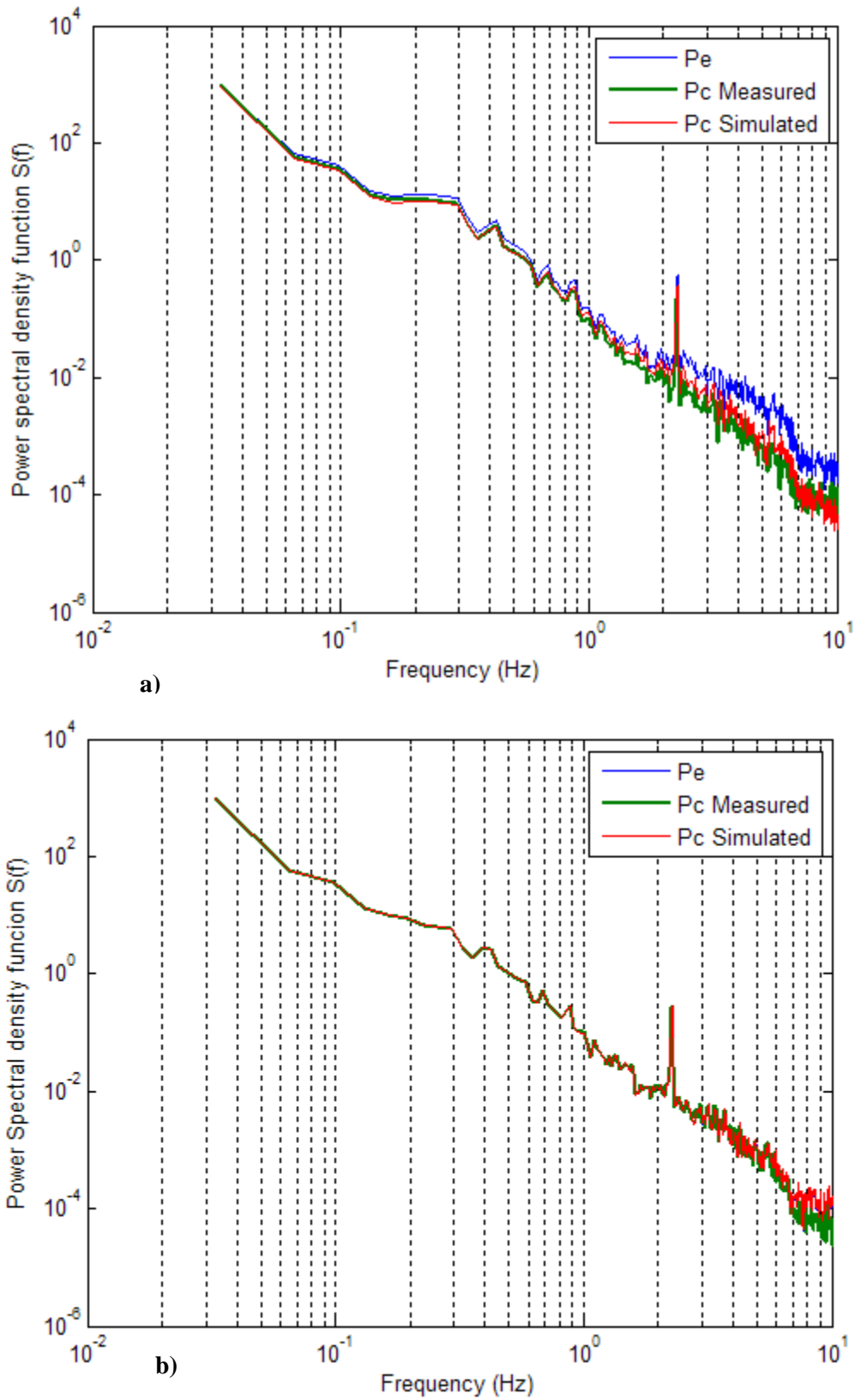
Figure 5.6 Spectral density functions for the cavity pressure for the wide face case **a)** $A_V = 0.022\%$ **b)** $A_V = 0.11\%$
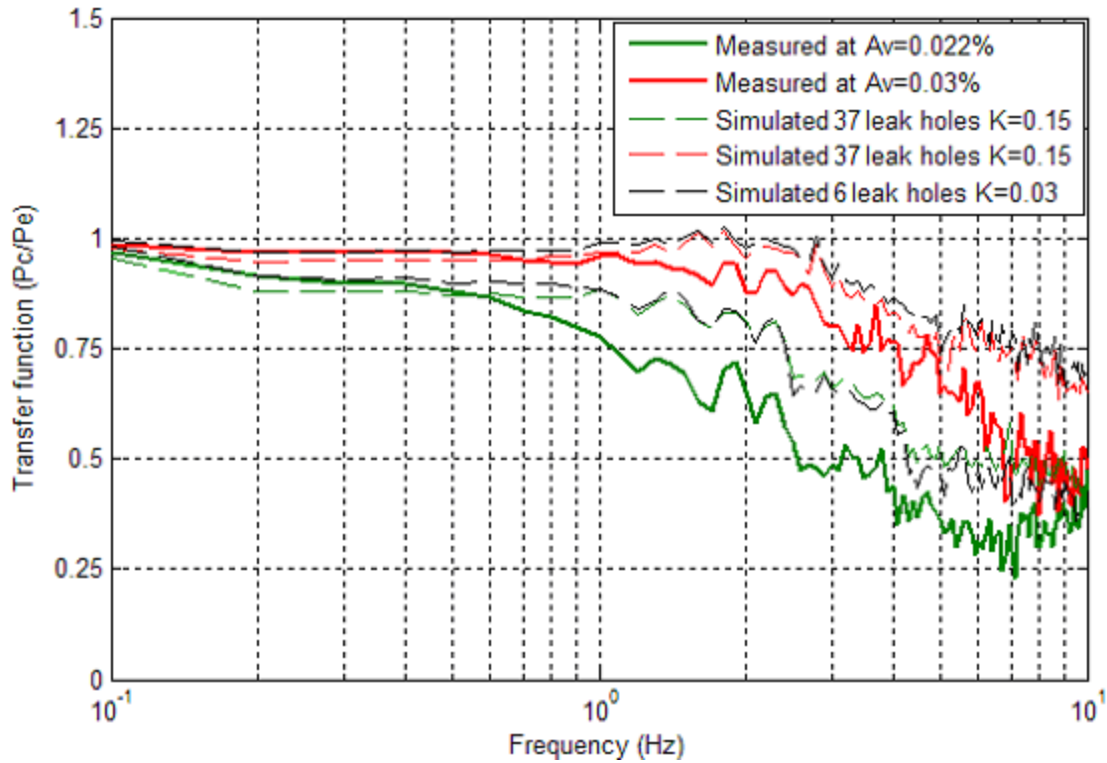
Figure 5.7 Effect of discharge coefficient and leakage holes on transfer functions
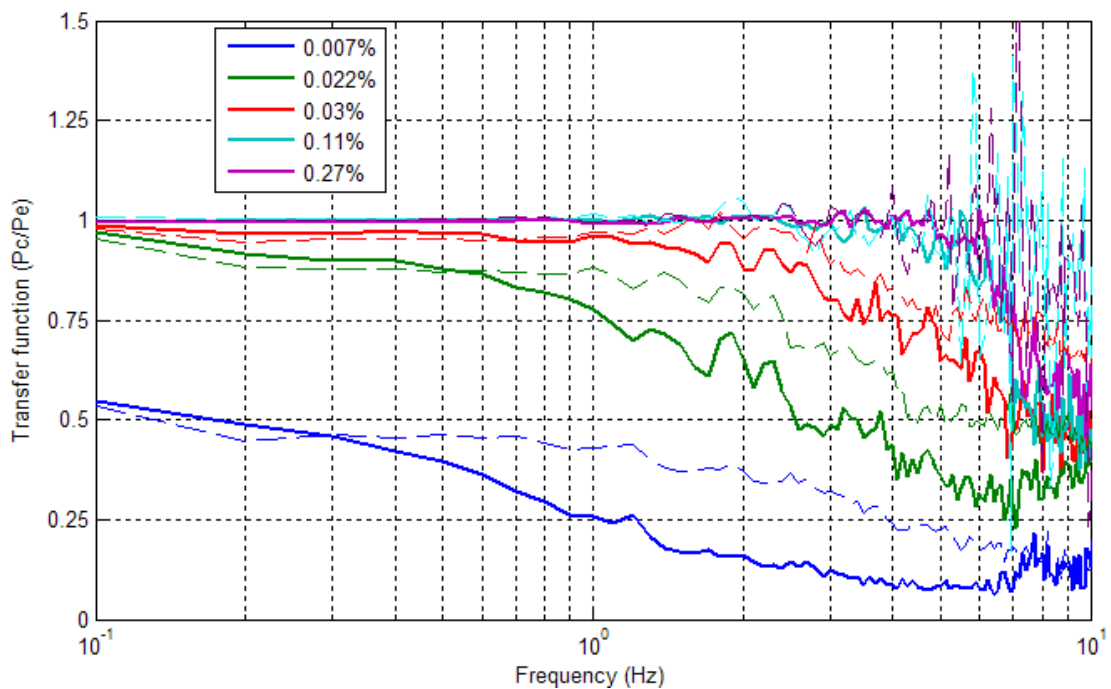

Figure 5.8 Comparison of measured and simulated cavity to external pressure ratios using transfer functions (wide face)

Therefore, in the case of simulations, higher frequencies of external pressure fluctuations are transmitted to the cavity, which was not expected from the comparison previously established between measured and simulated basic statistics. At high venting area ratios, the numerical model has the same qualitative behaviour of the experiment, but tends to slightly overpredict it.

In light of these results, we can admit that the model used for numerical simulations shows difficulties in predicting the cavity pressure at low rainscreen venting to wall area ratios; where the aerodynamic damping seems not to be fully captured, irrespective of the air barrier leakage area taken into account. Such performance might be explained by the possibility of other phenomena that are controlling the most the air movement at high frequencies (i.e. the three dimensionality of the flow) and which are not numerically simulated. In addition, another interpretation can be related to the numerical equations. In fact, when the number of vent holes becomes larger, the associated number of MDE equations is increased as per section 2.3.2; thus the number of damping associated terms increase and frequency fluctuations are predicted well. Therefore, the differences between measured and simulated data can be attributed to the way the damping term is linearized in terms of the air slug velocity $\dot{x}$. Moreover, there is maybe a certain damping term missing in the equations or it is not quite right and it depends on the area-venting ratio A_{rs}/A_w.

Inculet and Davenport (1994) with Kumar et al. (1998) found similar differences in transfer functions. Inculet and Davenport (1994) developed a numerical function based on Helmholz resonator model and they claimed that the discrepancy between experimental and computer model as a result of linearization of the damping term. The used range of rainscreen venting to wall area ratio was from to 0.02 % to 1%.

On the other hand, Kumar used a different method, which is the first principle model, and attributed the differences to the incorrect assumptions made in the model. Kumar combined all the rainscreen venting openings into one opening, and he applied the same concept to the air barrier leakage paths. He used then, as a single exterior

pressure input, the averaged exterior pressure as acting on a single opening rather than applying the exterior pressure data to each vent opening separately, as done in the current numerical simulations. Therefore, the proposed model did not use the appropriate damping flow term for each vent hole, instead, it considered the damping of flow through a single vent hole and the spatial non-uniformity of pressures acting on the panel were not taken into account; which is not the case here.

As the damping term seems to be the key parameter in the numerical simulations, the rainscreen discharge coefficient K was modified in order to see its effect on the predicted transfer function, based on an air barrier leakage to rainscreen venting area ratio $A_{ab}\big/A_{rs} = 0.125$ referring to 37 leakage holes. Figure 5.9 refers to the case of the wide face where $A_V = 0.022\%$. The plots show that the best match with the measured cavity to external pressure transfer function at low frequencies is associated with $K = 0.15$ as already revealed in Table 5.1. As K decreases, the underestimation of low frequencies fluctuations becomes more significant, while the gap between simulated and measured transfer functions is reduced, at first impression. However, all the simulated transfer functions, being parallel, start to roll-off at 2 Hz tending to collapse at higher frequencies, while the transfer function corresponding to the actual experiment rolls off at 0.7Hz. This behaviour proves, again, that there is a damping-related issue in the numerical model. The general behaviour of the simulated transfer functions is right, but the rolling is occurring at higher frequencies. Apparently, the equations are not exactly evaluating the critical damping frequency above which attenuations occur.

Such trend has been clearly described by Kumar et al. (1998), as Fig 5.10 shows. However the transfer functions curves appear as reversed, since the ordinates represent measures of the ratio of the differential pressure acting on the rainscreen, instead of the cavity pressure. In his test he had to lower the value of the discharge coefficient to 0.49 from the steady flow value of 0.61 to obtain the measured mean differential pressure across the rainscreen. Similarly, the slight overprediction at low frequencies gets wider in conjunction with a better match at higher frequencies.
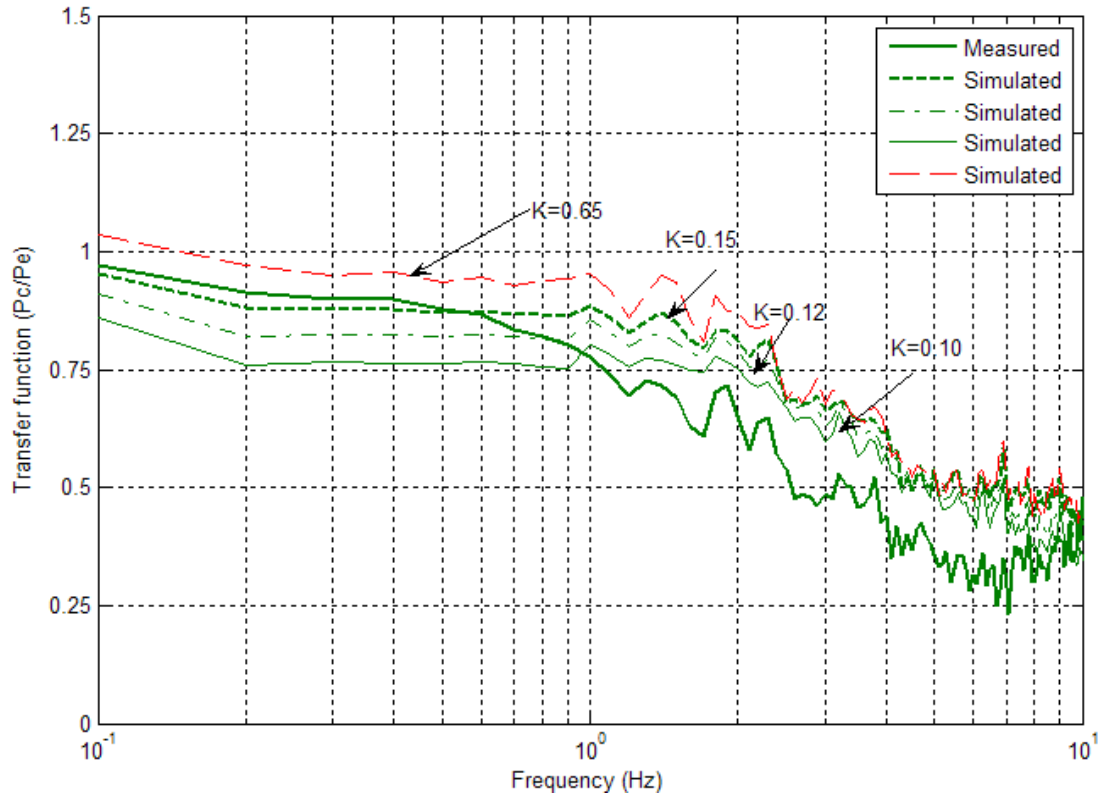
Figure 5.9 The effect of K on transfer function $A_v = 0.022\%$, d_c =25mm (wide face)
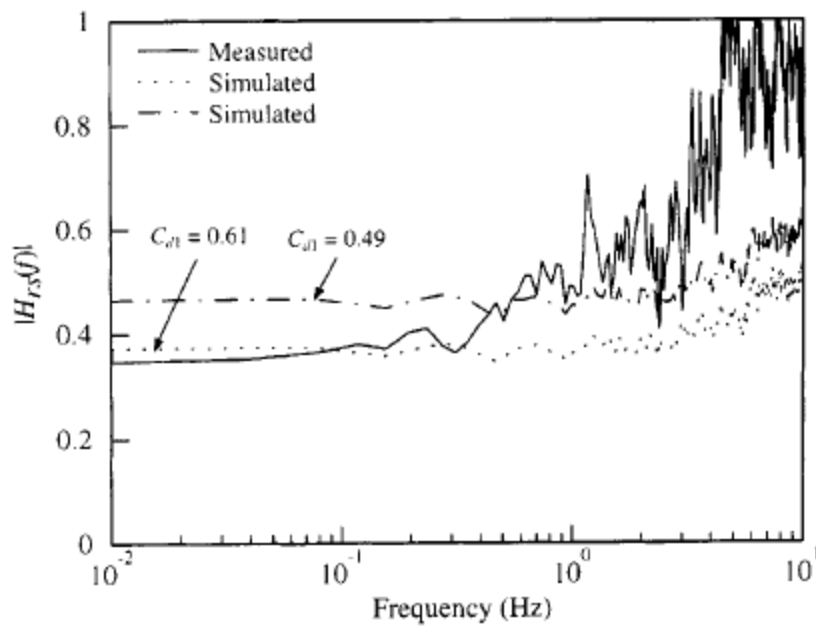
Figure 5.10 The effect of discharge coefficients on rainscreen pressures, reproduced from Kumar et al. (1999) $A_v = 0.15\%$ d_c =150mm

Inculet and Davenport (1994) had also to adjust K to 0.19 in order to have satisfactory agreement in terms of transfer functions, when having a leakage ratio of $A_{ab}/A_{rs} = 0.23$.

Figure 5.11 presents a comparison between simulated and measured cavity response pressures in terms of the phase angle established between the external applied and cavity pressures for each configuration. In this case, the match between numerical and experimental results is poor at low venting areas: the phase angle is much smaller in the case of simulations; it shows zero value at $A_V = 0.022\%$ and $A_V = 0.03\%$, thus the real trend disappears. This says, again, that the numerical model is highly underestimating the damping process. At high venting ratios, the phase angle presents a good agreement with a slight overprediction similarly to the transfer function numerical simulation.

According to the variation of the discharge coefficient K, it provides minor variations to the phase angle when it becomes lower, by taking into account the same amount of leakage holes (37 holes), which means that the value of the discharge coefficient is not the real obstacle for a good prediction (Figure 5.12). It does not affect significantly the phase shift established between applied and cavity pressure based on the numerical model. The problem is, rather, related to a whole term that depends on the rainscreen venting area ratio.
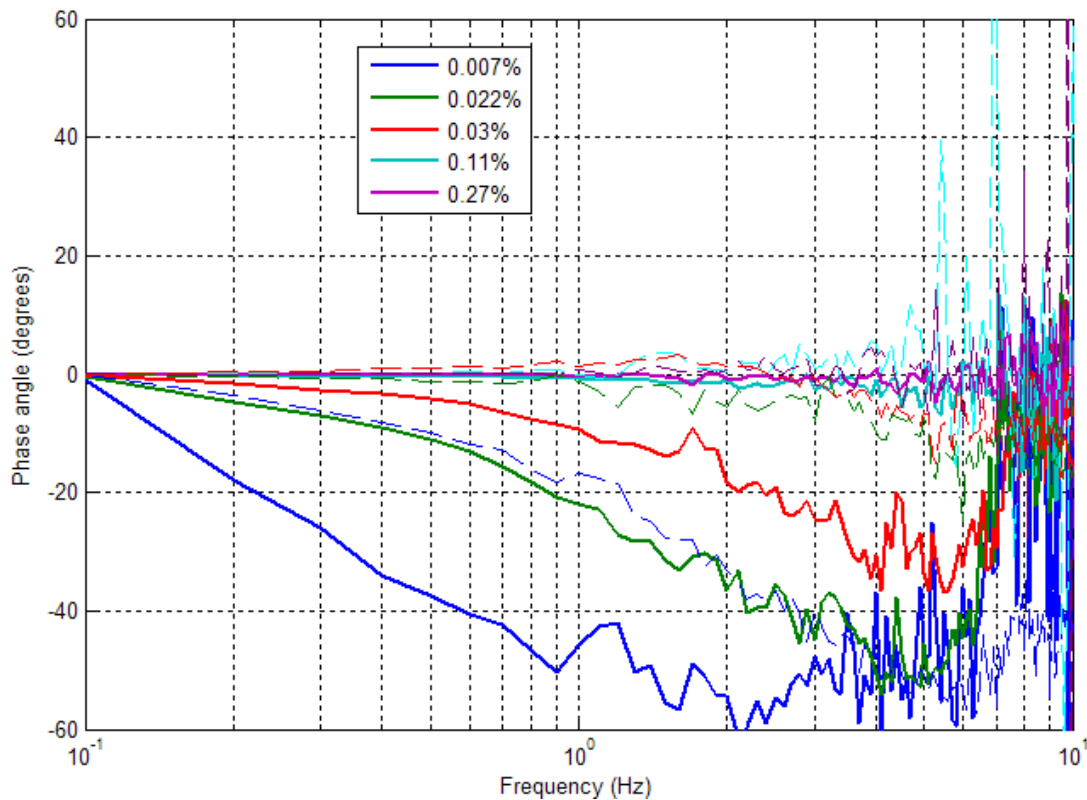
Figure 5.11 Comparison of measurements and simulations with phase angles (wide)
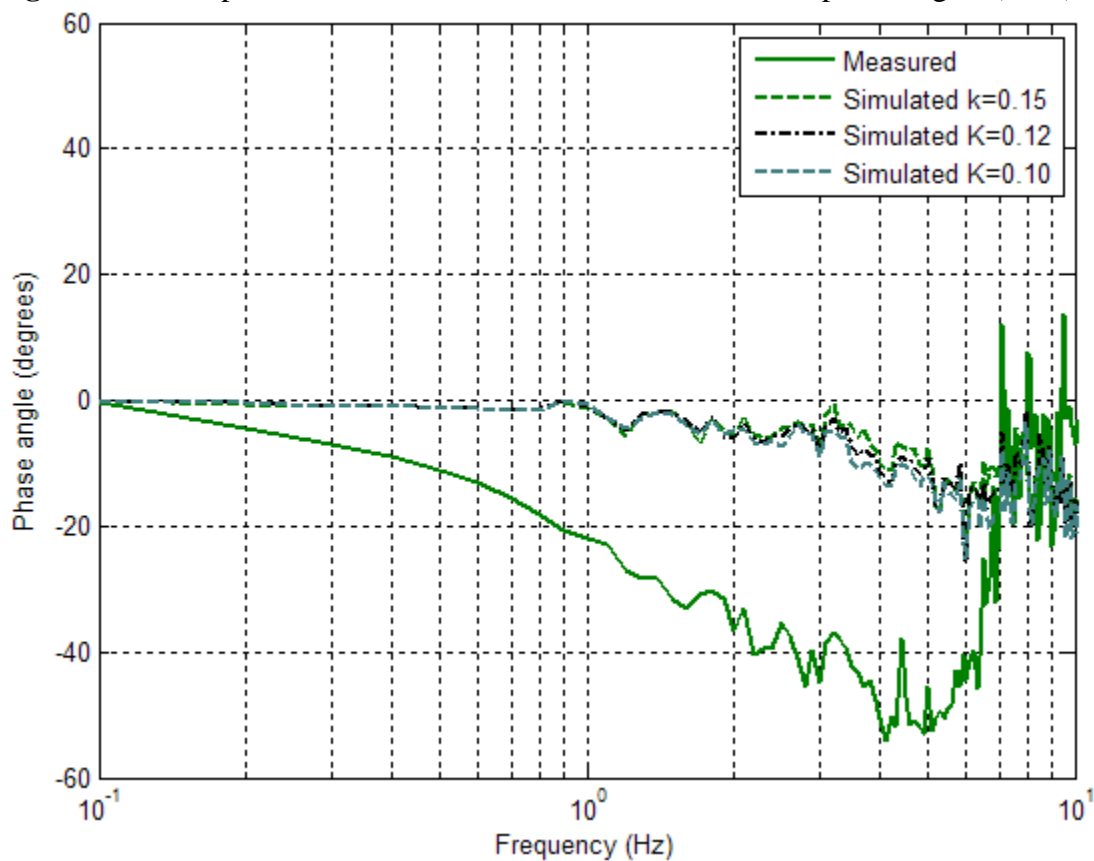
Figure 5.12 The effect of K on the phase angle $A_v = 0.022\%$ (wide face)
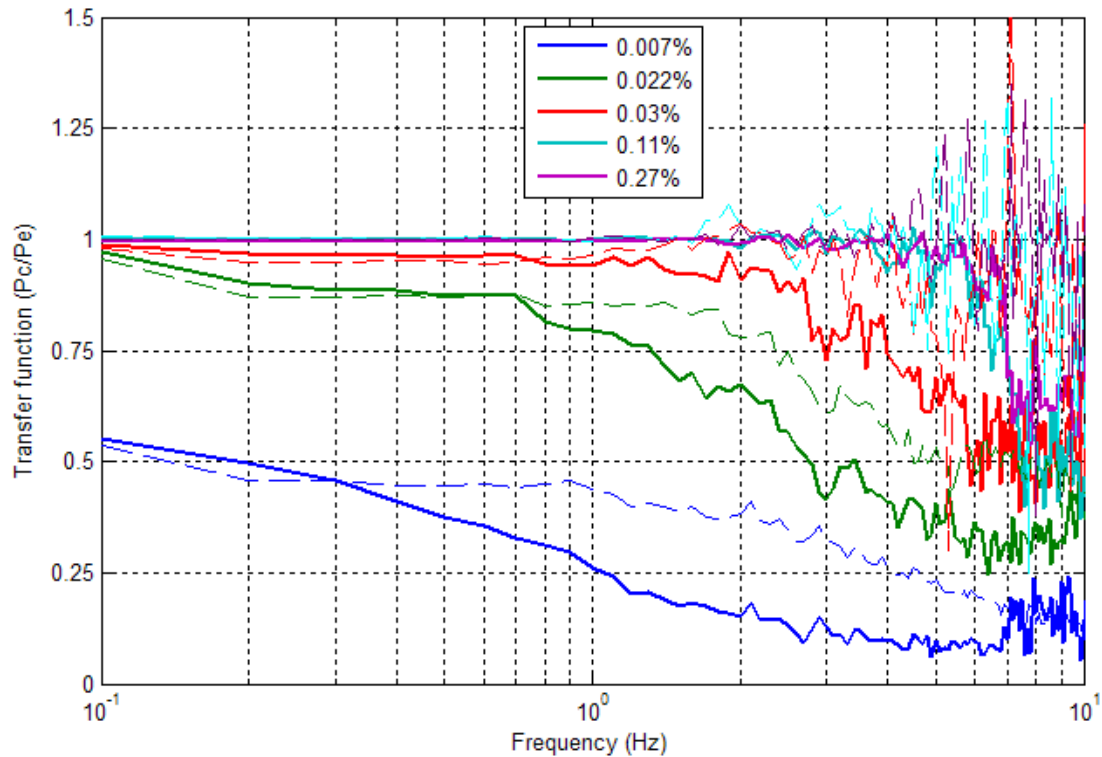
Figure 5.13 Comparison of measured and simulated cavity pressures using transfer functions (narrow face)

The narrow face case exhibits similar results to the wide face when comparing the simulated and measured transfer functions and phase angles, since it is subject to the same applied single signal. Figure 5.13 presents the transfer function plots for the five basic rainscreen venting configurations, solid lines refer to full-scale data while the numerical predictions are represented by the dashed line. The predicted transfer functions show a similar trend when comparing to the wide face case producing similar phase angle plots.

On the other hand, the predicted cavity pressure signal represents similar matching behaviour with the external pressure when the rainscreen venting openings are redistributed between top and bottom. At high venting areas, the agreement is satisfactory, while the damping process is not fully captured at low venting areas. Actually, the numerical model used in this project does not take into account the spatial distribution of the venting openings; it only uses the number of vents and the corresponding external pressures. Therefore, it does not distinguish between the vent location whether they are all at the bottom or not.

5.3.2 Three Different Pressure Signals

Numerical simulations are performed using the same computer program as in the previous case, with one difference in that the input pressures vary between the venting holes based on their locations under the three or six pressure boxes, as they refer to three applied different signals. Also, they are fed into the model as read in the experiment by the pressure transducers.

Number of holes	Venting Area ratio (%)	Rainscreen		Numerical / Experimental cavity pressure				Leakage holes (2mm)	Air barrier	
		n	K	mean	max	min	rms		n	K
3	0.022	0.5	0.15	1.08	1.00	1.00	1.06	37	0.7	0.6
4 (at bottom)	0.03	0.5	0.15	1.06	1.03	1.07	1.05	37	0.7	0.6
15 at bottom	0.11	0.5	0.15	1.06	0.98	1.00	1.04	37	0.7	0.6
		0.5	0.65	1.06	0.98	1.00	1.04	None	-	-
15 (top & bottom)	0.11	0.5	0.65	1.21	1.03	1.02	1.04	None	-	-
		0.5	0.15	1.20	1.03	1.02	1.03	37	0.7	0.6
36	0.27	0.5	0.15	1.04	1.00	0.97	1.01	37	0.7	0.6
		0.5	0.65	1.04	1.00	0.97	1.01	None	-	-

Table 5.2 Ratio of numerical and experimental cavity pressure for the three applied signals, wide face

Table 5.2 presents the numerical values for the equation coefficients as used in the numerical model for the wide face, taking into consideration the air barrier leakage characteristics as being constant for all configurations. These values apply also to the narrow face case, and they result in the best matching in terms of cavity pressure time series signals and transfer functions. Moreover, the inclusion of leakage holes does not affect anymore the cavity response pressure when the venting area becomes equal to 0.11% , despite the existence of an external pressure gradient. This is attributed to the high rainscreen venting to air barrier leakage area ratio $A_{rs}/A_{ab} = 40 > 10$; which leads to a full pressure equalization according to Ganguli and Dalgliesh (1988).
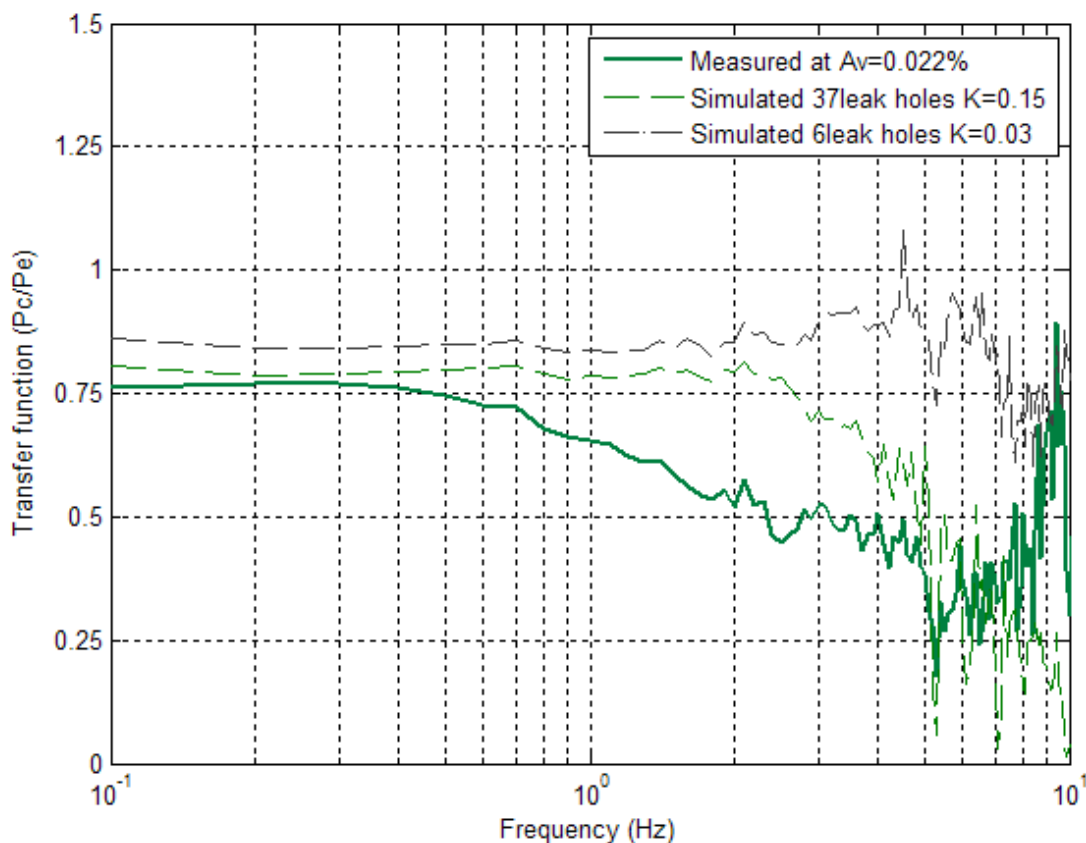
Figure 5.14 Effect of discharge coefficient and leakage holes on transfer functions

Unlike the single pressure signal, lowering the discharge coefficient to the extreme value of 0.03 and the leakage air barrier area to 6 leakage holes does not produce the same matching of the predicted signal with the experimental cavity pressure. As Figure 5.14 shows, the predicted frequencies get worse in low and high frequency regions when the leakage area is decreased. This means that a pressure gradient applied to the PER wall compartment might induce additional flow losses behind the rainscreen, which may be interpreted by a higher amount of air barrier leakage for the numerical model. However, such explanation may not be valid in the absence of proof for a pressure gradient inside the cavity.

On the other hand, the simulated statistics of the cavity response pressure with respect to the area-averaged pressure of the three applied signals are higher than the experimental values, when three different signals are applied to the PER wall model.
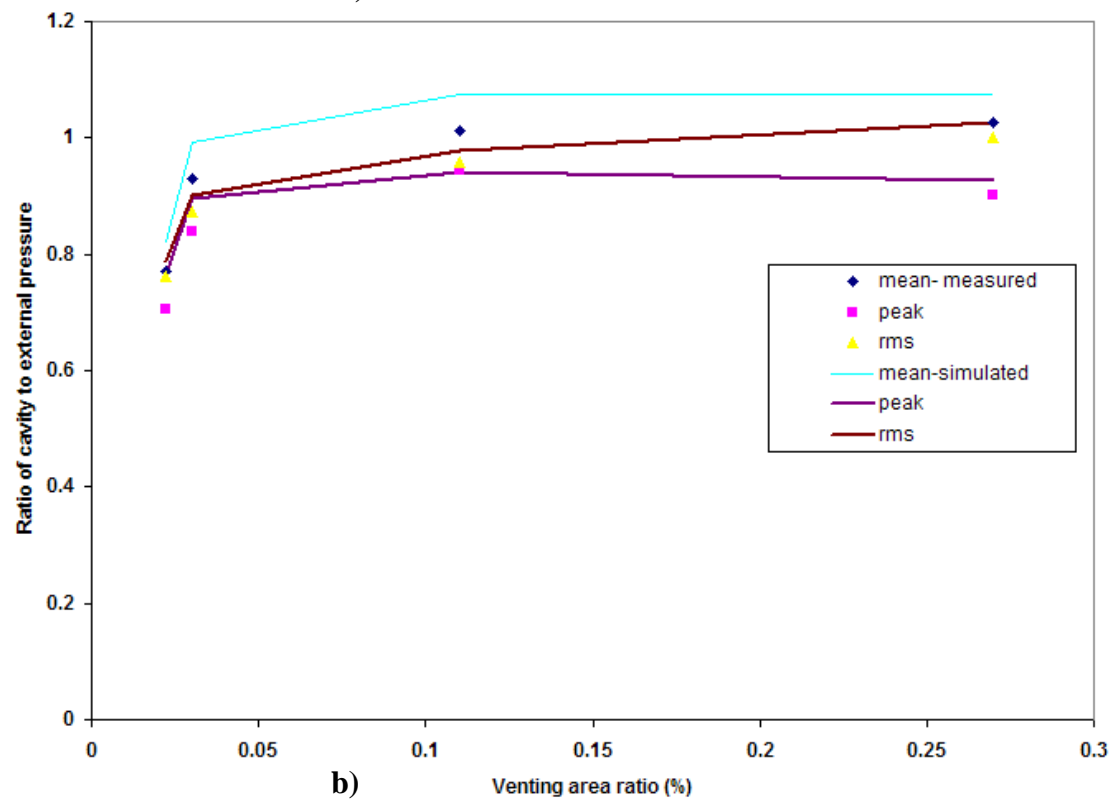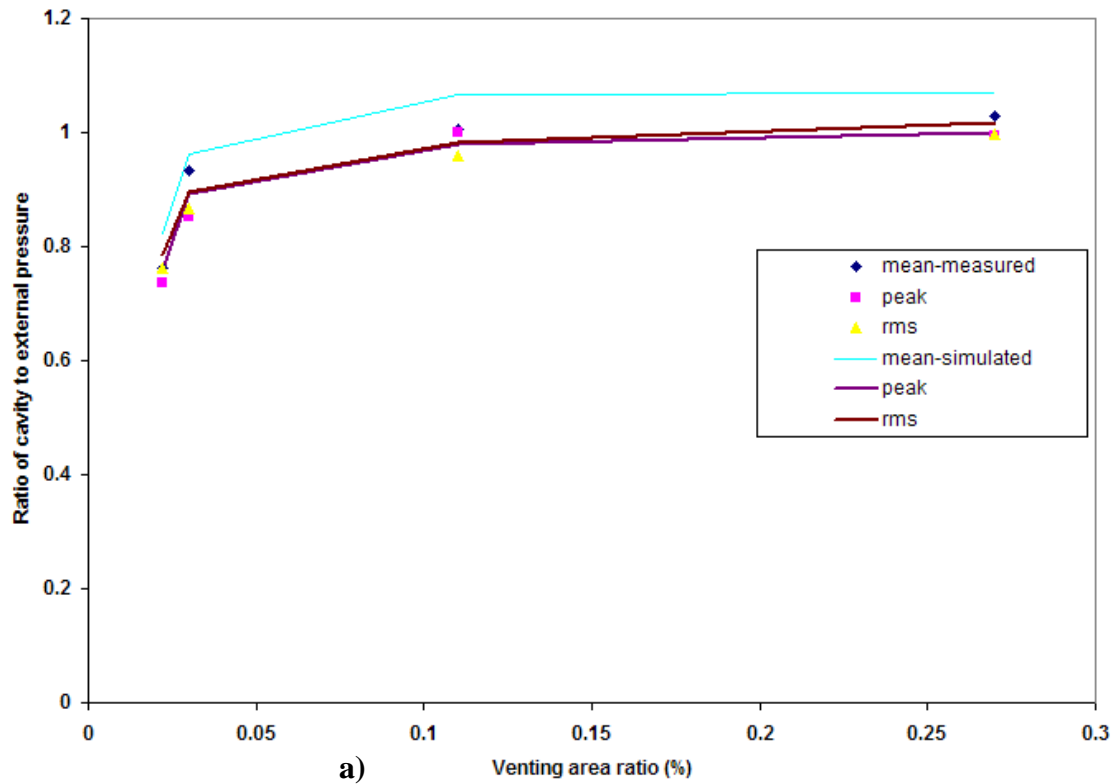
Figure 5.15 Basic statistics for the basic venting configurations for a) the wide face and b) narrow face
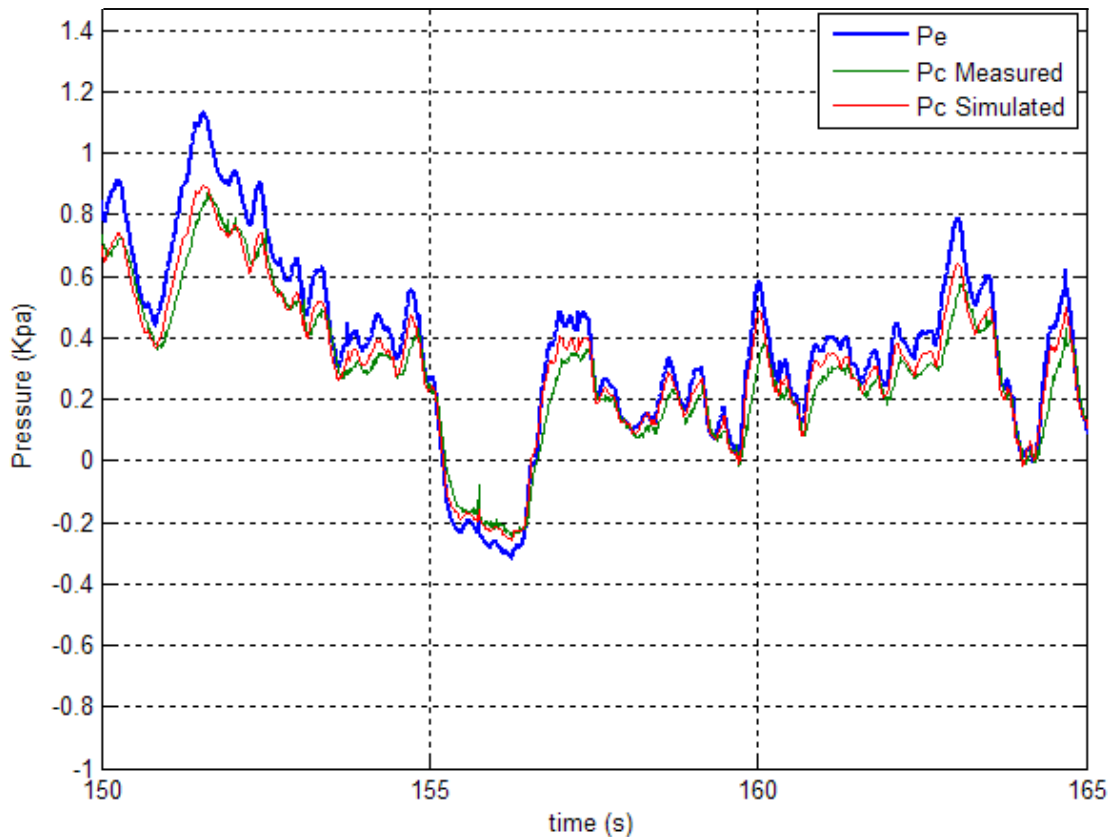
Figure 5.16 Cavity pressure for a single applied pressure signal for a wide face
($A_V = 0.022\%$)

The mean ratios are significantly overestimated in case of the simulations at all venting area for both the wide and narrow faces as seen in Fig 5.15. Also, the numerical values of peaks and rms ratios are higher than the full-scale data at low frequencies, while the agreement becomes much better at high venting ratios, which indicates that the model is able to capture the majority of external fluctuations. As a sample of time series prediction, Figure 5.16 shows the predicted cavity pressure response in case of the lowest venting area where $A_V = 0.022\%$ for the wide face. Clearly, the signal is overestimated with respect to the experimental cavity that is much smoother especially at high amplitudes. This is illustrated in Fig 5.17a where the magnitudes of the power spectral density function of the simulated cavity pressure are higher than the experimental results.
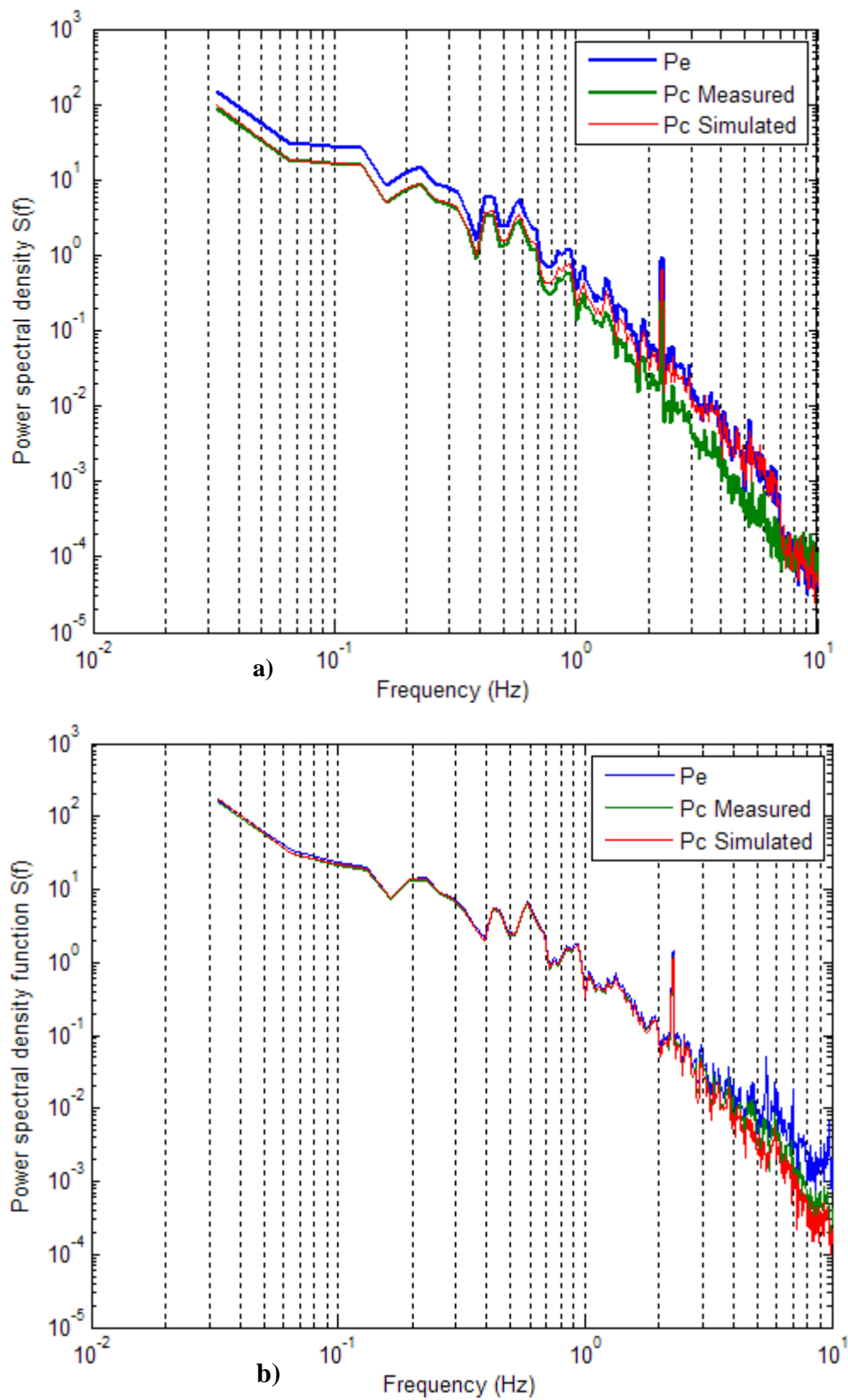
Figure 5.17 Spectral density function for the cavity pressure for the wide face
a) $A_V = 0.022\%$ b) $A_V = 0.11\%$

When the venting area ratio is increased, there is a fairly good agreement between the measured and simulated spectral function as shown in Fig 5.17b for $A_V = 0.11\%$. The transmission of external high frequencies seems, however, better in the actual experiment since the measured peak cavity to area-averaged pressure peak ratio is higher than the predicted value.

In terms of transfer functions, the agreement between measured and simulated transfer function of the cavity over the area-averaged pressure generally improves as the rainscreen venting area ratio increases, as previously shown for single applied pressure signal. However, slight differences are detected in the predicted transfer function when an external gradient pressure occurs. As Fig 5.18a shows, the transfer function for the simulated cavity pressure for the wide face case has in general a trend close to that of the measured signal at all venting configurations, with a slight over prediction at low frequencies. More specifically, at low venting area ratios where $A_V \leq 0.03\%$, the numerical model overpredicts the measurements, the simulated curves start rolling off at high frequencies, until they collapse with the measured transfer functions at around 5Hz; while the measured curves roll-off much earlier. This behaviour proves that the theoretical model has an issue with the damping prediction.

At higher venting areas ratios $(A_V > 0.03\%)$, the model is able to predict the critical damping frequency above which attenuations of the external fluctuations occur. However, the decay of the simulated transfer function seems too great in comparison with the measurements. In fact, the transfer functions are underpredicted in high frequency regions. The resultant gap between measured and simulated curves reduces, as the venting area gets higher.

When the three applied pressure signals refer to the narrow face case, the predicted transfer functions exhibit similar behaviour with respect to the venting area ratio and frequency regions, as shown in Fig 5.19.
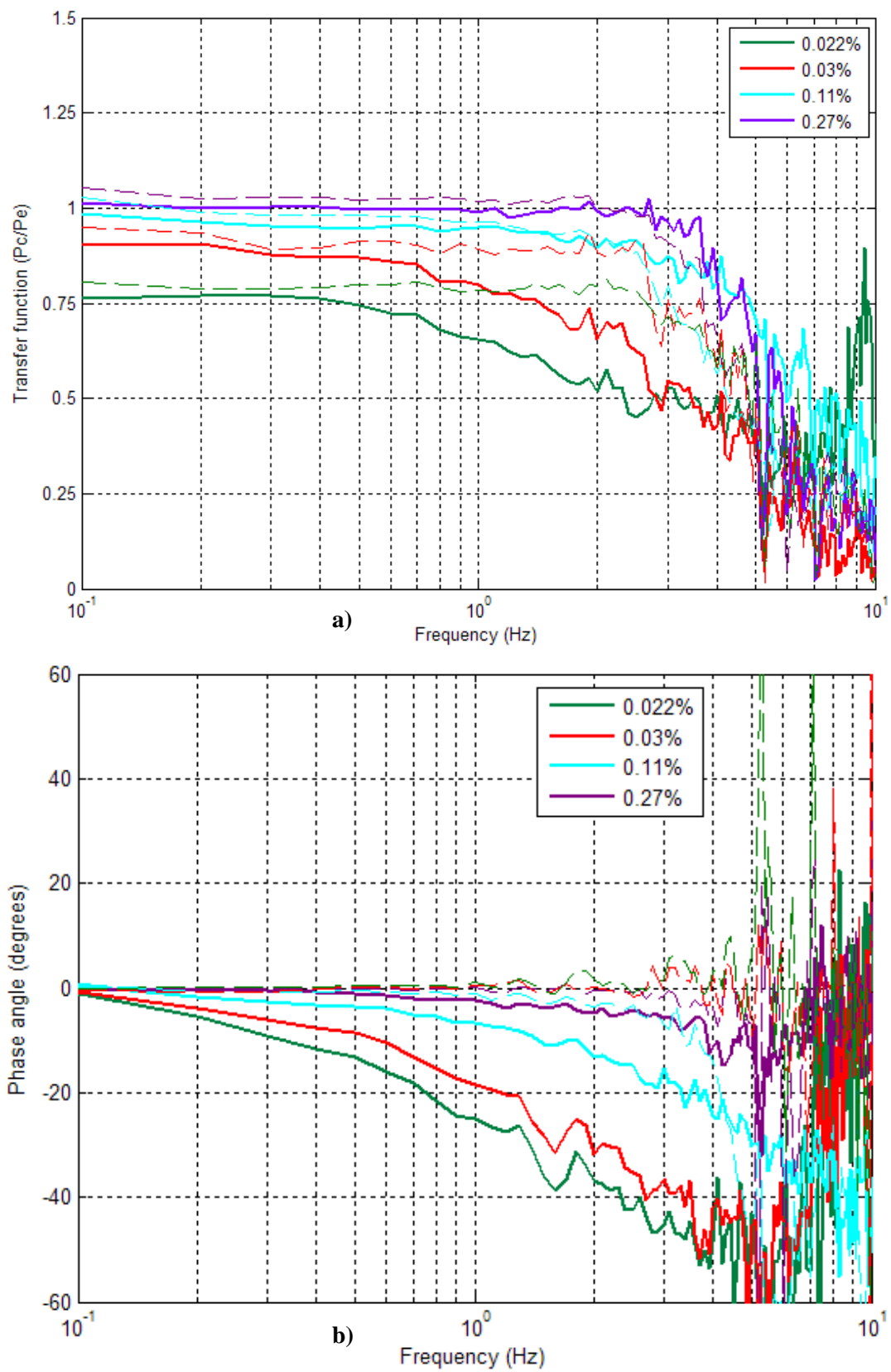
Figure 5.18 Measurements and simulations for the wide face a) transfer function b) phase
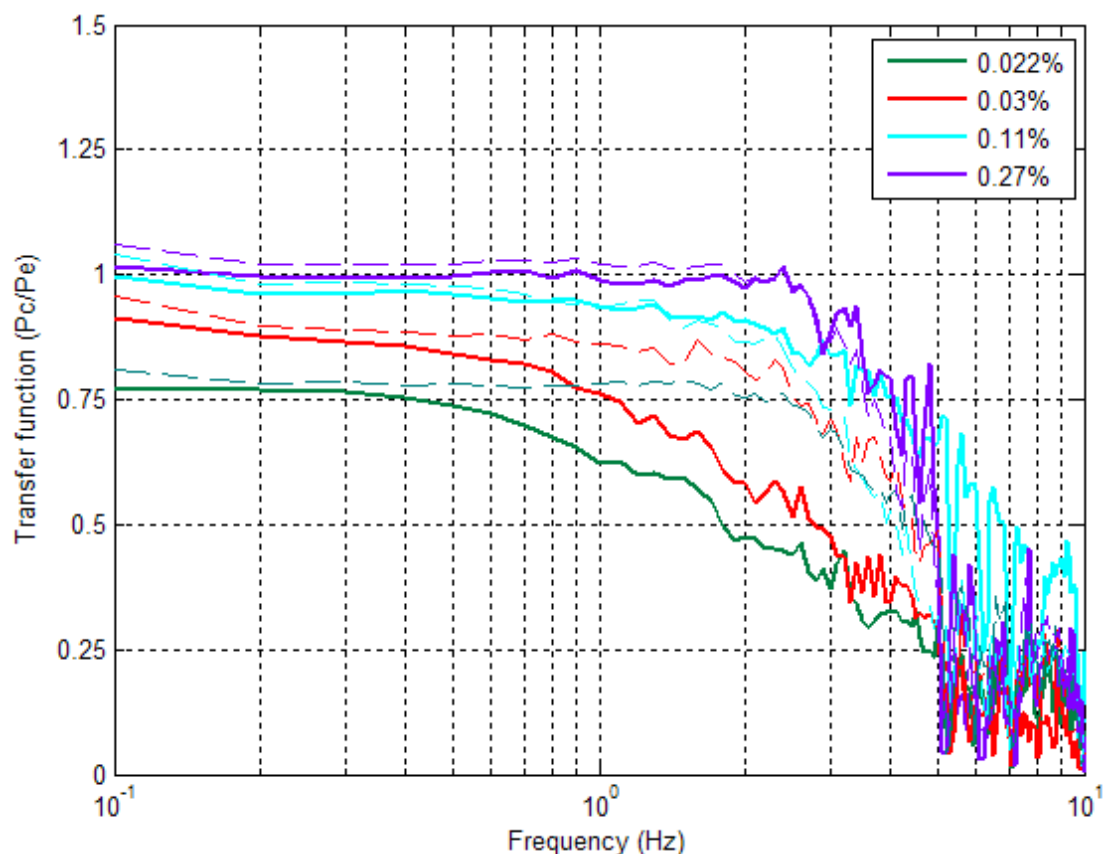
Figure 5.19 Comparison of measured and simulated cavity pressures for the narrow face transfer function

Figure 5.18b shows the predictions of the phase angle in the case of wide face. At low venting area ratios, the real phase lag between cavity and area-averaged external pressure is not captured at all by the numerical model; instead it is considered zero. At high venting ratios, the agreement between measured and numerical phase angle is not perfect as in the case of a single applied external pressure, which probably reflects the transfer function behaviour. The phase angles are overpredicted. At $A_V = 0.11\%$, the phase angle becomes underpredicted after 5 Hz.

Based on the results above, the numerical model presents better performance in the frequency domain at high venting area ratios when a single applied pressure is applied to the PER model. In case of an external pressure gradient, the underpredictions occurring in the simulations at high frequencies may be explained by the fact that the proposed model is not able to estimate the actual transmitted

frequencies associated with the different external pressure fluctuations that are simultaneously applied. At low venting configurations, the discrepancies are due, as before, to underprediction of the damping.

5.4 Numerical Prediction of Cavity Pressure at Various Depths

The same external pressure signals that are used in the previous simulations are provided again to the numerical model in order to predict the cavity response pressure at different cavity depths. The rainscreen and air barrier flow exponents are unchanged, as well as discharge coefficients.

Figure 5.20 presents the statistical peak cavity to external pressure ratios as predicted for a range of cavity depths varying from 50 to 300 mm for both single and three different applied signals for the wide face case; the value of 300 mm is usually the maximum cavity depth for PER wall used in the industry. As the continuity equation (Eqn (2.17)) from the Helmholtz resonator theoretical model infers, the cavity pressure is inversely proportional to the cavity volume. Therefore, at a constant rainscreen venting area, the cavity pressure is supposed to decrease as the cavity depth increases. Such a phenomenon is observed in Fig 5.20a at low venting area ratios, however it disappears as the rainscreen venting area increases. In addition, in the case of a pressure gradient, the cavity response pressure does not seem to be affected for any of the venting configurations, when increasing the cavity depth from 25 to 300mm. Predicted transfer functions can provide a better idea about the behaviour of the cavity pressure, especially in the frequency domain.
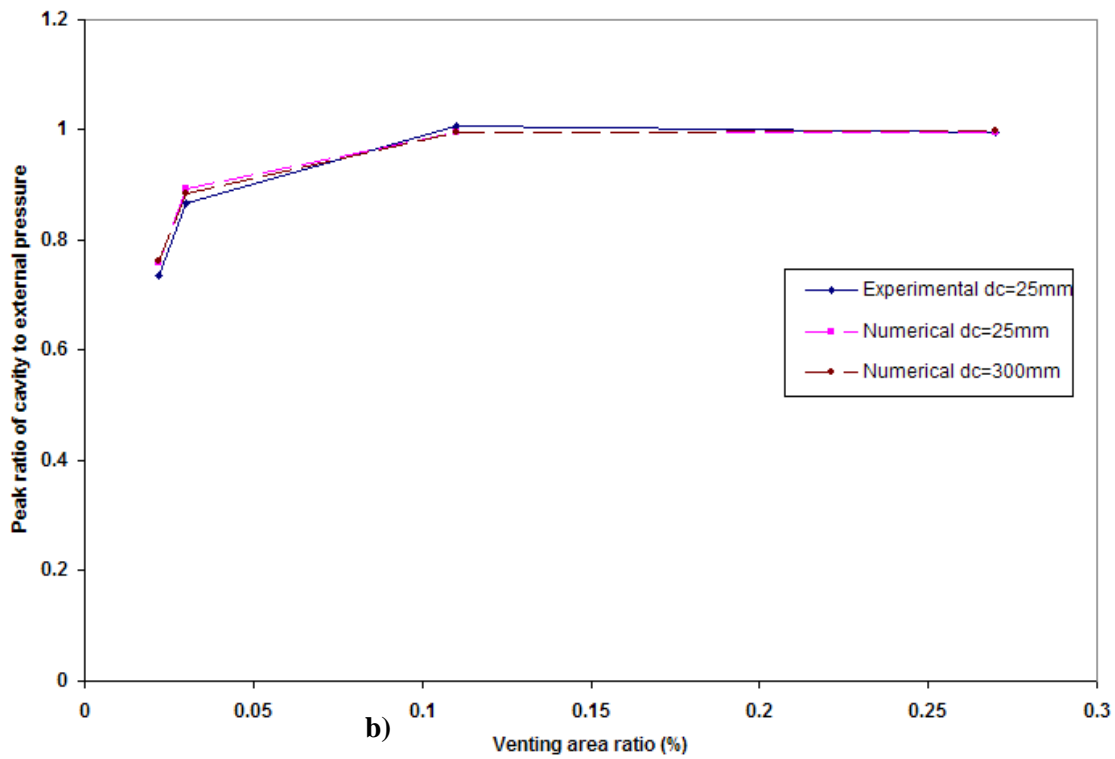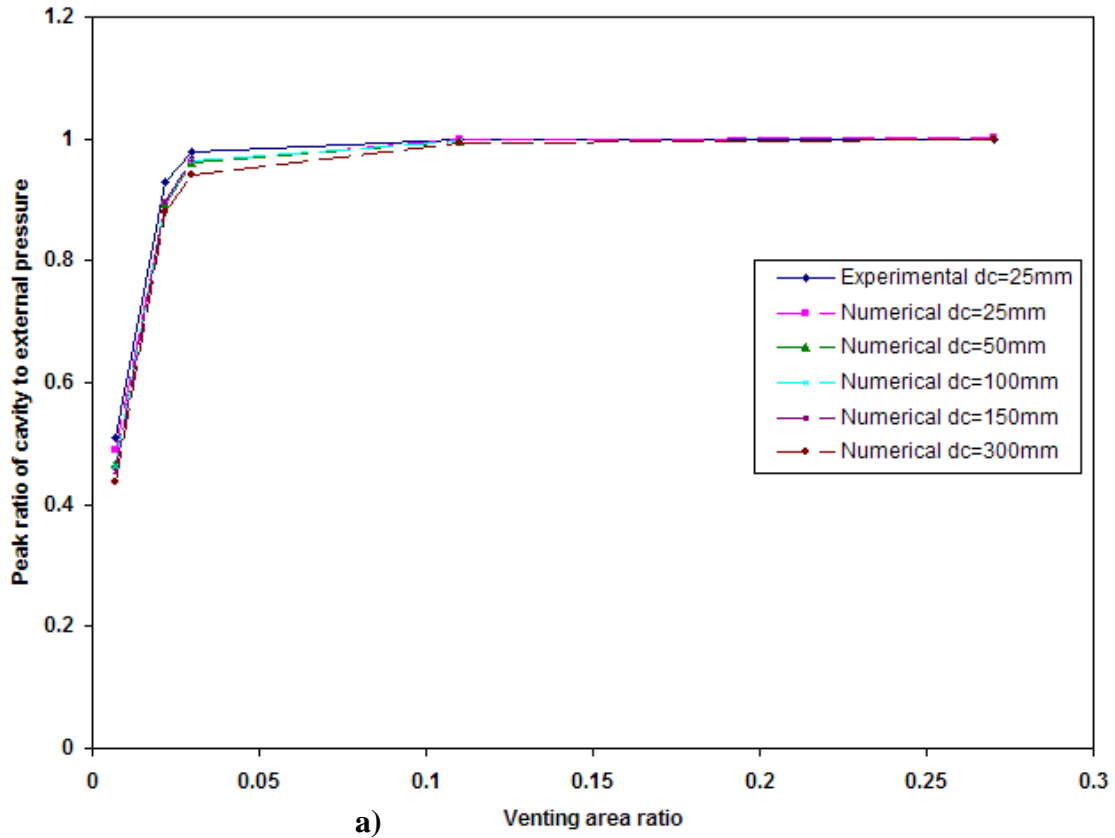
Figure 5.20 Peak ratio of cavity to external pressure for a) single and b) three different signals
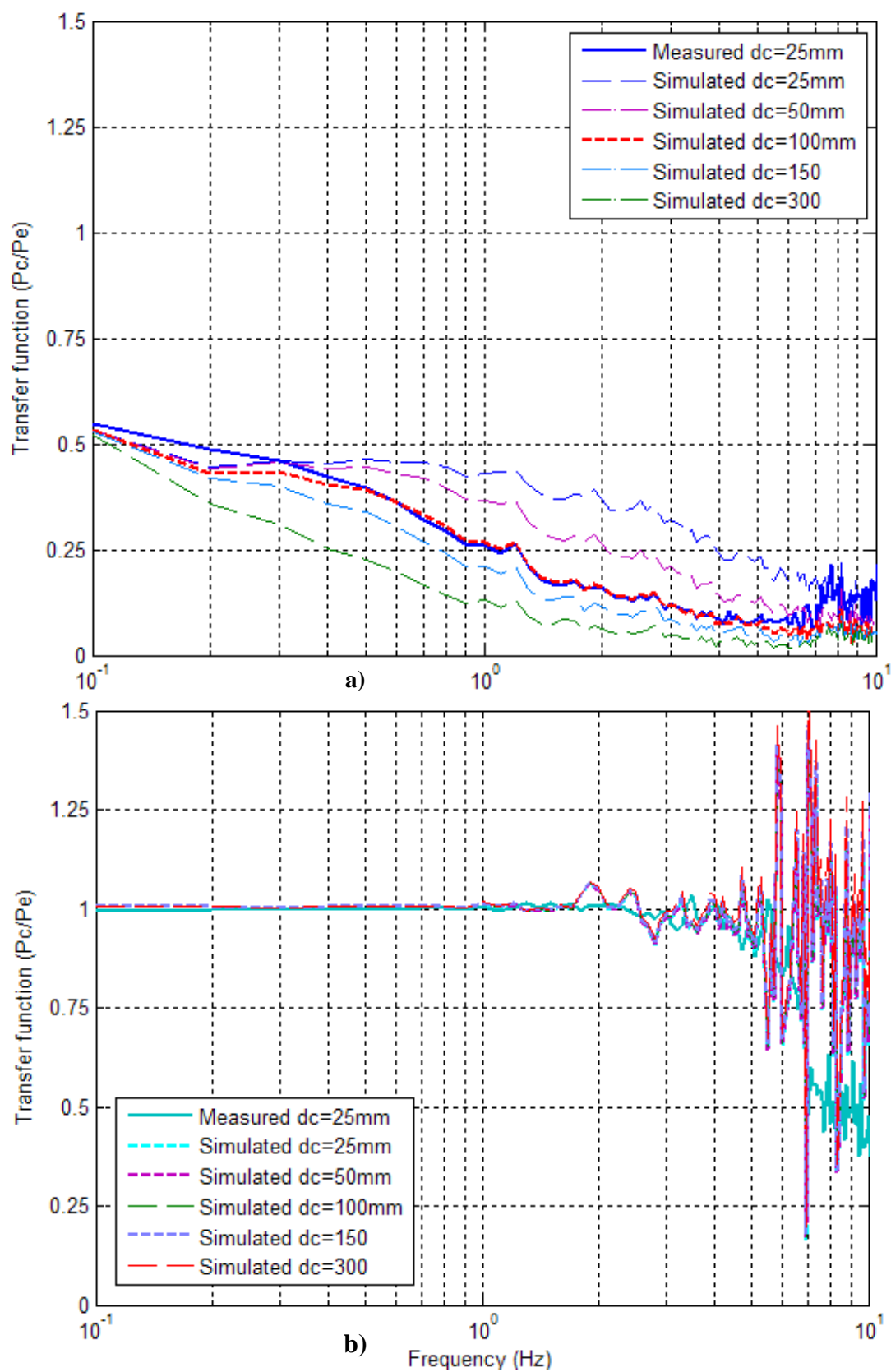
Figure 5.21 Transfer functions for single signal a) $A_V = 0.007\%$ b) $A_V = 0.11\%$ (wide face)
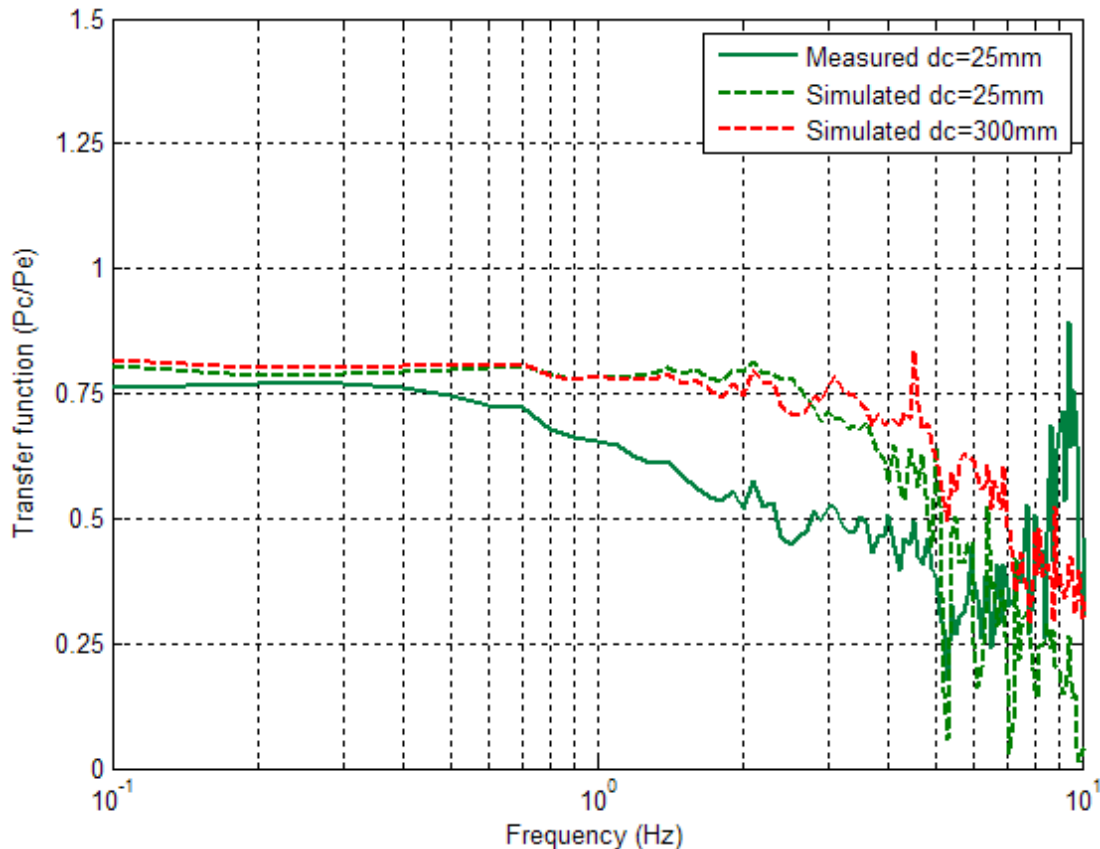
Figure 5.22 Transfer functions for three different applied signals $A_V = 0.11\%$ (wide face)

According to the applied single pressure, Figure 5.21 shows that for the low rainscreen venting area ratio the external load taken by the cavity decreases, as the cavity depth gets higher. At higher venting area, a similar amount of external fluctuations is transferred to the cavity in regardless of the cavity depth.

Figure 5.22 presents on the same plot the simulated transfer function at $d_c = 25mm$ and $d_c = 300mm$ at low venting area when three different pressures are applied to the PER wall model. There is no significant difference between the two cases. At a large cavity depth, the simulated transfer function has qualitatively the same trend, however, it starts to roll off at higher frequencies, allowing higher frequencies fluctuations to be transferred to the cavity. Since this would not practically be the case, we may deduce that the model could have also overpredicted the cavity pressure response as happened earlier for the smaller cavity.

Previous work has not tested the cavity depth variation effect on the pressure equalization process. The focus was more towards the rainscreen venting to air barrier leakage role in the PER walls performance. Apart from Garden (1963) who settled the minimum value at 25mm, only a few recommendations were mentioned in terms of determining a suitable cavity depth. The concept is that the cavity depth depends on both the rainscreen venting area and the total area of the panel. Inculet (1990) established the following relationship where $d_c \leq 10\sqrt{A_{rs}}\big/A_w$. Later, Kumar (2000) claims that an increase in venting for constant volume, or a decrease in volume for constant venting area, can improve the pressure equalization. This is proved in the numerical tests that have been done for the current project when a single pressure signal is applied. However, note that the external pressure signals used for all cavity depths were the same as for the lowest depth (25mm), which in practice could not be correct, taking into account the PLA errors at each configuration, and or the varying amount of leakage that may arise from the cavity volume change. Therefore, further full-scale experiments should be done, by varying the cavity depth to validate the theory.

5.5 Summary

This chapter has presented a comparison between the experimental and predicted cavity pressure measurements based on Helmholtz resonator model theory. The concept was to match the measured rms cavity pressure with the numerical value by adjusting the rainscreen discharge coefficient and including leakage holes in the air barrier simultaneously. When a uniform pressure was applied, the numerical model showed the same cavity response prediction at $A_V = 0.022\%$ and $A_V = 0.03\%$ under two different combinations: 1) six leakage holes at rainscreen discharge coefficient equal to 0.03 and, 2) 37 leakage holes with $K = 0.15$. While with a pressure gradient, only the second combination gave the best matching.

On the other hand, the predicted cavity pressure did not seem to be affected by the addition of leakage holes to the numerical model at venting area ratios higher than 0.11%.

In general, the results showed, for low venting area ratios, a satisfactory agreement in the low frequency regions between transfer functions of cavity to external pressures. At higher frequencies, the simulated transfer functions were overpredicted. At high venting area ratios, a good agreement was provided in terms of both transfer functions and phase angles.

Discrepancies were noticed when comparing the matching with respect to the applied external pressure. Basic statistical ratios of cavity to external pressures were underestimated under a pressure gradient and overestimated under a uniform pressure for low venting area ratios. Also, the simulated transfer functions were slightly underpredicted at high venting area ratios in the case of the application of a horizontal pressure gradient.

The numerical model was used to predict the impact of cavity depth variation on the pressure equalization process, using the external pressure values as applied to the model on site. The simulations showed that for low venting area ratios, increasing the cavity depth reduces the equalization process between external and cavity pressures under a uniform pressure. Under a gradient pressure, there was no effect of the cavity depth variation. Under a pressure gradient, the cavity pressure response did not change at both low and high venting area ratios.

The following chapter will explore the conclusions based on both the experimental and numerical findings of the current research. Also, it will present some recommendations for future experimental work.

CHAPTER 6

CONCLUSIONS AND RECOMMENDATIONS

A completely sealed full-scale model of a PER wall panel compartment measuring 2.2 m wide by 2m high was built in the IRLBH facility at the University of Western Ontario, to investigate the effect of various parameters on the pressure equalization process under normal wind pressure. PLAs were used to generate wind pressure time series signals based on wind tunnel experiments. Two types of external pressures were applied: 1) a single pressure signal and, 2) three different signals that create a pressure gradient across the rainscreen. The signals correspond respectively to a middle tap and edge taps signals of a windward façade associated to a pressure model already investigated. In each test configuration, the external data pressure signals of both wide and narrow faces were used. These faces are being tested each separately under a normal wind flow.

The configurations differed in the rainscreen venting area ratios, while the volume of the PER was kept constant at the cavity depth of 25mm. Also, in some cases, the layout of vent holes was changed for the same venting area. Data measurements provided the cavity pressure for each configuration which enables to evaluate the PER performance with cavity response to external pressure ratios. The experimental results were compared to a numerical model's predictions based on Helmholtz resonator theory. Furthermore, the effect of the compartment volume variation on PE was examined numerically by predicting the cavity pressure for a wide range of cavity depths, with respect to the rainscreen venting area ratio.

Contributions of the Current Research

Previous pressure equalized rainscreen wall system experiments were focusing most on the effect of rainscreen venting and air barrier leakage area ratios on the pressure equalization process. There was an agreement that a satisfactory PE process could be

attained by using an adequate rainscreen venting to air barrier leakage area ratio, all other factors remaining constant. However, other PER wall parameters or external flow conditions that might have an effective impact on the system performance, have not been extensively addressed before.

The current research has tested a PER compartment under a pressure gradient by the application of three different signals varying horizontally over the rainscreen panel. This experiment is considered to be unique in terms of setup and application. In fact, for the first time, such a test was performed in a controlled facility where the model is built as perfectly sealed. In addition, real wind traces were used corresponding to edge pressure signals, that were extracted from both a wide and narrow windward faces under a normal flow. Thus, the effect of two types of pressure gradients was examined. This test has provided a clear idea about the impact of a pressure gradient on the PER system performance, under a range of rainscreen venting area ratios and configurations.

Moreover, this project has examined the differential pressure differential across the rainscreen under a very low rainscreen to wall venting area ratio, which is 0.007%, a value that was never encountered before. Therefore, it was interesting to investigate the effect of such configuration on the model performance at the smallest cavity depth usually used, which is 25mm.

Finally, the vent openings layout impact on the PE process was experimentally investigated for the same rainscreen venting area ratio and cavity depth, under both the external uniform and gradient pressures. Previous studies have not separately examined this parameter.

Based on the experimental and numerical cavity pressure measurements, the data analysis have led to the following:

Conclusions

- The rainscreen venting to wall area ratio has a significant impact on the PER wall panel performance at constant volume. As the venting area increases, pressure equalization between external and cavity pressures improve, irrespective of the type of external applied pressure signals.

- Under both applied single pressure and pressure gradients, the cavity pressure is uniform at all rainscreen venting areas ratios.

- The change in the vent openings layout affects the process of pressure equalization. At high venting area ratios, the transfer functions magnitudes referring to the cavity to exterior pressures ratio are almost the same in case the vents are placed at bottom or distributed between top and bottom of the rainscreen. The difference is more pronounced at low venting area ratios, where the bottom location provides better pressure equalization.

- As the rainscreen venting area ratio gets larger, the critical damping frequency increases. Thus, the transfer functions of the cavity to external pressure ratio show less attenuation at low frequencies, with a reduction of the phase angle. In addition, better transmission of higher frequencies is observed.

- A full-pressure equalization results in a phase angle between the cavity and external pressure equal to zero, in conjunction with a complete transmission of low and high external frequency fluctuations in terms of transfer functions.

- The pressure gradient, caused by the application of three different signals, leads to a lower degree of pressure equalization with higher peak factors, in terms of differential pressure and frequencies. In the current research, the maximum PE is attained at $A_V = 0.27\%$, external area-averaged pressure frequencies higher than 3 Hz are not fully transmitted to the cavity. Under a uniform pressure, full PE was observed for $A_V = 0.11\%$

- A higher applied horizontal pressure gradient leads to higher residual loads on the raincsreen, which results in a slower pressure equalization process shown by the model.

- The numerical model based on Helmholtz resonator theory provides good matching with the experimental results at high rainscreen venting area ratios in terms of high frequencies external fluctuations. At low venting areas, the numerical model is not able to capture the real critical damping frequency, which shows an overprediction of the transfer functions and great reduction in phase angles. Such trend indicates that the model presents an issue in terms of the damping term, which is highly related to the area-venting ratio. A possible reason might be the linearization of the damping term in the equations.

- Under both a uniform and gradient pressures, the inclusion of leakage holes in the numerical model does not influence the predicted cavity response at $A_v \geq 0.11\%$

- Certain differences exist in the numerical predictions of cavity pressure response in the frequency domain depending on the applied external pressures. Under a uniform pressure, statistical values of the cavity to external pressure ratios are underestimated at low venting areas ratios by numerical simulations, and the experimental transfer function is in fairly good match at high venting are ratios. Under a pressure gradient, there is overestimation of the statistical ratios; also, the transfer function becomes underpredicted at higher frequencies for larger venting.

- Based on the numerical model prediction, the cavity depth variation shows that the effect of the volume change is more significant at low venting areas. At a constant rainscreen venting area, the pressure equalization is reduced as the cavity depth increases when a uniform pressure is applied. However, no significant change is observed when the PER is subject to a pressure gradient.

Recommendations for Future Experimental Work

- It would be very useful to conduct more tests at various depths in order to see the effect of cavity volume change on the PE performance of the current model, especially under a pressure gradient. Such experiment may either validate the current project's results, or settle new recommendations for an optimum cavity depth.

- More test configurations are recommended involving the inclusion of intentional leakage openings in the air barrier, which will help to check the impact of the rainscreen venting to air barrier leakage areas ratios on the model performance under a uniform pressure and pressure gradient.

- Various other experiments may be performed at different wind angles, compartment size and vent openings layout to collect the volume of data required for design guidelines settling.

- The numerical model as used in this project needs further investigation for better predictions at low venting areas. A possible solution is to find a certain method in doing the computations without the linearization of the equations and damping terms.

- The wind-driven rain impact may be also investigated using the current PER wall model. By applying simultaneously wind pressure and rain droplets, we would experimentally observe the process of the water penetration into the cavity through the various vent openings. Such test would require improvement in the way of wind application to avoid losses, especially at low venting areas.

- A rainscreen venting area ratio less than 0.11% is not recommended for a PER system at a compartment cavity depth of 25mm

REFERENCES

Baskaran, B. A. and Brown, W. C. (1992). "Performance of pressure equalized rainscreen walls under cyclic loading". *J. Thermal. Ins. and Build. Envelop*. **16**, 183-193.

Baskaran B.A. (1992). "Review of Design Guidelines for Pressure Equalized Rainscreen walls". *Institute for Research in Construction, National Research Council* Canada, internal report, issue 629.

Birkeland, O. (1962). "Curtain walls". *Norwegian Building Research*.

Bloxham, C. and Vickery, B.J. (1989). "An experimental investigation of internal pressure dynamics with a dominant front wall opening", University of Western Ontario, Faculty of Engineering and Science. *BLWTL-SS46-1989.*

British Standards, BS 8200:1985. "Code of practice for design of non-load bearing external vertical enclosures of buildings".

Brown, W.C, Rousseau, M.Z and Dalgliesh, W.A.(1995). "Field testing of pressure-equalized rainscreen walls". *Building Envelope Performance and Durability*, IRC Technical Seminar, 59-69, Canada.

Canadian Construction Materials Centre (CCMC), 2000. "A method for Evaluating Air barrier Systems and Materials." *National Research Council's Institute for Research in Construction, Construction Technology*, Issue 46.

Chaplin, G.C, Randall, J.R and Baker, C.J.(2000). "The turbulent ventilation of a single opening enclosure." *J. Wind Eng. Ind. Aerodyn.,* **85,** 145-161.

Choi E., C.C. and Wang, Z. (1998). "Study on pressure-equalization of curtain wall systems". *J. Wind Eng. Ind. Aerodyn.,* **73,** 251-266.

Davenport, A.G. and Surry, D. (1984). "The Estimation of Internal Pressures due to Wind with Application to cladding pressures and Infiltration." *Wind Pressure Workshop,* Brussels, Belgium.

Fazio, P. and Kontopidis, T. (1988). "Cavity Pressure in Rain Screen Walls". *Building and Environment*, **23**,137-143.

Garden, G.K. (1963). "Rain Penetration and its control". *Division of Building Research, National Research Council* Ottawa, Canada, Canadian Building Digest, issue 40

Ganguli, U. and Quirouette, R.L. (1987). "Pressure equalization performance of a Metal and Glass curtain wall." *Proceedings, CSCE Centennial conference*, **1**,127-144, Montreal, Canada.

Ganguli, U. and Dalgliesh, W.A. (1988). "Wind pressures on open rain screen walls: Place Air Canada." *J. Struct. Eng.,* **114**, 642-56.

Ginger, J.D and Letchford, C.W (1999). "Net pressures on a low-rise full-scale building". *J. Wind Eng. Ind. Aerodyn* , **83**, 239- 250.

Harris, R.I. (1990). "The propagation of internal pressures in buildings." *J. Wind Eng. Ind. Aerodyn,* **34**, 169-184.

Holmes, J.D. (1979). "Mean and fluctuating internal pressure induced by wind", *Proc.5th International Conference on Wind Engineering*, 435-450, Colorado State University.

Holmes, J. D. (2001). "Wind loading of structures". *Spon press*, London, England.

Inculet, D. (1990). "Pressure Equalization of Rainscreen Cladding". The university of Western Ontario. MESc thesis. Faculty of Graduate studies. London, Canada.

Inculet, D. (2001). "The Design of cladding against wind-driven rain". The university of Western Ontario. PhD thesis. Faculty of Graduate studies. London, Canada.

Inculet, D.R and Davenport A.G. (1994). "Pressure-equalized rainscreens: A study in the frequency domain". *J. Wind Eng. Ind. Aerodyn,* **53**, 63-87.

Inculet, D. and Surry, D. (1997). "Optimum Vent locations for Partially-Pressurized Rainscreens". The University of Western Ontario, London, Canada. *BLWT-SS30.*

Inculet, D., Surry, D. and Davenport, A.G. (1997). "Unsteady pressure gradients and their implications for pressure-equalized rainscreens". *Proceedings of the International Conference on Building Envelope Systems and Technology,* Bath, England.

Inculet, D., Surry, D. and Davenport, A.G (2001). "An experimental study of pressure gradients and their implications for the design of pressure-moderated rainscreens." *Proceedings of the International Conference on Building Envelope Systems and Technologies*, 1, 101-106, Ottawa, Canada.

Irwin, P.A., Schuyler, G.D. and Wawzonek, M.A. (1984). "A wind tunnel investigation of rainscreen wall systems. *Morrison Hershfield Limited. Prepared for CMHC.*

Kala, S., Stathopoulos, T. and Kumar, K. S. (2008). "Wind loads on Rainscreen walls: Boundary-layer wind tunnel experiments". *J. Wind Eng. Ind. Aerodyn.*, **96**, 1058-1073.

Kumar, K.S. (1998). "Pressure equalization performance of rainscreen walls: Experimental investigations", *Proceedings of the 2nd East European Conference on Wind Engineering*, Prague, Czech Republic, September 1998.

Kumar, K.S. (1999). "A study on pressure equalization of rainscreen facades: full-scale experiments and computer simulations." *Technical Report, FAGO 99.40.k, Faculteit Bouwkunde*, Technical University of Eindhoven, Eindhoven, The Netherlands.

Kumar, K.S. and Wisse, J.A. (1999). "A full-scale study on pressure equalization of rainscreen facades", *Proceedings of the 10th International Conference on Wind Engineering*, Copenhagen, Denmark, June 1999.

Kumar, K. S., Van Shijndel, A.W.M (1999). "Prediction of pressure equalization performance of rainscreen walls". *Wind Struct,* **2**, 325-345.

Kumar, K. S. (2000). "Pressure equalization of rainscreen walls: a critical review."*Building and Environment*, **35**, 161-179.

Kumar, K. S., Stathopoulos, T. and Wisse, J.A. (2003). "Field measurement data of wind loads on rainscreen walls". *J. Wind Eng. Ind. Aerodyn.*, **91**,1401-1417.

Killip, I.R. and Cheetham, D.W. (1984). "The prevention of rain's penetration through external walls and joints by means of pressure equalization*." Building and Environment*, **19**, 81-91.

Kimura, R.I (1977). "Scientific basis of air conditioning". *Applied Sciences*, 175-186.

Kopp, G.A., Morrison, M.J., Gavanski, E., Henderson, D.J. and Hong, H.P. (2010). "Three Little Pigs" Project: Hurricaine Risk Mitigation by Integrated Wind Tunnel and Full-Scale Laboratory Tests. *Natural Hazards,* **11***,* 151.

Latta, J.K. (1973). "Walls, windows and roofs for the Canadian climate- a summary of the current basis for selection and design". *Special Technical Publication,* Issue 1. *NRCC 13487.*

Malecki, I. (1969). "Physical foundations of technical acoustics." *Pergamon Press, Oxford and New York.*

Morrison Hershfield Limited (1998). "Rain penetration control: Applying current knowledge". *CMHC, Canada,* issue 2972033/2.

Oh, J. H., Kopp, G. A. and Inculet, D. R. (2007). "The UWO contribution to the NIST aerodynamic database for wind loads on low buildings: Part 3. Internal pressures." *J. Wind Eng. Ind. Aerodyn,* **95**,755-779.

Rayleigh, L. (1945). "The theory of sound, 2nd Edition". *New York, NY: Dover Publications*

Rousseau, M.Z., Poirier, G.F. and Brown, W.C. (1998). "Pressure Equalization in Rainscreen wall systems*". National Research Council of Canada. Construction Technology Update.* Issue 17.

Schijndel Van, A.W.M. and Schols, S.F.C. (1998). "Modeling pressure equalization in cavities." *J. Wind Eng. Ind. Aerodyn,* **74**, 641-649.

Shaw, C.Y. (1981). "Air tightness: supermarkets and shopping malls. *ASHRAE J.23*

Sharma, R.N and Richards, P.J. (1997). "The effect of roof flexibility on internal pressure fluctuations." *J. Wind Eng. Ind. Aerodyn,***72**, 175-186.

Sharma, R.N. and Richards, P. J. (2003). " The influence of Helmholtz resonance on internal pressures in a low-rise building". *J. Wind Eng. Ind. Aerodyn*, **91**, 807-828.

Skerlj, P.F and Surry, D. (1994). " A study of mean pressure gradients, mean cavity pressures and resulting residual mean pressures across a rainscreen for a representative building". *Interim Progress Report to CMHC*, Boundary Layer Wind Tunnel Laboratory, University of Western Ontario.

Vickery, B. J. (1986). "Gust factors for internal pressures in low-rise buildings." *J. Wind Eng. Ind. Aerodyn,* **23,** 259-271.

Vickery, B. J. and Bloxham, C. (1992). "Internal pressure dynamics with a dominant opening." *J. Wind Eng. Ind. Aerodyn,* **41**, 193-204.

APPENDIX A

A-1 Rainscreen Sketches for Different Venting to Wall Area Ratio Configurations

A-2 Verification of the Air Barrier and Rainscreen Stiffness

A.3 - Uncertainties in Measurements

A.1- **Rainscreen Sketches for Different Venting to Wall Area Ratio Configurations.**
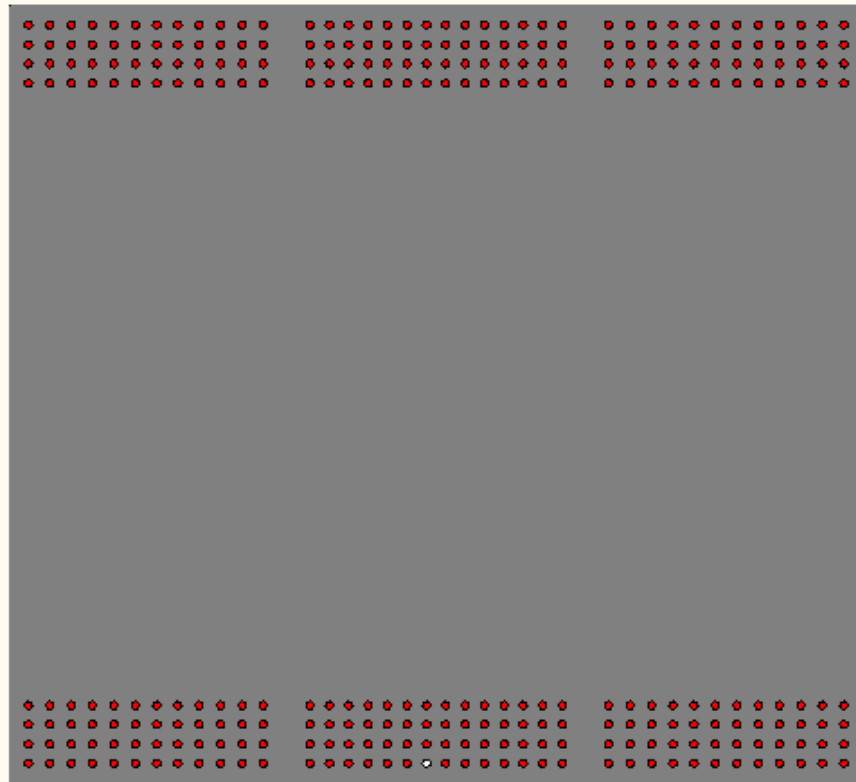
Configuration a) $A_v = 0.007$ %

Configuration b) $A_v = 0.022\%$

127
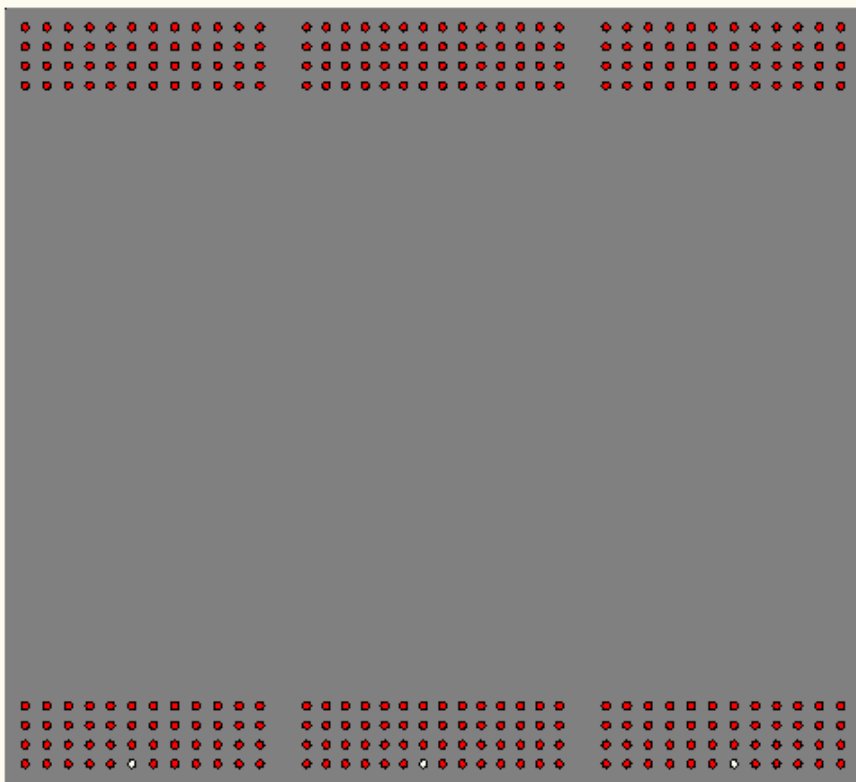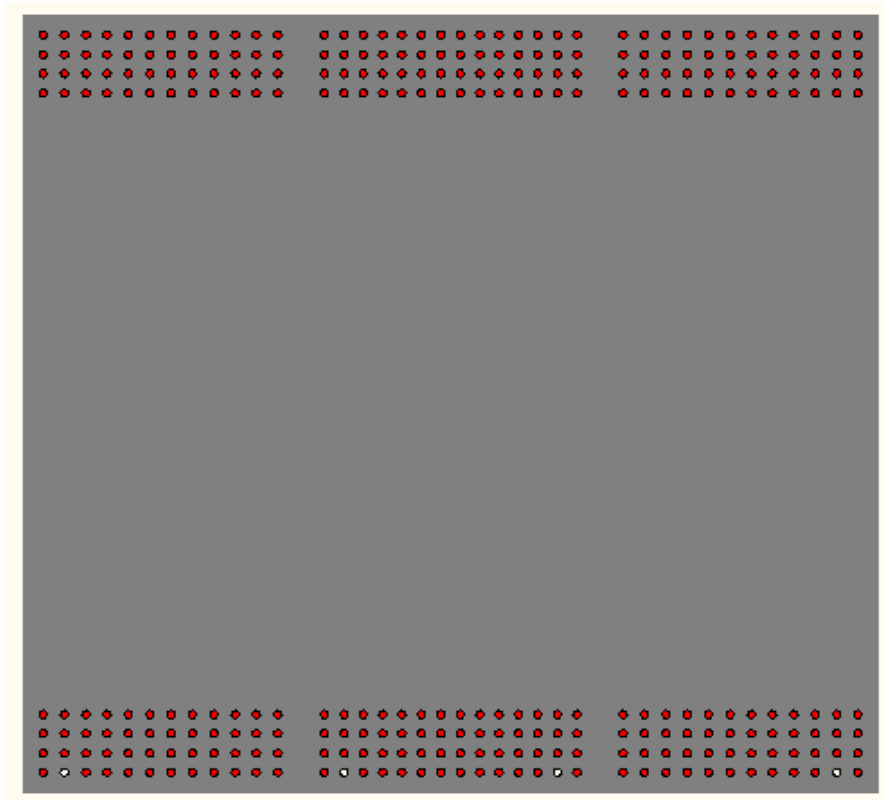
Configuration c) $A_V = 0.03\%$
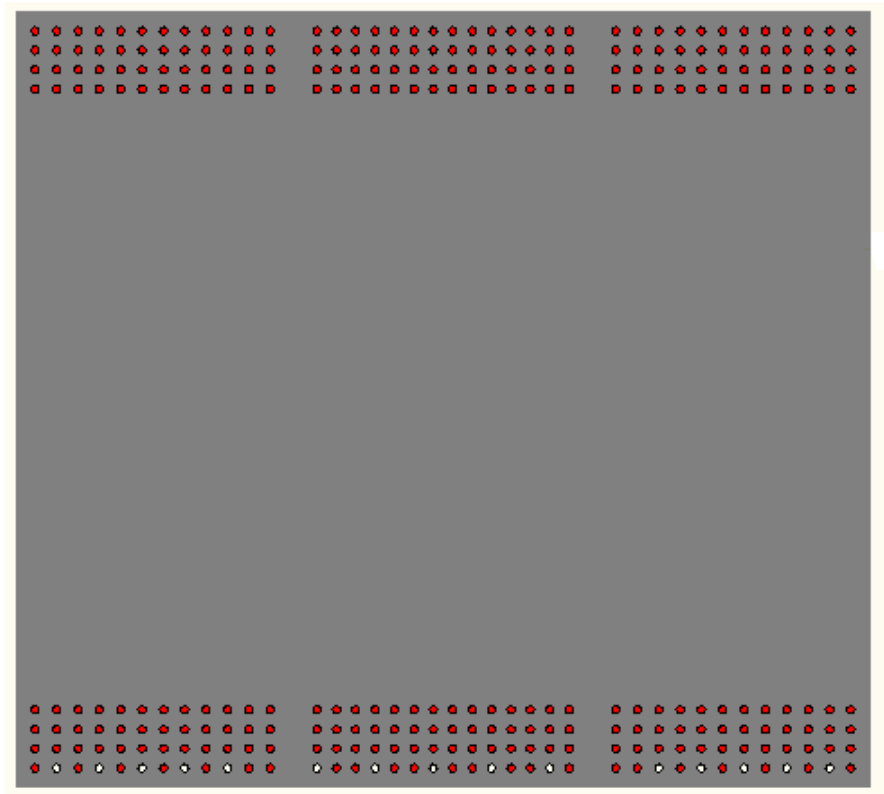
Configuration d) $A_V = 0.11\%$
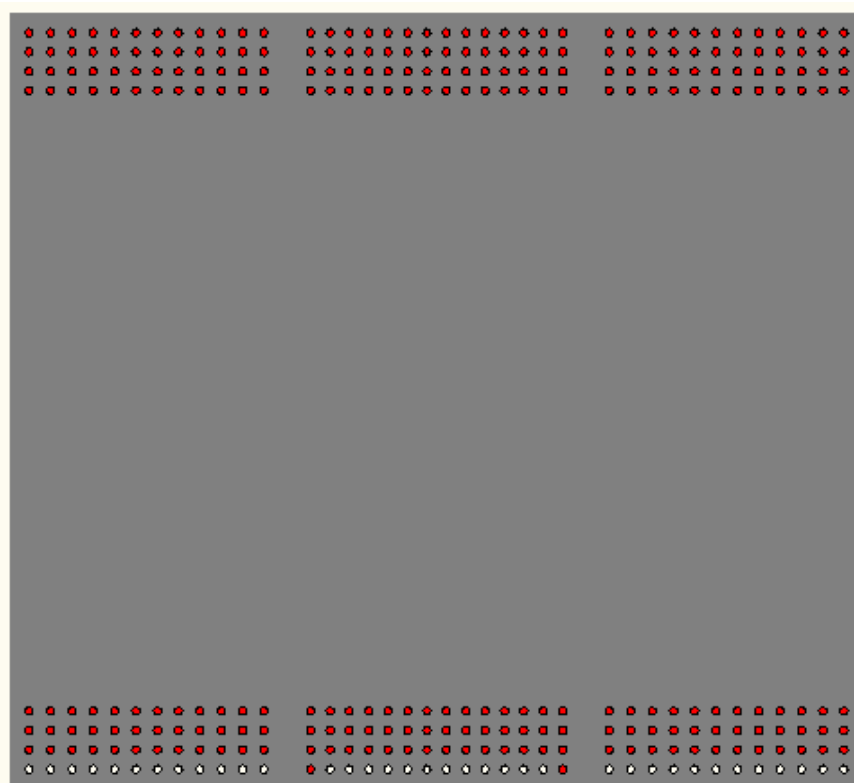
Configuration e) $A_V = 0.27\%$
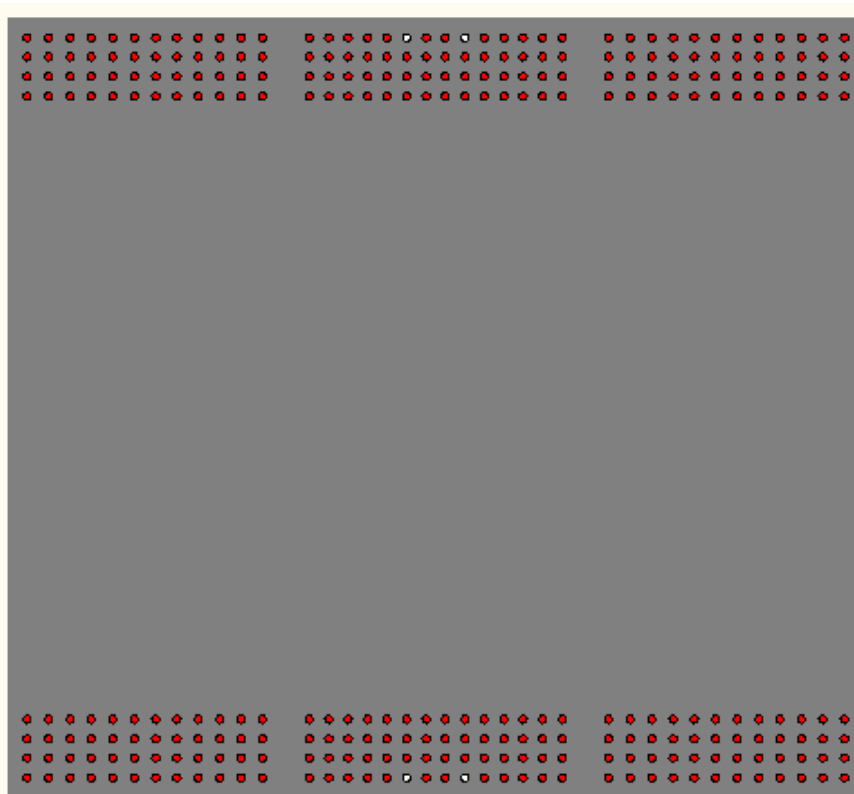
Configuration f) $A_V = 0.03\%$
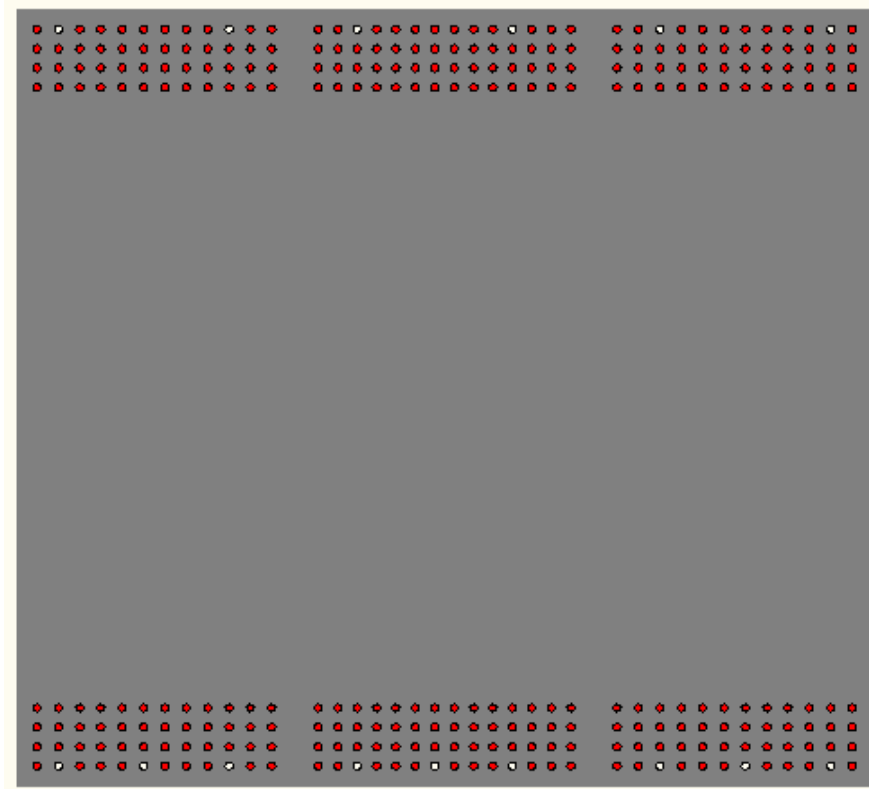
Configuration g) $A_V = 0.11\%$

■ **:** Plugged hole   ▫ : unplugged hole

Figure A1 Rainscreen venting area configurations

A.2 - Verification of the Air Barrier and Rainscreen Stiffness

It is absolutely important to keep the air volume inside the cavity constant during the tests configurations. For this reason, the PER wall panel is built with installing studs from the front and the back to eliminate any probability for deflection.

A.2.1 Aluminium deflection

Since the 2 wood pressure boxes (20 x 71 x 2200 cm³) ensure the rigidity of the aluminium rainscreen at top and bottom, we have to check the deflection of the remaining section (60 x 2200 cm²). The panel is assumed to be exposed to a (1.5 kPa) normally distributed load, thus the maximum deflection Δ is calculated based on Roark's Formulas for Stress & Strain (6th edition) for a rectangular plate under uniform pressure where

$$\Delta = \frac{C_0 p_0 b^4}{E h^3}$$

$p_0 = 1.5$ Kpa

b is the longest dimension

$E = 7.13 x 10^9$ Kg/m²   is the elastic modulus of the aluminium

h= 0.00635 m is the rainscreen thickness

C_0 depends on the end supports and the aspect ratio of the plate.

In case 4 vertical studs are installed at 45 cm, and 2 are placed horizontally at 20 cm, then

the aspect ratio $\dfrac{b}{a} = 2.25$ and $C_0 = 0.12$; the deflection for each section (20 x 45 cm²) is

around 1 mm.

A.2.2 Wood deflection

The deflection limit of the plywood wall of the air barrier at the back of the (PER) wall is

equal or less to $\dfrac{l}{240}$; $\Delta_{\lim it} \leq 9 x 10^{-3} m$ for $l = 2.2m$

The deflection of the wooden studs is calculated with the formula: $\Delta = \dfrac{5wl^4}{384EI}$

w is the uniformly distributed load supported by the stud, l is the stud span

$E = 1.04 x 10^9$ Kg/m²   is the elastic modulus of the wood, I is the inertia moment

Taking into consideration a uniform load of 0.54 Kg/m, each of the 6 (3 x 18 cm²) cross section studs at 36cm having a span $l = 1.5m$ (crossing 2 horizontal wood plates at top and bottom) has deflection around 0.1 mm. Such value theoretically gives a volume increase inside the cavity of 0.044%.

A.3 - Uncertainties in Measurements

A.3.1 Errors from Pressure loading Actuators (PLAs)

These errors are issued from the performance of the PLAs that are supposed to generate the same pressure signal in each configuration of the test. However, slight changes are observed in the achieved pressures due to the change in the fan performance of the PLAs, function of the ambient temperature and the number of holes in the rainscreen. For this

reason, the pressure equalization is examined in function of the cavity to the exterior pressure ratio, instead of the cavity pressure evaluation itself.

The error computed here refers to the Accuracy in percentage, which is the ratio of the deviation $\Delta\delta$ value to the target pressure value δ

Configuration	Mean pressure (kPa)			Peak pressure (kPa)		
	Achieved	Deviation	Accuracy	Achieved	Deviation	Accuracy
a	1.3068	0.0132	1.0%	2.697	0.1175	4.0%
b	1.3222	-0.0022	-0.1%	2.829	-0.0145	-0.5%
c	1.3231	-0.0031	-0.2%	2.715	0.0995	3.5%
d	1.3182	0.0018	0.1%	2.765	0.0495	1.7%
e	1.3185	0.0015	0.1%	2.774	0.0405	1.4%
f	1.3018	0.0182	1.3%	2.767	0.0475	1.6%
g	1.3154	0.0046	0.3%	2.839	-0.0245	-0.8%

Table A.1 Achieved single exterior pressure signal for the wide face

Table A.1 shows the mean and peak pressure values achieved by the PLAs in each configuration, with the associated deviation; corresponding to the wide face when one single exterior pressure signal is applied to the rainscreen. The deviation $\Delta\delta$ is the difference between the actual (demand) and measured value for each case; knowing that the accurate value δ refers to the target pressure (given to the PLA) where the mean and peak are respectively $\overline{P}_e = 1.32 Kpa$ and $\hat{P}_e = 2.8 Kpa$.

In case several PLAs are functioning within the same setup, the measured (achieved) value taken into account is the one read by the PLA controller, which is related to the second airbox at the bottom of the rainscreen. This PLA is fed with the demand signal and all others must follow it reproducing the same signal simultaneously. Such process is supposed to reduce the errors that might come in case the PLAs are working independently; based on preliminary tests we've done before.
Setting this apart, the data clearly demonstrates that the PLA controller never reproduces the same pressure signal with the exact statistical values, which gives us a deviation range of the achieved pressure with respect to the demand.

As an example, the first Accuracy error values are calculated as follows:

For the mean pressure:

$$Accuracy : \frac{\Delta \delta}{\delta} = \frac{0.0132}{1.32} = 0.01 = +1.3\%$$

For the peak pressure:

$$Accuracy : \frac{\Delta \delta}{\delta} = \frac{0.1175}{2.8} = 0.041 = +4\%$$

	Single applied signal		Three applied signals	
Mean pressure	Wide face	Narrow face	Wide face	Narrow face
Accuracy	-0.2% to +1.3%	-0.7% to +1.4%	-1.3% to +1.2%	-1% to +5%
Peak pressure				
Accuracy	-0.8% to +4%	-1.8% to +1%	+1% to +13%	-7% to +10%

Table A.2 Summary of accuracy errors ranges for PLAs performance

Table A.2 shows a summary of the errors ranges of the PLAs for both the wide and narrow faces cases. In case three different pressures are applied, the errors seem higher especially with respect to the peak pressures values. The accurate pressure here is assumed to be the area-averaged pressure on the pressure boxes, and the PLAs are working separately without following any controller. So as each PLA related to each pressure box is generating a different signal, the errors would be accumulated from all the machines, since the demand pressures are different and the PLAs are working without assured synchronization. Therefore, the production of demand peak pressures is inconsistent from one test to another.

A.3.2 Errors from pressures transducers readings in the same pressure box

Errors also occur between the different pressure transducers that are supposed to read the same achieved pressure within the same test configuration. However, they record different values because they have different positions on the outer pressure boxes, so each tackles the signal generated by a certain PLA; and since each PLA has its own performance, the pressure transducers present different readings, even if the PLAs are generating the same signal.

Configuration	Wide face	Narrow face
Horizontal error		
b	+0.4%	-0.4%
c	-2% to −2.2%	-3%
d	-0.2% to 2%	-1.5% to 0%
g	-0.4%	-0.3% to −1%
e	±0.5%	+0.03% to +0.6%
Vertical error		
f	-0.4%	-0.2%
g	-0.9% to −0.4%	-0.3% to −0.1%

Table A.3 Accuracy errors between pressure transducers of the same test configuration

Table A.3 shows the Accuracy errors for all configurations for both the wide and narrow face when one single pressure signal is applied. The errors calculated in this case are the differences (in percent) between the mean pressures values measured by the pressure transducer of the PLA contoller airbox; and those located on the adjacent pressures boxes (Horizontal error) and the top and bottom boxes (Vertical error).

It is obvious that the higher range of Accuracy errors belongs to configuration c, where four holes are distributed as two under the second air box and one under each edge box. Since the pressure transducer located on the middle airbox, that covers the two holes, reads the accurate pressure value, there is certainly a discrepancy between this value and the others located at the edge boxes. In general, the airflow blown by the PLA is function of vent holes area, thus the PLA controller will perform the signal differently from the others, and the errors are higher because there is no equal distribution of the vent holes between the three boxes.

Appendix B

B.1 Numerical Method

B.1 Numerical Method

The numerical code written in Matlab 7.1 is supposed to provide the solution for the Helmholtz resonator theory system equations, which include the "Multiple discharge equations for unsteady flow through multiple openings or leaks (MDE)",

$$\rho_a l_{ei} \ddot{x}_i + \left(\frac{1}{K_i}\right)^{1/n_i} \left(\frac{\rho_a}{2}\right)^{1/2n_i} \dot{x}_i \left|\dot{x}_i\right|^{(1/n_i)-1} + \frac{32\mu l_{0i}}{d_i^2}\dot{x}_i = p_{ei} - p_c \qquad (B.1)$$

and an additional Continuity Equation (CE)

$$\rho(a_1 x_1 + a_2 x_2 + ... + a_m x_m) = \frac{\rho V_0}{\gamma P_0}p_c \qquad (B.2)$$

showing m+1 unknowns for a number (m) of vent openings: the cavity pressure and the air slug distance for each opening ($p_c, x_1, x_2, ... x_m$), (i=1,2...m)

Since the non –linear (MDE) equations with first and second order differential terms do not have a general analytical solution; they are transformed into a set of linear equations using a backward differencing approximation (a concept that is issued from the expansion of Taylor series about a single variable) in addition to iterations. Therefore, the first order and second order derivatives of the air slug movement distance are respectively expressed with respect to the time interval Δ as:

$$\dot{x}^j = \frac{x^j - x^{j-1}}{\Delta}$$

$$\ddot{x}^j = \frac{x^j - 2x^{j-1} + x^{j-2}}{\Delta^2}$$

where j designates a step of time.

Using the bulk of modulus $K_A = \gamma P_0$, the continuity equation (CE) is rewritten as

$$p_c^j = \frac{K_A}{V_0}\sum_{k=1}^{m} a_k x_k^j \qquad (B.3)$$

Substituting the derivatives of the distance x, and the cavity pressure p_c with the numerical approximate expressions, the (MDE) system equations become

$$\frac{\rho_a le_1}{\Delta^2}(x_1^j - 2x_1^{j-1} + x_1^{j-2}) + \frac{(C_{L_1})^{1/n}}{\Delta^2}(\frac{\rho_a}{2})^{1/2n}(x_1^j - x_1^{j-1})\left|x_1^j - x_1^{j-1}\right|^{(1/n)-1}$$

$$+\frac{32\mu l_0}{d^2\Delta}(x_1^j - x_1^{j-1}) = p_{e_1}^j - \frac{K_A}{V_0}\sum_{k=1}^{m}a_k x_k^j$$

$$\frac{\rho_a le_2}{\Delta^2}(x_2^j - 2x_2^{j-1} + x_2^{j-2}) + \frac{(C_{L_1})^{1/n}}{\Delta^2}(\frac{\rho_a}{2})^{1/2n}(x_2^j - x_2^{j-1})\left|x_2^j - x_2^{j-1}\right|^{(1/n)-1}$$

$$+\frac{32\mu l_0}{d^2\Delta}(x_2^j - x_2^{j-1}) = p_{e_2}^j - \frac{K_A}{V_0}\sum_{k=1}^{m}a_k x_k^j$$

$$\dots$$

$$\frac{\rho_a le_m}{\Delta^2}(x_m^j - 2x_m^{j-1} + x_m^{j-2}) + \frac{(C_{L_1})^{1/n}}{\Delta^2}(\frac{\rho_a}{2})^{1/2n}(x_m^j - x_m^{j-1})\left|x_m^j - x_m^{j-1}\right|^{(1/n)-1}$$

$$+\frac{32\mu l_0}{d^2\Delta}(x_m^j - x_m^{j-1}) = p_{e_m}^j - \frac{K_A}{V_0}\sum_{k=1}^{m}a_k x_k^j \tag{B.4}$$

Once the initial approximations of the values of x^j are recognized, these equations can be solved simultaneously with (m) unknowns $(x_1, x_2, ... x_m)$. The row vector of the slug movements x is found from the multiplication of two matrices ($mat1$) and ($mat2$) issued the reorganization of the terms in the (MDE) equations.

Figure B1 shows the flow chart for the computational programming of the (MDE) and (CE) equations in order to predict the cavity pressure P_c.
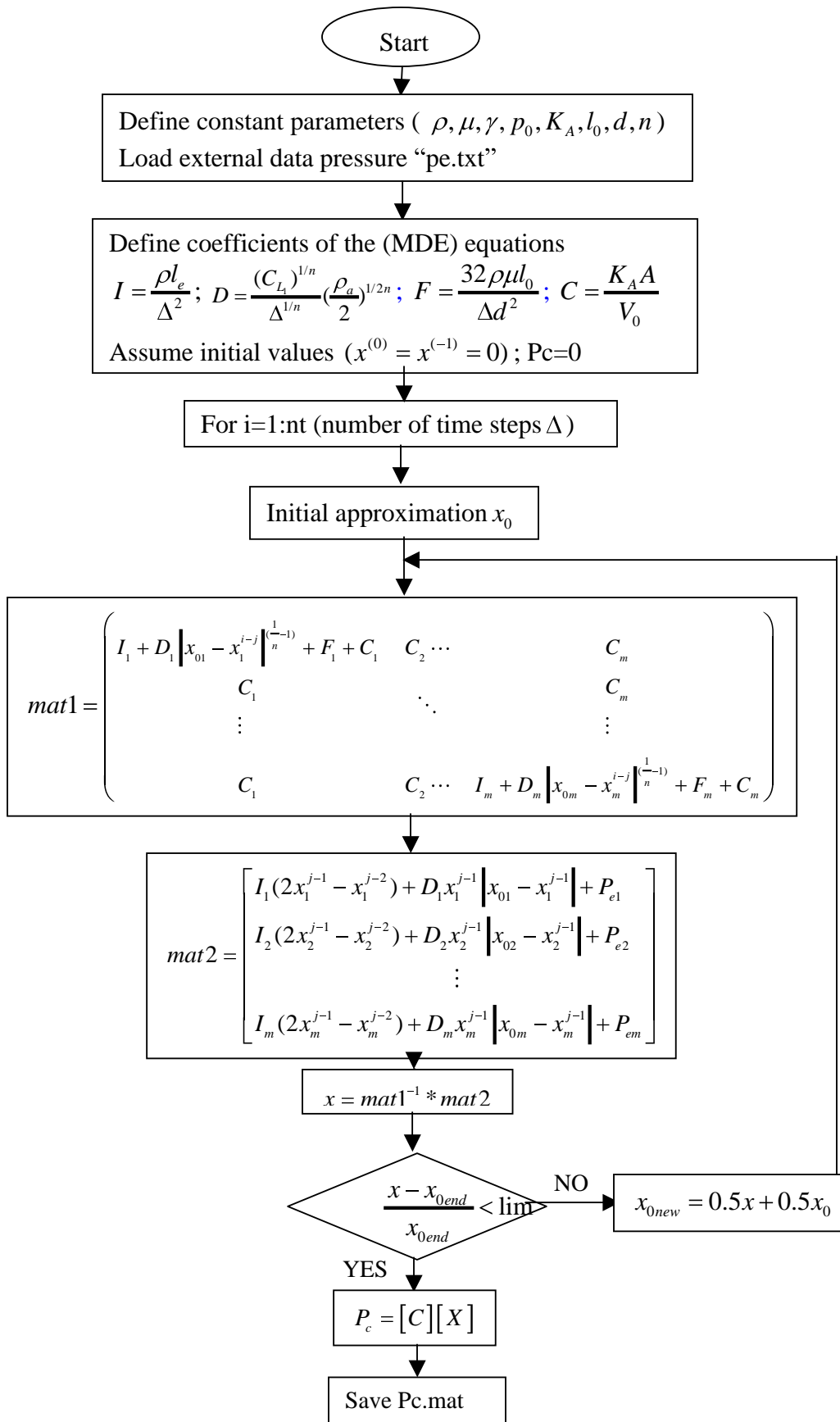
```
                          ┌─────────┐
                          │  Start  │
                          └─────────┘
```

Start

Define constant parameters ($\rho, \mu, \gamma, p_0, K_A, l_0, d, n$)
Load external data pressure "pe.txt"

Define coefficients of the (MDE) equations

$$I = \frac{\rho l_e}{\Delta^2}; \quad D = \frac{(C_{L_1})^{1/n}}{\Delta^{1/n}}(\frac{\rho_a}{2})^{1/2n}; \quad F = \frac{32\rho\mu l_0}{\Delta d^2}; \quad C = \frac{K_A A}{V_0}$$

Assume initial values ($x^{(0)} = x^{(-1)} = 0$) ; Pc=0

For i=1:nt (number of time steps Δ)

Initial approximation x_0

$$mat1 = \begin{pmatrix} I_1 + D_1\left|x_{01} - x_1^{i-j}\right|^{(\frac{1}{n}-1)} + F_1 + C_1 & C_2 \cdots & & & C_m \\ C_1 & & & & C_m \\ \vdots & & \ddots & & \vdots \\ C_1 & & C_2 \cdots & I_m + D_m\left|x_{0m} - x_m^{i-j}\right|^{(\frac{1}{n}-1)} + F_m + C_m \end{pmatrix}$$

$$mat2 = \begin{bmatrix} I_1(2x_1^{j-1} - x_1^{j-2}) + D_1 x_1^{j-1}\left|x_{01} - x_1^{j-1}\right| + P_{e1} \\ I_2(2x_2^{j-1} - x_2^{j-2}) + D_2 x_2^{j-1}\left|x_{02} - x_2^{j-1}\right| + P_{e2} \\ \vdots \\ I_m(2x_m^{j-1} - x_m^{j-2}) + D_m x_m^{j-1}\left|x_{0m} - x_m^{j-1}\right| + P_{em} \end{bmatrix}$$

$$x = mat1^{-1} * mat2$$

$$\frac{x - x_{0end}}{x_{0end}} < \lim$$

NO → $x_{0new} = 0.5x + 0.5x_0$

YES

$$P_c = [C][X]$$

Save Pc.mat

Figure B1 Flow chart for computational programming for (MDE) equations in Matlab 7.1

The program shows that the computation starts with a "for" Loop, that is based on the time step between each measurement during the sampling period. Also, there are iterations, and each time the value of x is computed, it gives new approximation $x_{0new} = 0.5x + 0.5x_0$, that is supposed to get closer to the final solution. The solution is determined when the convergence limit is reached so $\dfrac{x - x_{0end}}{x_{0end}} < 10^{-6}$; meaning that the provided distances get close enough to the true values. This convergence criterion is chosen by trial, the values of x seemed constant at this limit.

Finally, the pressure is generated by multiplying the two vectors $[C]$ and $[X]$, based on the Continuity Equation as rewritten in Eqn (B.3).

VITA

NAME: Samar Darwich Dernayka

PLACE OF BIRTH: Tripoli, Lebanon

POST-SECONDARY EDUCATION AND DEGREES:

B.E.S.C
Lebanese University, Faculty of Engineering
Branch I
2006

MESC Thesis
The University of Western Ontario
Faculty of Civil and Environmental
Engineering
2009-2011

RELATED WORK EXPERIENCE:

Structural Engineer
DEC- Design and Construction Engineering
Tripoli, Lebanon
2006-2008

Teaching Assistant
The University of Western Ontario, Canada
2009-2011

PROFESSIONAL LICENSE:

Order of Engineers and Architects
Tripoli, Lebanon